MF2077 Machine Design Advanced Course Part II

CubeSat Evaluation and Design for Tribological Testing

Ananthakrishna Ayankalath Thekkepat
Harun Gungør
Dannel Jacob
Abhay Menon
Samantha Rosenberg

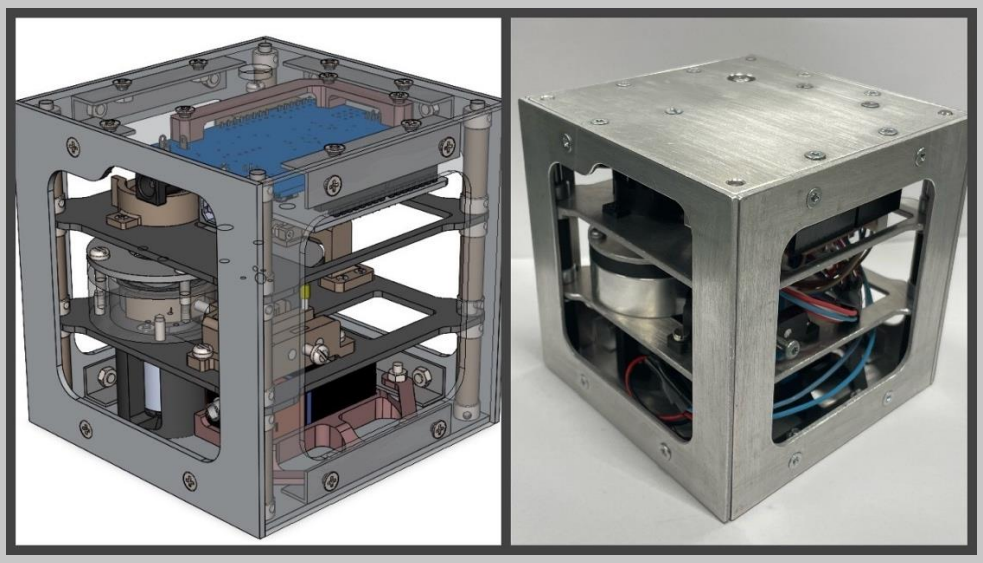

Machine Design Advanced Course Part II (MF2077)
School of Industrial Engineering and Management
Autumn 2023

ABSTRACT

CubeSats are versatile low-cost satellites used in academia and industry. Designing and implementing these CubeSats require careful consideration of mission objectives, electronic systems, communication setups and testing protocols. This project focuses on utilizing CubeSats for tribological testing to evaluate the performance of different lubricants for space applications. This project evaluates an existing design of a CubeSat tribometer which previously failed to meet its objectives and works to redesign it. A design twin of the space compatible CubeSat was manufactured and tribological testing was conducted, as a proof of concept, to evaluate frictional properties of lubricants.

Keywords: CubeSat, Friction, Lubricants, Space, Tribometer.

ACKNOWLEDGMENTS

The successful completion of this project was made possible through the invaluable guidance and support of several individuals whom we gratefully acknowledge.

First and foremost, the authors would like to thank Dr. Ian Sherrington and Dr. Sergei Glavatskih for their valuable supervision and continuous support throughout every phase of this project. Their expertise and mentorship were instrumental in shaping the outcome of the project.

We extend our heartfelt gratitude to Dr. Kjell Andersson and Dr. Akepati Bhaskar Reddy for guiding us and providing us with the opportunity to contribute to this meaningful project.

A special mention goes to Seshagopalan Thorappalli Muralidharan from the mechatronics department for his invaluable advice and help in design and procurement of the printed circuit board. His expertise significantly enhanced the quality of our work.

The authors would also like to thank Anton Boström, Lars Hässler and Thomas for their pivotal role in manufacturing the essential components crucial to the realization of the project. We would also like to thank Peter Carlsson for helping in placing the orders for all the components bought for this project.

We express our heartfelt gratitude to all mentioned above, as well as to numerous others who directly or indirectly contributed to the successful completion of this endeavour.

TABLE OF CONTENTS

LIST OF FIGURES

LIST OF TABLES

1. INTRODUCTION

CubeSats are standardized modular satellites. One unit of a CubeSat measures exactly $10\ cm\ \times 10\ cm\ \times 10\ cm$ and weighs under 1.3 kg. CubeSats emerged in the early 2000s as a cost-effective platform for educational research. Due to their design modularity allowing for easy integration of different systems and components, CubeSats have found diverse applications. This modular approach also enables easy and efficient assembly and testing of CubeSats as compared to traditional satellites. Due to their low cost and versatility, CubeSats excel in facilitating various scientific experiments and space observations.

This specific project focuses on the development and testing of a CubeSat tribometer capable of testing lubricant oils and greases in both terrestrial and space environments. A pin-on-disc tribometer and a bearing tribometer are used in the CubeSat to study the properties of lubricants in space. The data collected from this CubeSat can be used to improve the design and performance of satellites and other space technologies. The main objective of the project is to evaluate the design of an existing CubeSat tribometer which has failed to meet its objectives and redesign it. The design of the tribometers was changed significantly and many new components were used. A design twin of the space-based CubeSat was manufactured for testing in terrestrial conditions.

1.1. Project Goals

The project aims to

- Conduct a formal evaluation of the existing design and use this evaluation to inform the preparation of suitable Product Design Specification for the new CubeSat.
- Develop and evaluate concepts for design of two tribometers: pin-on-disc and bearing tribometers. These tribometers will be constructed using some of the existing CubeSat components, frame, motors, bearings etc.
- The new design must be commissioned, calibrated, tested, and operated to collect friction data.
- Redesign the theoretical space-borne system using the terrestrial system as a “design-twin” to inform its structure. (Construction of this device is not required due to the high cost it would incur.)

1.2. Scope

- Requirements, specifications, and time plan.
- Concept development, evaluation, and selection of the best concept.
- Detailed design of components, selection of parts, driving systems, and sensors.
- Manufacturing and assembling of the modular instruments.
- Basic functional tests to commission the modular instrument.

1.3. Customer Profile

The potential consumer base of a CubeSat tribometer is restricted by its cost and its extremely specific purpose. The following entities were identified as potential users of the CubeSat tribometer proposed in this project:

- Space agencies interested in testing lubricants in space.
- Research institutions.
- Aerospace industry.
- Start-ups in the space industry.

- Commercial lubricant manufacturers.
- Universities with an interest in space tribology.

The customer requirements for the CubeSat can be divided into four categories: Spatial, functional, cost and ecological.

Spatial requirements:

- Miniaturization: The tribometers must fit within the 10 cm x 10 cm x 10 cm CubeSat form factor.
- This space must house all the control systems and functional elements of the tribometers.

Functional requirements:

- The tribometers must be able to operate in both terrestrial and space environments.
- The tribometers must be versatile enough to be capable of testing a variety of lubricants.
- The tribometers must be able to measure friction and wear.
- The tribometers must be able to operate for at least 1 year in space.
- The system must be able to operate autonomously and transmit data back to earth.
- The tribometer should be able to accurately measure friction torque under variable loads and operating speeds.
- The tribometer must consume minimal power due to limited power resources.
- The tribometer must withstand the harsh conditions to which it is deployed.
- The tribometer design must have hardware redundancy.

Cost requirements:

- The tribometers must use off-the-shelf components as much as possible to minimize cost.
- Scope of repairability must be ensured.

Ecological requirements:

- The materials and the manufacturing process used must have minimum impact on the environment.
- The CubeSat tribometer must use renewable energy sources.
- Repurposing of existing components to minimize carbon footprint.

1.4.Project Charter

A project charter is a contract between the sponsor and the project manager, signed by both at the start of the project. It is used throughout the product life cycle and includes the project's goals, scope, objectives, specifications, approach, timeline, milestones, deliverables, and identified risks. The project charter is a critical document that provides a clear understanding of the project's purpose, goals, and objectives, and serves as a reference for the project team and stakeholders throughout the project. It helps to ensure that the project stays on track and that everyone involved in the project is working towards the same objectives. See *Appendix 1*.

1.5.Work Breakdown Structure

The Work Breakdown Structure (WBS) is a hierarchical decomposition of the work to be executed by the project team to achieve project objectives and deliverables [1]. WBS breaks down the project into individual components, making it more manageable and less overwhelming. WBS has a levelled structure and provides a roadmap for different levels of

teams working under individual components. The project is broken down into different subdivisions like initiation, planning, execution, control, and closure as shown in Fig.1. The initiation process includes project charter, project goals and deliverables, and literature survey. The planning phase is subdivided into Gantt chart, communication, and project plan. The execution process involves status updates to stakeholders, execution, documentation, and task management. The control process includes managing changes, tracking tasks and delays, and managing resources. The closure process involves lessons learned, final presentation, handover of documents and prototype. See *Appendix 2.*

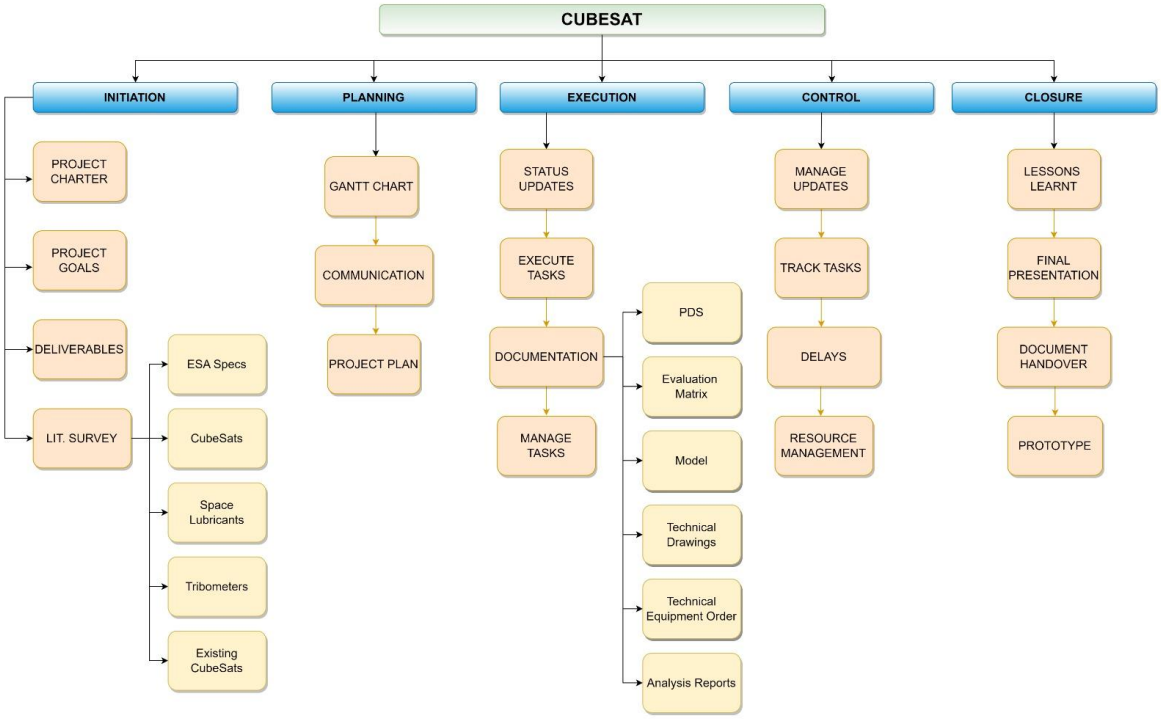

Figure 1: Work Breakdown Structure

1.6.Gantt Chart

The project schedule is represented graphically using a Gantt chart. It is used to display all the activities based in the WBS. For this project, the Gantt chart is divided into four phases and work has been scheduled for each week. The Gantt chart is used to track progress against the project timeline and to identify potential delays or risks. Phase 1 encompasses start-up meetings, literature survey, requirement analysis, WBS and product design specifications. In Phase 2, Concept generation, evaluation and selection will be carried out. In phase 3, design and simulation of the selected concept is performed, and the manufacturing drawings will be prepared. Phase 4 encompasses manufacturing, assembly, testing and implementation of the prototype. See *Appendix 3.*

1.7.Product Design Specification

The product design specification (PDS) defines what the product should provide and is based on the customer's requirements. It serves as a reference for the design objectives and forms the basis for design. The PDS is subject to change, but it becomes firm at the production or manufacturing stage. In this project, the properties, and parameters of the PDS were determined based on information from literature studies and ESA specifications. The PDS is presented as

short and concise information for each property, and the document is tracked for edits. As the document is a structured statement of properties, it is presented as a short and concise detail of each property, and document tracking showing edits of the said properties. See *Appendix 4.*

1.8.Eco-Design

Eco-design integrates the sustainability concepts into the design without compromising on the quality, functionality, and performance [2].

The CubeSat was designed, and material selection was done using ANSYS Granta edupack keeping in mind that there is minimal effect on the environment. Additionally, in the terrestrial design-twin which was manufactured, all the 3D printed parts were made through fused deposition modelling of Polylactic Acid (PLA). PLA is a biodegradable and recyclable plastic. Furthermore, all critical components were 3D printed to check for conformity between the parts. By doing so, it was possible to make necessary design changes before actual milling of metal parts. This made sure to prevent waste. Some of the parts used in the CubeSat were obtained from the previous model of the CubeSat. This included motors, Arduino Uno, jumper cables, and the amplifier for load cell. The rest of the components were ordered from Swedish online markets which sourced these components from local vendors with minimal pollution caused by logistics. All machined parts were manufactured inhouse at KTH using Aluminium alloy and can be recycled easily.

The CubeSat was designed to burn up on re-entry, thereby not causing it become space junk.

2. LITERATURE REVIEW

2.1. CubeSat

CubeSats, also known as nanosatellites, have emerged as a disruptive technology in the field of space exploration and research. They are nanosatellites of the dimensions 10x10x10cm with a maximum mass of 1.3 kg, which can house various tech for experimentation across broad areas of science [3]. The concept of CubeSat was conceived at California Polytechnic State University and Stanford University in the late 1990's keeping cost reduction, educational opportunities, and rapid technology advancements in mind. The CubeSat was developed keeping modularity in mind, allowing for combination with other CubeSats that support the same main purpose. A single CubeSat is termed 1U, combined with another CubeSat is called 2U, and three combined together is called 3U.

The CubeSat has a diverse range of applications across areas including Earth observation, communication, scientific research, technology demonstration, and education. The major advantages of these nanosatellites include their low cost, rapid development cycles, and their ability to support a variety of missions. It is also augmented with challenges related to limited payload capacity, power constraints, communication limitations, and orbital decay. The CubeSat that our team intends to design must be able to support tribological testing in the harsh environment of space to understand and analyse the working of certain novel lubricants and to expand the data pool regarding how to apply the right tribological practices to ensure the smooth operation of space missions.

2.2. Tribology

Tribology in space applications is a topic still under high scrutiny due to the issues with the harsh environment of space and the harsh conditions components have to withstand during initial launch into space. Issues related to cold welding and seizing is a potent risk to certain

parts of a system, leading to the mission failing. Lubrication of moving components in space is a very tricky area of tribological contacts due to the harsh nature of space, with high range of operating temperatures (-40, +80) ºC and vacuum conditions with pressure 10e-6. Normal lubricants used on earth's surface cannot be applied, and only lubricants with the following properties are considered - High viscosity index, low pour point, exceptionally low vapour pressure and low volatility. Some examples of such lubricants are mineral oils, Perflouropolyalkylethers (PFPAE), polyesters and multiply-alkylated cyclopentanes [4].

Greases are also a good option for lubrication. Solid lubricants can also be used to lubricate several components in a system used in space. The following types are used in space applications – soft metal films, lamellar solids, polymers and other low shear strength materials. There are many methods to add this solid lubricant to the system, most common way is to apply it to metal surface as film or coating. Solid lubricant powder can be incorporated into a liquid binder system. The retainer in rolling element bearings can be made of solid lubricant which keeps adding material for lubrication purposes as it further wears out. There are many advantages and disadvantages to weigh against liquid and solid lubrication, the key point being that solid lubricant cannot be tested in air for use in vacuum i.e., on Earth's surface [5].

2.3. Critical Design Review

The Critical Design Review (CDR) is a crucial milestone in the engineering design process, aimed at ensuring the feasibility, functionality, and safety of a project and has a vital role in assessing the maturity of a design before proceeding to the manufacturing and implementation stages. The CDR should represent a complete and comprehensive presentation of the entire design. CDRs are conducted to demonstrate that the detailed design is complete and ready to proceed with coding, fabrication, assembly and integration efforts. The key elements that are usually evaluated during the design process are design completeness, system integration, technical performance, risk assessment, and compliance with requirements and standards.

The process of conducting a CDR involves various stages and activities such as preparation, documentation, presentations, reviews, and decision-making. It also discusses the roles and responsibilities of different stakeholders, such as project managers, engineers, subject matter experts, and external reviewers. The iterative nature of the CDR creates a feedback loop that helps enhance the design and create mitigation strategies for future issues. The design review process helps identify design flaws, technical challenges, and potential risks at an early stage, leading to improved project outcomes, cost savings, and schedule adherence. It is important to highlight some of the pre-requisites to ensure a robust and holistic CDR. Some of them being:

- Successful Completion of PDR
- Preliminary CDR agenda
- Success Criteria
- Updated project documents – Charter, PDS, WBS,
- Build-to specifications of hardware and software items
- Fabrication, assembly, integration & test plan procedures
- Operational limits and constraints
- Updated reliability, and risk assessments and mitigation
- Verification and validation plan
- Updated cost and schedule data
- Software design documents (Interface design)
- System safety analysis and verifications

2.4. Design Evaluation

The evaluation of design using predefined rubrics to understand the robustness of a system is pertinent to select the best possible concept before implementation of the same to create a tangible product. Through research we have understood that there are two types of evaluation methods, which are discursive evaluation methods and intuitive evaluation methods. Discursive evaluation methods rely on arguments and reasoning to decide on design whereas intuitive evaluation methods use intuition and feel when deciding on a design/product. Focus shall be placed on discursive evaluation methods as it works based on quantifiable engineering data [6]. The overarching theme of evaluation activities can be categorized into three parts:

- Define Goals: Describe and define target directions of a good solution in a concrete and solution-independent way.
- Collect Information: Generate the alternative solutions and predict the solutions' behaviour, i.e., which properties they will possess under given circumstances.
- Evaluate Information: Determine an alternative's value for how well it solves the given design task.

Permeating from this we can clearly define the phases of evaluation for Discursive evaluation methods as:

- Establish criteria, including their scoring scales,
- Establish weighting factors per criterion,
- Determine the decision rule that will be followed,
- Determine the scores per criterion and total scores,
- Examine the (sub-) scores of the alternatives,
- Decide on one alternative (based on a decision rule).

2.5. Friction Models

Ball bearing involve complex lubrication conditions, where high loads are found in extremely low scale areas of contacts between the balls and the raceway. Running in period, speed of rotations, viscosity of lubricants, base oil of said lubricants, materials of the ball and raceway are some of the many important rubrics one must understand to be able to model approximate models to calculate the friction moment in the system. Several models were studied such as the SKF model, the Hysteresis model, and the Palmgren model. The team ran calculations based on the inertia and power loss of the system, but this model was only applicable for dry contacts [7]. The SKF model was chosen as the most appropriate model to use as not only was the bearing manufactured by SKF; they also provided a tool that would output the frictional moment values of rolling and sliding based on varied input parameters. This tool is greatly helpful in crosschecking the validity of our written codes and adds another layer of robustness to our system. The Hysteresis model looks into deeper physical phenomena of hysteresis between the two raceways and balls, and also includes the pivoting movement and inertia of the ball in its friction calculations [8]. This model was used to compare the results of the SKF model to understand if it holds true when placed against different lines of thinking.

2.6. Sensors

The CubeSat design and usage required the integration of several different sensors to be able to retrieve accurate and usable values. These sensors included load cells, pressure sensors, temperature sensors and optical encoders. The load cell was used to measure the frictional force on the pin and disc system and the pressure sensor measured the applied radial force on the ball

bearing, these values being comparatively low. To ensure the load cell and pressure sensor was calibrated at the right working range, calibration methods were researched and implemented. These calibration methods included using known weights to retrieve calibration factors for the load cell and pressure sensor, which was calculated by creating a linear model of best fit and retrieving the same factor by progressively increasing the weights with the same step. The optical encoder required calibration to ensure the smooth measurement of speed of the bearing, hence appropriate time averaged methods were researched, with the Resor method being identified as the most appropriate [9].

2.7. Contacts in Space

2.7.a. Reaction Wheels

Reaction wheels are pivotal components in satellite attitude control systems, designed to manage and stabilize a spacecraft's orientation in space. These devices exploit the conservation of angular momentum, utilizing spinning wheels mounted along different axes to induce controlled rotations. By adjusting the speed and direction of these wheels, a spacecraft can finely tune its orientation without the need for traditional methods such as thrusters or external forces. Typically arranged along three orthogonal axes (X, Y, and Z), reaction wheels enable three-axis control, ensuring precise pointing and alignment. They operate based on the principle that changing the angular momentum of the wheels induces an equal and opposite rotation in the spacecraft, adhering to the conservation of angular momentum. Redundancy is often built into satellite systems with multiple reaction wheels to enhance reliability, and momentum unloading mechanisms, such as magnetic torquers or thrusters, prevent wheel saturation over time. Reaction wheels offer an efficient and fuel-conserving means of controlling satellite orientation, making them essential for missions with limited fuel resources or extended operational lifetimes in space.

Figure 2: Momentum wheels used in space missions.

2.7.b. Pin Contact for Unfurling of Antennas

Standoff pins were used in the partially compromised Galileo mission which involved its usage in the unfurling of its high gain antenna as it approached its target destination close to

the atmosphere of the planet Jupiter [10]. High vibrations during the transport and storage phase of the mission while on Earth had led to irreversible wear in this particular mechanism, which lead to compromised unfurling of the antenna as the standoff pin had got jammed in place. A small component such as this is also extremely critical for the success of any mission, as a single component failure leads to critical failure of the system due to the lack of redundancy in these mechanisms. Thus, an expansive study of the response of such contacts at varied conditions must be studied to understand how to mitigate unwanted responses of the system.

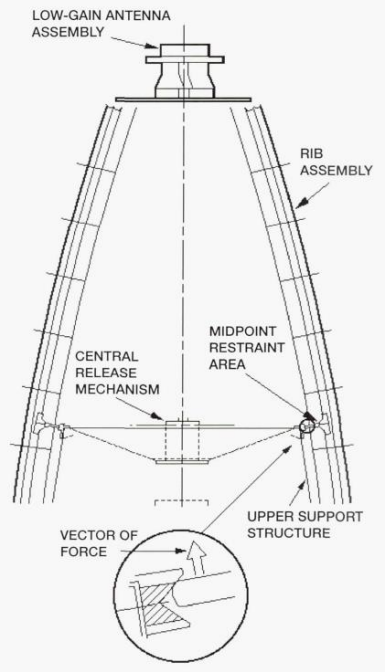

Figure 3: Pin-Socket mechanism for unfurling of communication antenna.

2.8. Control System

Although the CubeSat is a compact system of just 10*10*10cm dimensioning, it involves the working of several components such as motors and its controller, sensors such as load cells, pressure sensors, temperature sensors and optical encoders. These components need to be integrated with a robust microcontroller that allows for accurate sensor readouts and controlled motor operation. Based on previous experience, competency and level of user friendliness, the Arduino Uno was chosen and integrated into the system.

3. DESIGN EVALUATION AND REVIEW

3.1. Introduction

The Critical Design Review (CDR) is a pivotal stage in the engineering design process where a thorough assessment is conducted to evaluate the maturity, feasibility, and functionality of a project's design. It serves as a critical milestone before moving forward with manufacturing and implementation. During the CDR, key elements such as design completeness, system integration, technical performance, risk assessment, and compliance with requirements and standards are evaluated. The significance of the CDR lies in its ability to identify design flaws, technical challenges, and potential risks early on, leading to improved project outcomes, cost savings, and schedule adherence. It ensures that the design aligns with project objectives, stakeholder expectations, and regulatory requirements. Here, we perform CDR on the existing CubeSat model from 2022.

3.2. Changes Made Since CDR

3.2.a. Changes to Project Plan

The changes made to project plan includes adding the requirement of mandatorily placing the control modules (Includes controllers for actuators and motors to control and monitor CubeSat) inside the $10 \times 10 \times 10\ cm$ dimensions of the CubeSat, with none of the same appearing outside the CubeSat, to fully realize the optimization of space in the CubeSat. The load applicators used in the terrestrial CubeSat will consist of spring mechanism or fine screw loading to provide a variable load. The space compatible twin of this CubeSat will involve variable loading using servo motors to vary the force applied. For an added dimension of safety, there will be a pin that will separate CubeSat power system from the rest of the circuitry, which is removed when CubeSat is placed in dispenser before launch to activate the entire system. In line with this added dimension of safety of robustness, additional tests such as vibrational test, shock test and FlatSat test will be conducted.

3.2.b. Changes to Tribometer Configurations

The Tribometers used are Pin-on-disc and ball bearing configurations to test novel lubricants. The major areas of focus when it comes to improving the manufacturability and configuration of these tribometers was handling misalignment issues, which can be addressed by using two pins placed diametrically opposite to each other to create a dynamically loaded system that mitigates any unwanted wobble. The space optimization of the CubeSat can be further improved by creating a one motor shaft system i.e., placing two tribometers on a shaft connected to one motor. Changes are made in sensor placement to account for space optimization and mounting issues. Alternatives for various loading mechanism were accounted for based on requirement, which included loading using fine screws and spring loading for fixed loading and variable loading using servo motors. The measurement of forces is taken up by the introduction of load cells to measure force applied due to deflection.

3.2.c. Changes to Electronics

The position of controller module and wiring for all the electronics and motors in the CubeSat will be fit inside the CubeSat completely as a requirement. There must be no part that juts out of the CubeSat system i.e., the electronic system must confine to space optimization requirement of CubeSat design. The specifications include Arduino Uno rev3 used as

controller, motor driver used being L298N, HX711 load cell amplifier and Thermistor NTC-10K temperature system being integrated into the system.

3.2.d. Analysis of Results

The previous CubeSat frame had several L brackets that mated the different parts in place and these L brackets had nuts and bolts jutting out of the system, which cause major instability in the entire system. Vibrations caused due to launch processes and other activities will be enhanced due to this bulkiness, leading to probability of damage and failure increasing. The jutting of certain parts does not comply to the strict space requirements of the Dispenser system for launching. The integration of frame and plates does not provide enough space inside to allow for all CubeSat levels and components to fit inside the CubeSat, hence failing an essential requirement of efficient space optimization. The intrinsic and important property of modularity is not realized in the design, which reflects the need for smoother and more streamlined design of frame and structure.

3.2.e. Manufacturing and Assembly

The frame and plates were cut using Jet cutting and the material thickness used was 2mm. Due to variations in dimensioning from original drawings due to manufacturing issues, after-processing was required. The CubeSat was erected level by level individually, while keeping in mind certain constraints and sensitivities that were pertinent to each individual floor. Certain floors were preassembled to prevent damage to components such as motor shaft. Each level was fasted to the frame and calibrated to specific heights using shaft collars. The Arduino level did not fit inside the CubeSat frame due to interferences with wiring and other levels, hence was placed outside the CubeSat Frame.

3.2.f. Design Integrity

The CubeSat frame is held together using L brackets with bolts and nuts jutting out that affects the overall stability of the system, which can lead to critical issues. The jutting of certain components is in direct conflict to the space requirements to be loaded into a Dispenser. The CubeSat Frame must envelope all levels and components, which is not the case here due as the Arduino level had to be placed on top of the frame due to the space inside not being optimised to the fullest.

3.2.g. Design Review

The project aimed to conduct experiments to determine the frictional properties of lubricants in space environment. The speed of the motors was controlled using a transistor and Arduino board, and a tachometer was used to measure the speed. The ball bearing and pin-on-disc setups rotated at 80 rpm and 30 rpm, respectively.

To measure the applied load and friction force, two load cells were used in each setup. These load cells were connected to amplifiers, and the Arduino collected data from the experiment. Calibration of the load cells was performed using a known weight, and then they were mounted into the CubeSat. Mounting the load cells on the pin-on-disc tribometer and ball bearing tribometer enabled precise measurement of the friction force.

However, there were challenges in the experimental setup. The load cell in the pin-on-disc setup was attached to the load cell holder using tape, which increased the thickness and caused a misalignment between the load cell plunger and the pin. This misalignment affected the measurement of the applied load on the pin-on-disc tribometer.

In the ball bearing tribometer, the load cell attached to the loading screw was broken due to overload. Additionally, the flexible arm shell had alignment issues caused by rough and uneven

inner surfaces. This misalignment resulted in an incorrect attachment of the load cell plunger to the flexible arm, leading to random force distribution during load application. Despite collecting friction force data, the applied load could not be accurately measured, even after changing the load cell.

Overall, the prototype of existing project successfully controlled the speeds and measured friction force, but there were limitations in accurately collecting the applied load. These challenges needed to be addressed to ensure the robustness of long-term tests, as the final application was intended for continuous operation in space for one year.

4. CONCEPT

Considering the outcomes of the thorough Critical design review outlined earlier, diverse concepts were developed. The CubeSat tribometer setup explored numerous approaches for creating, transmitting, and applying loads, alongside diverse sensor arrays and control mechanisms. This allowed for a broad spectrum of combinations that could meet project requirements. Nevertheless, factors such as cost, weight, and the stakeholders' preference to salvage parts from the current model limited the scope of generated concepts. The morphological chart in the following section illustrates some of the combinations incorporated in these concepts.

1.1. Concept Generation

The morphological chart is an effctive tool used to explore and generate a wide range of possible solutions for the design concepts. It has been a great tool that assists in finding innovative and optimal designs. The morphological chart shown in Fig. 4 and 5 shows morphological chart for pin-on-disc and bearing tribometer containing different concepts of the CubeSat tribometer. Each coloumn represents different solutions for the requirement stated in the respective rows. Each coloured line represents a combination of these solutions which helps to form the design.

Contact Type	**Pin-on-disc**					
Create Load	Piezoelectric	Loading Screw	Servo Motor	Pneumatic	Hydraulic	
Transmit Force	Direct	Spring	Rack-pinion	Chain		
Apply Load	Single actuator	Double actuator				
Create Torque	BDC motor	BLDC Motor				
Measure Applied Load	Load cell	Strain Gauges	Capacitive sensor	Inductive Sensors		
Measure Friction Force	Load cell	Strain Gauges	Capacitive sensor	Inductive Sensors		
Controller	Arduino Uno	Raspberry Pi				

Figure 4: Morphological Chart for pin-on-disc tribometer.

Contact Type	**Bearing**					
Create Load	Piezoelectric	Loading Screw	Servo Motor	Pneumatic	Hydraulic	
Transmit Force	Direct	Spring	Rack-pinion	Chain		
Apply Load	Single actuator	Double actuator				
Create Torque	BDC motor	BLDC Motor				
Measure Applied Load	Load cell	Strain Gauges	Capacitive sensor	Inductive Sensors		
Measure Friction Force	Load cell	Strain Gauges	Capacitive sensor	Inductive Sensors		
Controller	Arduino Uno	Raspberry Pi				

Figure 5: Morphological Chart for bearing tribometer.

1.2. Concepts

Using the morphological charts explained in the previous section, different concepts were generated for the pin-on-disc and the bearing tribometers. These concepts are described in the following sections.

1.2.1. Pin-on-disc Tribometer Concepts

Concept 1 for the pin-on-disc tribometer is shown in Fig. 6, where the motor is connected to a main shaft. The disc is mounted on the main shaft. The bearing inner ring is connected to a bevel gear assembly which transmits motion from the main shaft. The load is created using either a servo motor or a loading screw and is transmitted to both the pin-on-disc tribometer and the bearing tribometer using a rack and pinion assembly. The applied load is measured using load cells and the frictional force is measured using strain gauges.

Concept 2 for the pin-on-disc tribometer is shown in Fig. 7, where the disc is rotated using a motor. The load is generated using a loading screw at the centre of the loading arm. The loading arm is cut horizontally for the placement of two load cells to measure the applied force. Two pins apply load on the rotating disc at diametrically opposite points. The frictional force is measured using strain gauges. The design also includes grooves on the loading arm for running the cables for connecting the sensors. The loading arm is meant to be 3-D printed.

Concept 3 for the pin-on-disc tribometer is shown in Fig. 8 and is very similar to the previous concept. Here, the load is applied closer to the two pins and a single load cell is used to measure the applied load. The frictional force is measured using another load cell placed on the side of the loading arm. The loading arm and the load cell attachments are meant to be 3-D printed.

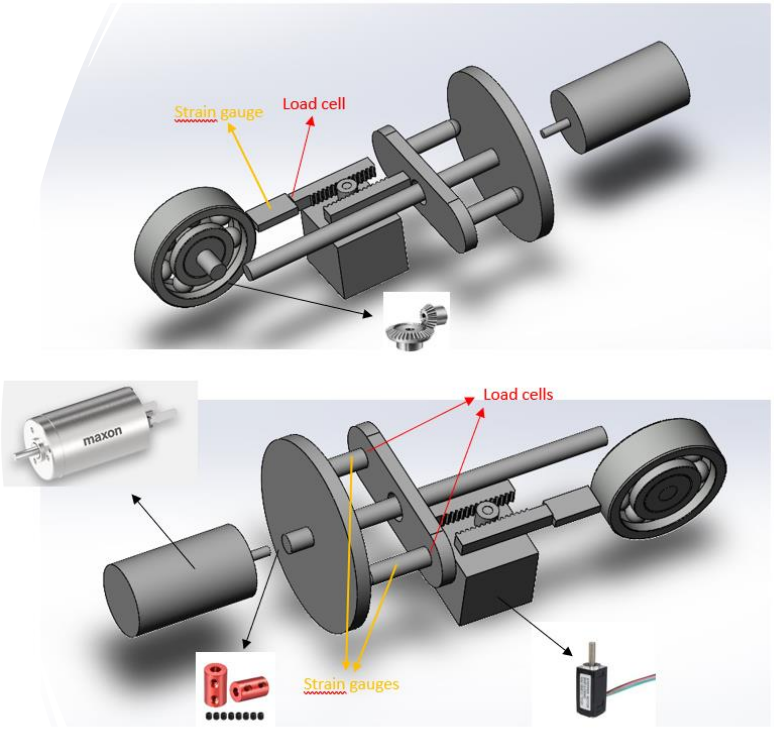

Figure 6: CAD illustration of concept 1 of pin-on-disc tribometer

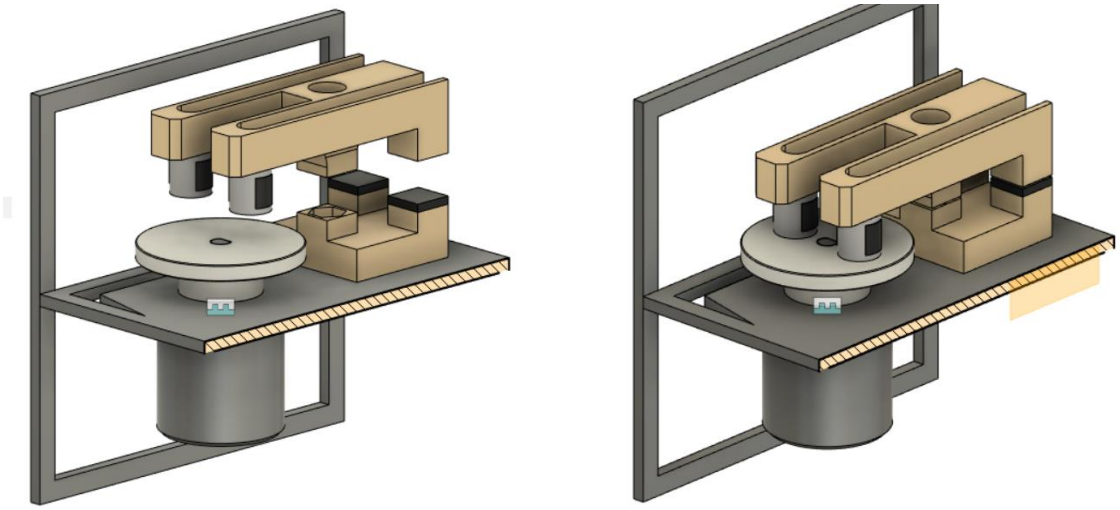

Figure 7: CAD illustration of concept 2 of pin-on-disc tribometer

Concept 4 for the pin-on-disc tribometer is shown in Fig. 9, where the disc is rotated using a motor. The load is generated using a screw loading mechanism. The load cell holder and the pin holder are integrated into the same system to optimize space. The frictional force is measured using a load cell.

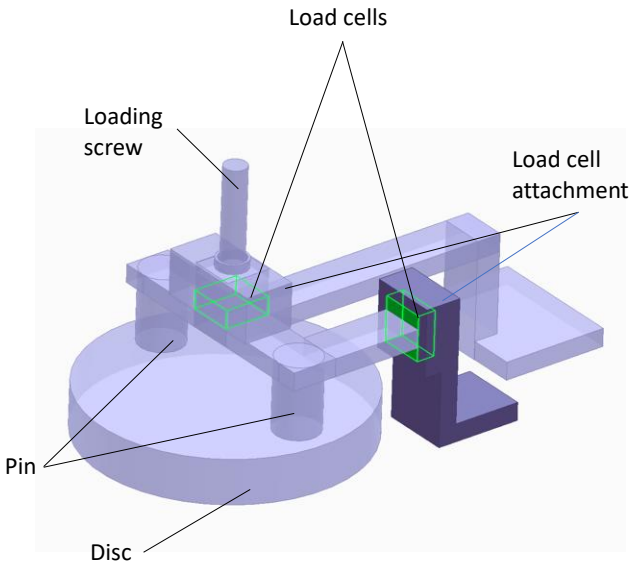

Figure 8: CAD illustration of concept 3 of pin-on-disc tribometer

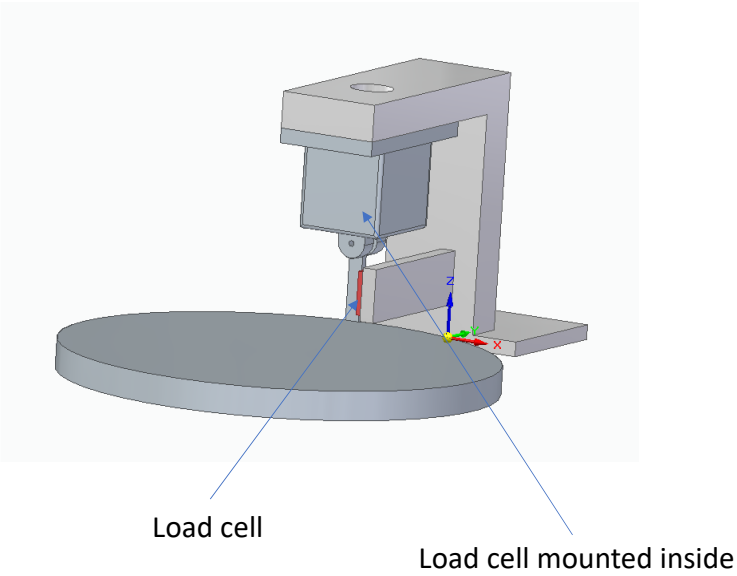

Figure 9: CAD illustration of concept 4 of pin-on-disc tribometer

Concept 5 for the pin-on-disc tribometer is shown in Fig. 10, where the disc is mounted on a motor. The applied force is generated using a servo motor and transmitted using springs. Here the load is applied diametrically using a dual actuator setup. The applied load is measured using a load cell mounted near the springs. The frictional force is measured using strain gauges placed on the loading arm.

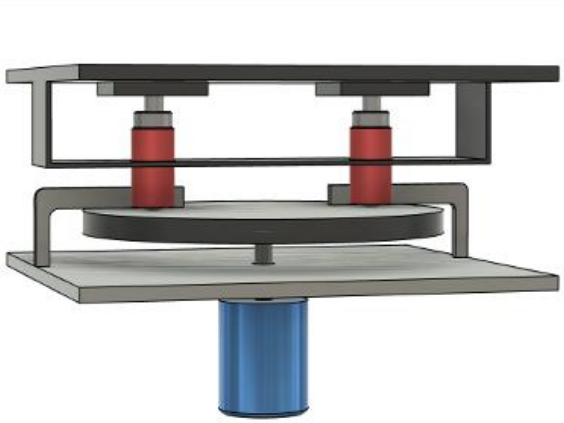

Figure 10: Illustration of concept 5 of pin-on-disc tribometer

1.2.2. Bearing Tribometer Concepts

Concept 1 for the bearing tribometer is shown in Fig. 11, where a motor drives the main shaft. This shaft rotates the inner ring of the bearing and has a bevel gear assembly at the other end which drives a disc. The applied load is transmitted through a spring to the loading mechanism which transmits force onto the outer ring of the through a flexible arm. A load cell is used to measure the applied load and the frictional force is measured using strain gauges.

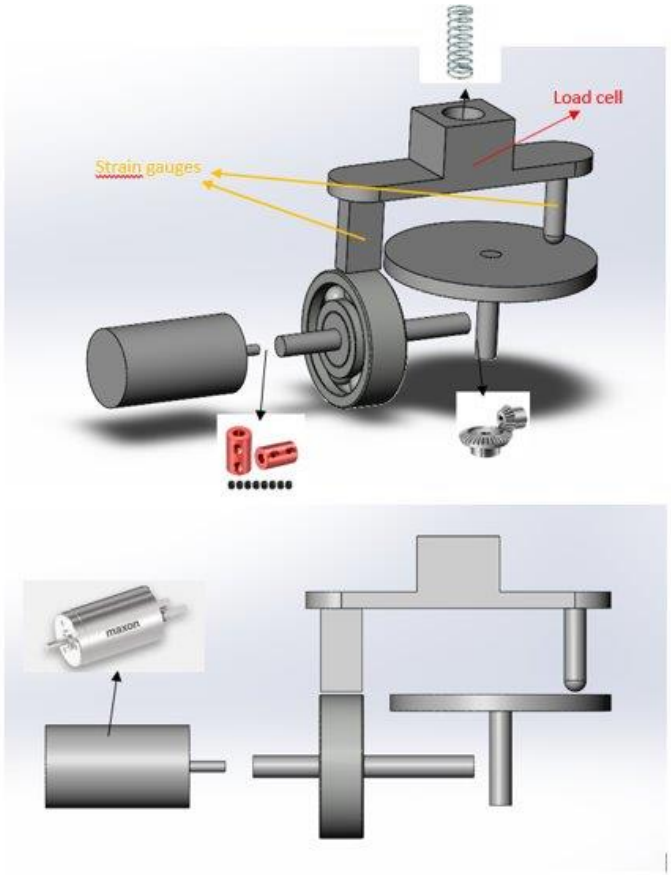

Figure 11: CAD illustration of concept 1 of bearing tribometer

Concept 2 for the bearing tribometer is shown in Fig. 12, where the bearing inner ring is driven by a motor. The applied load is generated using a loading screw and is transmitted through a flexible arm. A load cell placed before the flexible arm measures the applied load. The frictional force is measured using a load cell mounted on a load cell attachment. The whole setup is meant to be 3-D printed.

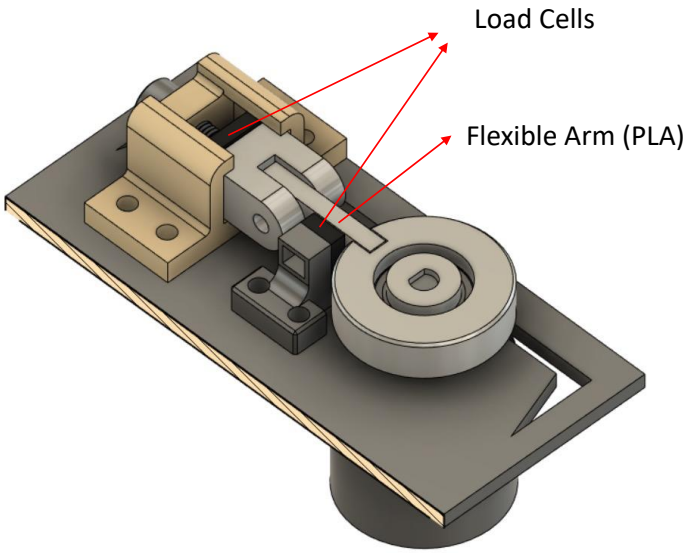

Figure 12: CAD illustration of concept 2 of bearing tribometer

Concept 3 for the bearing tribometer is shown in Fig. 13, where a motor drives the inner ring of the bearing. A prismatic load cell holder, to be manufactured using 3-D printing, holds the load cell which measures the applied load. The load is generated using a loading screw. The friction force is measured using a strain gauge.

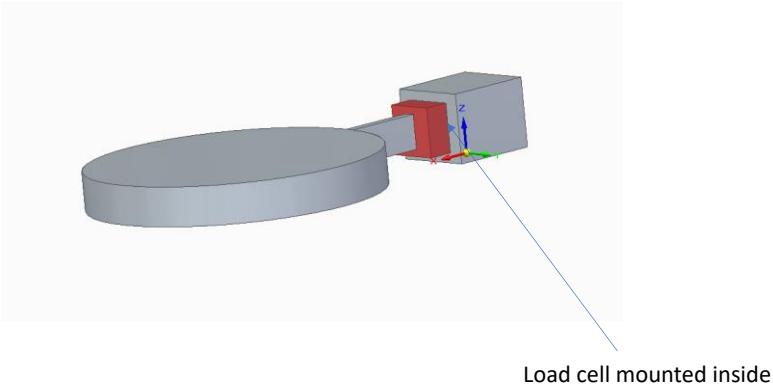

Figure 13: CAD illustration of concept 3 of bearing tribometer

Concept 4 for the bearing tribometer is shown in Fig. 14, where a motor drives the inner ring of a bearing. The applied load is generated using a servo motor, which transmits the force through a loading screw on to a spring. The load cell attached at one end of the spring measures the applied force which is applied at the outer ring of the bearing through a flexible arm. A strain gauge placed on the flexible arm measures the frictional force.

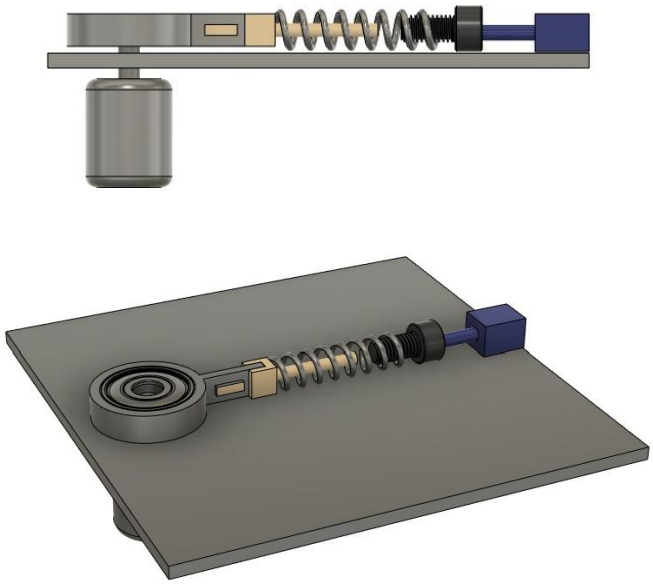

Figure 14: CAD illustration of concept 4 of bearing tribometer

1.3. Concept Evaluation

The concepts generated using the morphological chart are evaluated using the following criteria explained in Table 1. These criteria are used further in weighted evaluation matrix and Pugh evaluation matrix.

Table 1: Criteria for evaluation of concepts

Criteria	**Explanation**
Mass	Total mass excluding the frame – Lower the better
Manufacturability	Ease and efficiency of manufacturing – cost effective
Ease of Assembly	Modular, design for accessibility, self-aligning and locating
Sensor Placement	Direct measurement of forces
Cost	Cost of all components used – Lower the better
Compactness	Use lesser space – Lower the better
Frictional contact	Number of frictional contacts – Higher the better
Redundancy	Functional and component redundancy
Power	Power consumption – Lower the better
Robustness	Sensitivity to noise – Lower the better

1.3.1. Pugh Evaluation Matrix

Here, a Pugh evaluation matrix is used to quickly sift through different design concepts and improve upon these concepts. Here, the previous design of the CubeSat tribometer is considered as the reference and is given a score of 0. The new deisgn concepts are evaluated

against this reference for each criteria. If the new design is better, a score of +1 is given, where as a worse design is given a score of -1 for that criteria. If the reference is same in comparison to the new concept, the score given is 0. The sum of all scores for the concept gives the total score of the concept. Tables 2 and 3 shows the Pugh evaluation matrices for the pin-on-disc and bearing tribometer respectively.

Table 2: Pugh evaluation matrix for concepts of the pin-on-disc tribometer.

Pugh Evaluation Matrix – Pin-on-disc Tribometer						
Parameters	**Reference**	**Concept 1**	**Concept 2**	**Concept 3**	**Concept 4**	**Concept 5**
Mass	0	-1	1	1	1	-1
Manufacturability	0	0	1	1	1	1
Ease of Assembly	0	-1	1	0	1	-1
Sensor Placement	0	-1	0	0	0	-1
Cost	0	-1	1	1	0	0
Compactness	0	0	0	1	1	-1
Frictional Contact	0	1	1	1	1	1
Redundancy	0	-1	0	0	0	0
Power	0	0	0	0	0	-1
Robustness	0	0	1	0	0	1
Total Score	0	-4	6	5	5	-3

Table 3: Pugh evaluation matrix for concepts of the bearing tribometer.

Pugh Evaluation Matrix – Bearing Tribometer					
Parameters	**Reference**	**Concept 1**	**Concept 2**	**Concept 3**	**Concept 4**
Mass	0	0	1	1	-1
Manufacturability	0	1	1	1	1
Ease of Assembly	0	1	0	0	1
Sensor Placement	0	0	0	0	0
Cost	0	0	1	1	1
Compactness	0	-1	0	0	0
Frictional Contact	0	0	0	0	0
Redundancy	0	-1	0	0	0
Power	0	1	0	0	-1
Robustness	0	1	1	1	1

Total Score	0	2	4	4	2

1.3.2. Weighted Evaluation Matrix

To evaluate the concepts, a weighted evaluation matrix was used. Each concept was given a score between 1 to 5 for all the criteria based on their perfoemance in that criteria. Each criteria is also given a weight between 1 to 5 to show the importance of the criteria. Power consumption, mass, compactness and robustness are given very high weights because of their importance in space applications. The total score of a concept is calculated and the concept with the highest score is selected. Tables 4 and 5 shows the weighted evaluation matrices for the pin-on-disc and bearing tribometer respectively.

Table 4: Weighted evaluation matrix for concepts of the pin-on-disc tribometer.

Weighted Evaluation Matrix – Pin-on-disc Tribometer						
Parameters	**Weights**	**Concept 1**	**Concept 2**	**Concept 3**	**Concept 4**	**Concept 5**
Mass	5	3	4	4	4	3
Manufacturability	4	3	5	4	3	4
Ease of Assembly	4	1	4	3	4	3
Sensor Placement	3	3	3	4	4	3
Cost	4	3	3	3	3	3
Compactness	5	1	3	3	4	2
Frictional Contact	3	3	5	5	3	5
Redundancy	4	1	5	3	3	5
Power	5	2	3	4	4	1
Robustness	5	1	3	3	3	3
Total Score	0	85	157	149	148	129

Table 5: Weighted evaluation matrix for concepts of the bearing tribometer.

Weighted Evaluation Matrix – Bearing Tribometer					
Parameters	**Weights**	**Concept 1**	**Concept 2**	**Concept 3**	**Concept 4**
Mass	5	4	3	3	3
Manufacturability	4	4	4	2	4
Ease of Assembly	4	3	3	3	3
Sensor Placement	3	3	5	5	3
Cost	4	3	3	2	3
Compactness	5	2	4	4	4
Frictional Contact	3	3	3	3	3

Redundancy	4	1	3	3	3
Power	5	4	3	3	2
Robustness	5	3	3	3	3
Total Score	0	127	141	129	130

1.4. Concept Selection

Using the results from the Pugh evaluation matrix and weighted evaluation matrixdiscussed in the previous sections, a concept was chosen from pin-on-disc tribometer and bearing tribometer concepts. For the pin-on-disc tribometer, the Pughs evaluation matrix gives the highest score to the concept two. For the bearing tribometer, both concept 2 and 3 are ranked the same by the Pugh evaluation matrix. So, we use the weighted evaluation matrix to select the bearing tribometer concept and concept 2 was selected because of the high score. Fig. 15 shows the selected concepts.

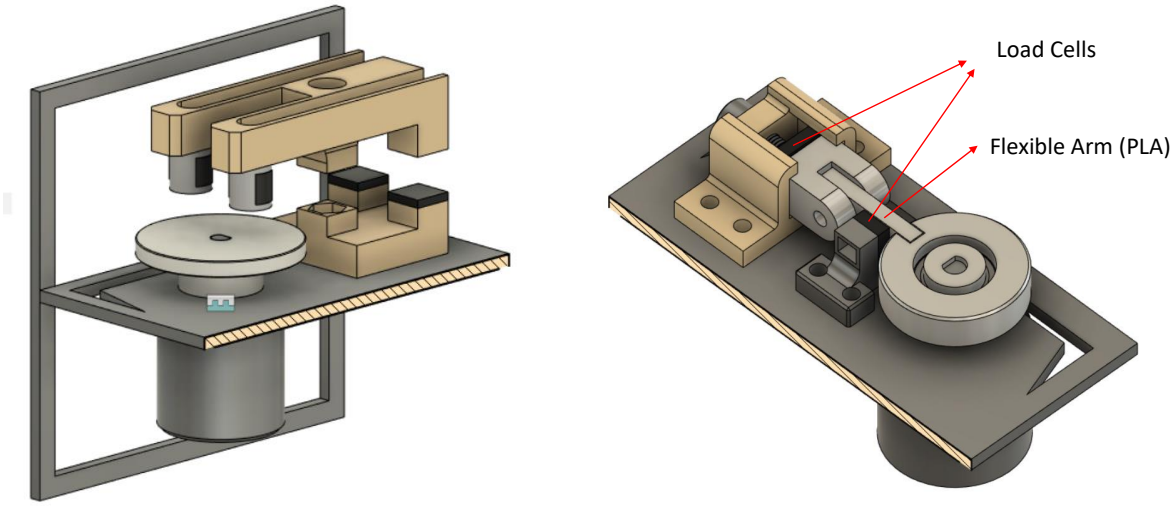

Figure 15: CAD illustration of selected concepts for the pin-on-disc and bearing tribometer.

5. CALCULATIONS AND THEORY

Friction is a physical phenomenon that occurs at scales of up to several nano meters. When two surfaces mate and slide or roll on each other, a force is developed that opposes this motion of the bodies, leading to power losses in the entire system. These power losses are heavily dependent on individual properties of each surface, such as the surface roughness, the elastic modulus of the material and their surface energy. Friction forces are sensitive to the inputs related to the speed with which the surfaces interact with each other and the force that is applied directly by one body on the other. If we magnify and view the working of the surface interactions between the bodies, we see that the surface of the body c be discretized into several crests and troughs, i.e. the surface is not flat. These rises and dips on the surface creates an uneven topology, which is the base cause of friction in systems. These rises and dips are called asperities, and the relative scale of these asperities between the contacting bodies creates the basis of a unit opposing friction force. This can be explained by considering the interaction of a unit asperity of the first body on a unit asperity of the second body. The area of contact,

presence of lubrication, speed of movement and the applied perpendicular force creates an opposing force between these asperities. The assimilation of these individual opposing forces over the length of the surfaces gives us the total Friction force between the two bodies. The coefficient of friction μ describes the amount of friction force that will be generated between the bodies and is an empirical dimensionless value calculated by dividing the total friction force by the total applied force. This coefficient is extremely critical to understand the physical working of systems and the expected percentage of losses, data which is required to understand if a system is a viable to be accepted. Friction forces must always be minimized, this is done so by increasing the quality of the surface finish on the bodies such as to reduce the interaction of asperities. Lubrication involves adding material, which can be greases, oils, gases and also some solids, between the interacting bodies. These lubricants have extremely low coefficient of frictions, and as they serve as the contact surface between the bodies, they inherently reduce the total friction forces that would develop between the surfaces. When it comes to space applications, we see there is a lot of intermittent use of systems. The momentum wheels, solar array drives etc. are not continuously used but required to function at full capacity for short periods after being left at standstill over a much larger period of time. These systems involve the use of ball bearings and also involve simple connection such as pin joints. Although in space, these mechanisms still experience friction losses, and the response of the system varies to Earth conditions due to factors such as the vacuum pressure of space and absence of oxygen that translated to the absence of low friction oxide layers. High friction values can lead to the jamming of the contact due to excessive wear and cold welding of surfaces, leading to catastrophic failure of the entire mission.

To understand this intermittent working of these mechanisms, a tribological experiment was set up using a standard SKF ball bearing and another using a simple pin on disc mechanism. Each tribological experiment is further elaborated below.

5.1. Ball Bearing

Ball bearings are essential components that allow for the attachment of rotating elements to static systems such as housings. Ball bearing are essential components in momentum wheels and solar array drives, and a failure of the ball bearing ultimately leads to failure of the entire system. Hence the selection of ball bearing used and lubricant augmented with it is critical to ensure smooth working of systems.

In the experiment a ball bearing is attached to a motor and allowed to intermittently rotate at varied speeds over set time periods. The RPM of the attached inner ring of the bearing is measured using an optical encoder and this value is inputted into certain models to evaluate the coefficient of friction between the balls and raceways that it is in contact with. From this we can understand the wear phenomena between the balls and raceways, a response which can be used to understand the optimum inputs required to minimize this wear.

5.1.a. SKF Model

SKF, or Svenska Kullagerfabriken AB (Swedish Ball Bearing Factory AB), is a Swedish multinational company that specializes in manufacturing and supplying bearings, seals, lubrication systems, and related products and services. SKF is one of the world's leading

suppliers of rolling bearings and has a significant presence in the global industrial market. Using their expertise and knowledge in the field of tribological phenomena, their engineers have created a model that can approximate the total friction force in bearing based on the inputted speed, applied force, materials of the bodies and viscosity of the lubricant used.

Bearing friction is not constant and depends on certain tribological phenomena that occur in the lubricant film between the rolling elements, raceways and cages.

The SKF model for calculating the frictional moment closely follows the real behaviour of the bearing as it considers all contact areas and design changes and improvements made to SKF bearings, including internal and external influences. The SKF model for calculating the frictional moment uses the form:

$$\mathbf{1.}\quad \boldsymbol{M = M_{rolling} + M_{sliding}}$$

The SKF model is derived from more advanced computational models developed by SKF. It is valid for grease or oil lubricated bearings and is designed to provide approximate reference values.

Further expanding each component:

5.1.a.1.Rolling Friction

The rolling frictional moment can be calculated using the form:

$$\mathbf{2.}\quad \boldsymbol{M_{rolling} = \varphi_{ish}\varphi_{ors}G_{rr}(\vartheta n)^{0.64}}$$

A fraction of the overall quantity of oil within a bearing passes through the contact area; only a tiny amount is required to form a hydrodynamic film. Therefore, some of the oil close to the contact area is repelled and produces a reverse flow. This reverse flow shears the lubricant and generates heat, which lowers the oil viscosity and reduces the film thickness and rolling friction. For the effect described above, the inlet shear heating reduction factor can be estimated using

$$\mathbf{3.}\quad \Phi_{ish} = \frac{1}{1+1.84*10^{-9}*(n*d_m)^{1.28}*\vartheta^{0.64}}$$

For oil-air, oil jet, low level oil bath lubrication (i.e. oil level H lower than the centre of the lowest rolling element) and grease lubrication methods, continuous over-rolling displaces excess lubricant from the raceways. In applications where viscosity or speeds are high, the lubricant may not have sufficient time to replenish the raceways, causing a "kinematic starvation" effect. Kinematic starvation reduces the thickness of the hydrodynamic film (decreasing k value) and rolling friction. For the type of lubrication methods described above, the kinematic replenishment/starvation reduction factor can be estimated using.

$$\mathbf{4.}\quad \Phi_c = \frac{1}{e^{[(K_{re}*\vartheta*n*(d+D)*\sqrt{\frac{K_Z}{2*(D-d)}}}}$$

Further elaboration on friction calculations can be found in *Appendix 3.*

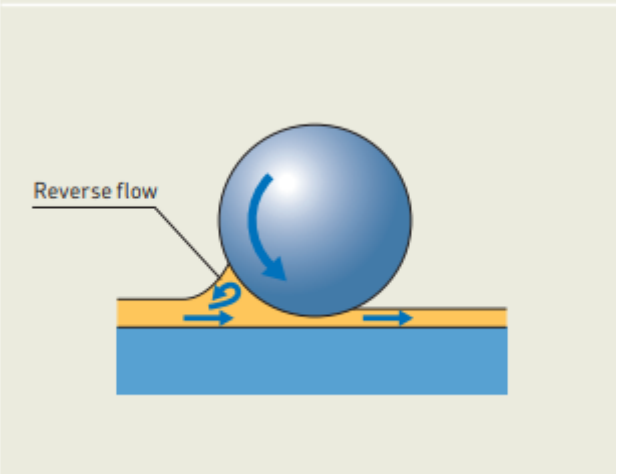

Figure 16: Reverse lubricant flow leading to heating

5.1.a.2. Sliding Friction

The sliding friction component is calculated using the form:

$$5. \quad M_{sl} = G_{sl}\mu_{sl}$$

The SKF model is derived from empirical data that is run only in the Hydrodynamic full film lubrication segment of the Stribeck curve, which follows that form of increased friction as total speed increases. Our test runs must follow the same characteristic to be considered as successfully implemented in the system.

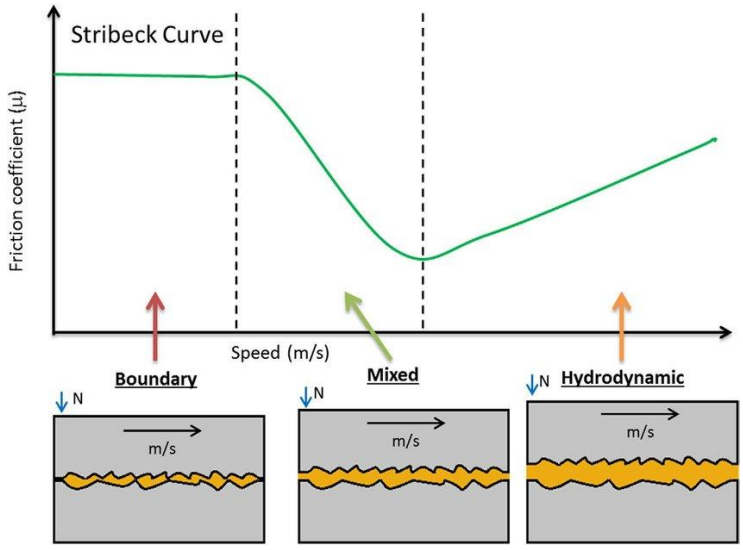

Figure 17: Stribeck curve

5.1.1.c. SKF Model Calculations

SKF provides an extremely helpful tool that can be used to calculate the total friction moments and its components by inputting values for axial and radial loading, total RPM and type of SKF grease used. A look into this tool is given in the figure x.

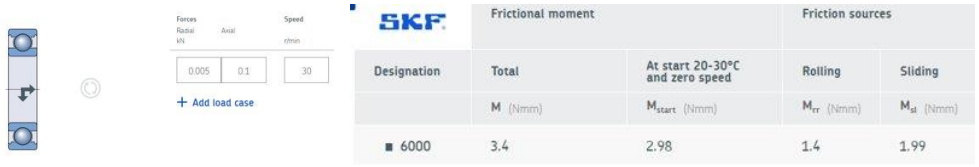

Figure 18: *SKF tool to calculate friction moments*

A code was written to simulate the same model in MATLAB such that the same could be implemented in the testing of the ball bearing in the CubeSat. This code gave similar values as the SKF tool, hence adding a layer of robustness to the calculation of friction torques.

RPM	Total Friction Moment	Rolling Friction Moment	Sliding Friction Moment
30	3.4368	1.4048	1.9983

Figure 19: MATLAB results

5.1.2. Hysteresis Model

There are several other theoretical models that can be used to calculate the friction torque in a ball bearing. These include the Hysteresis and Palmgren model. The Hysteresis model is chosen to act as a mode of comparing values to that of the SKF model to verify if the inferred values held water when put up against similar models.

The Hysteresis model evaluates the extremely critical component friction moment generated due to the elastic hysteresis that occurs between the raceway and the ball [8]. Methods are given to calculate friction torques generated due to hydrodynamic rolling forces, pivoting forces and the energy required to overcome the inertia of the balls is paramount too. This model is extremely robust due to its inclusion of extremely important physical phenomena, but lacks from accuracy due to the exclusion of friction forces generated by the cage of the ball bearing assembly.

The equation is of the form:

$$6.\quad T_Z = \frac{MER * d_m}{d_b} + FR * d_m + MP - \frac{F_{ib} * d_m}{4}$$

5.1.3. Comparison of Simulated Results

Codes that evaluated the results of coefficient of friction for three different lubricants of varying viscosity (LGLT2 - 17mm^2/s, LGWM1 - 200 mm^2/s, LGEM2 - 500 mm^2/s) across the working range of the encoder were run and simulated for both the SKF model and the Hysteresis mode. The simulated graphs largely followed the same trends and gave similar values, the values of the Hysteresis model being lower due to absence of friction force due to cage and the approximations in density and pressure-viscosity coefficient of the lubricant.

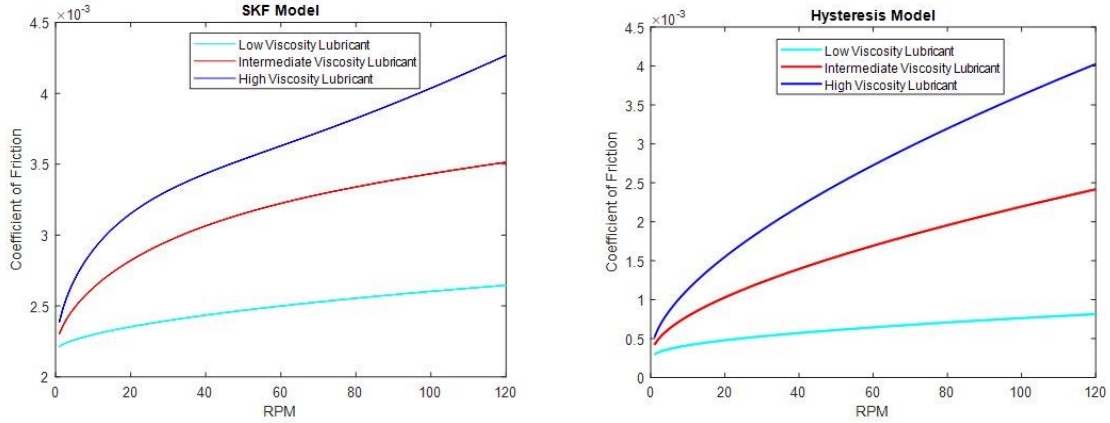

Figure 20: SKF Model vs Hysteresis Model

5.2. Pin-on-Disc

Pin-on-disc calculations are much more straightforward due to the set-up of the system. It involves two diametrically opposite pins applying constant load on a rotating pin, with the force caused due to friction between the contacts being directly measured by a calibrated load cell. This force can be directly divided by the applied axial force to retrieve the kinetic coefficient of friction at that particular loading. This method holds true for both dry and lubricated contacts, thus greatly reducing the complexity of the system.

Theoretical models can be modelled by calculating the force required to pull two contacting asperities from each other, this force value being dependent on complex calculations of the surface energy of the bodies and their interfacial surface energy. Lubricated contacts can involve the usage of the Hamrock Dawson equation to understand the lubricants response to the system a hence calculate approximate values of friction moments.

$$7. \quad \mu = \frac{f}{F}$$

The coefficient of friction depends on the measured friction force f divided upon the applied force in the contact **F**.

6. DESIGN

After completing initial researches, we worked on the detailed design phase for a tribometer instrument intended for space testing. Developing a fully compliant CubeSat tribometer unit is expensive and time-consuming, especially to meet the European Space Agency (ESA) and National Aeronautics and Space Administration (NASA) specifications. To address these challenges and costs we designed a prototype tribometer unit that closely mimics the features of a space-compatible CubeSat. This prototype serves as a cost-effective testing model here on Earth. The plan is to refine and adapt this proven prototype into a full-fledged space compatible. This staged approach helps optimize costs and ensures that the final design aligns seamlessly with space requirements.

6.1 CubeSat Prototype Design

Prior to the extensive process of designing a fully space-compatible CubeSat for launch, a comprehensive and detailed prototype was designed and tested on Earth under simulated space conditions. Due to budget and time constraints, we tailored the design of the prototype based on the features needed for space compatibility. This prototype holds significant importance, serving as a crucial setup and initial analysis for the eventual space-compatible CubeSat designs for tribological testing. The figure below illustrates the configuration of the prototype 1U CubeSat model.

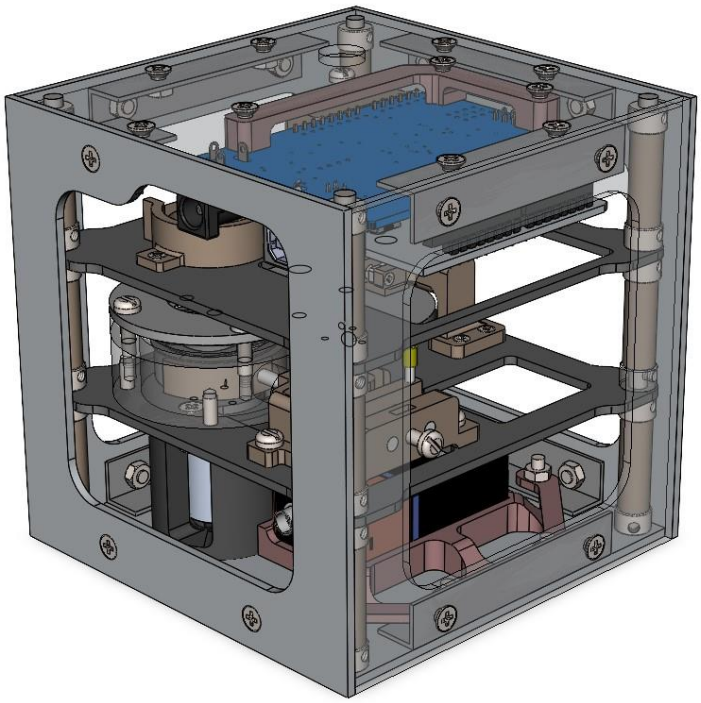

Figure 211: CubeSat prototype model

6.1.a CubeSat Frame

To keep costs in check, we came up with a new and simpler frame design for the prototype CubeSat, as shown in the figure.

The frame consists of two identical plates for the top and bottom, two identical plates for the sides (left and right), and two different plates on the other sides (back and forward). All frames made of 2 mm aluminium sheet. Additionally, there are four 4mm support rods to keep floors and frames in right positions and to increase the structure integrity. The plates are connected using custom L brackets, which are made from angle profile aluminium. This design not only simplified the manufacturing process but also significantly reduced the overall cost.

The top and bottom frames are connected to the side frames using custom L brackets, secured with 2 M3 bolts and nuts on each side. All L brackets are the same, except for one that is used to connect the top frame to forward frame. This specific L bracket is different to accommodate the USB and power ports on the Arduino, requiring a bit more space. Through these holes on frames and L brackets the other CubeSats can be attached together to get more unit of CubeSats.

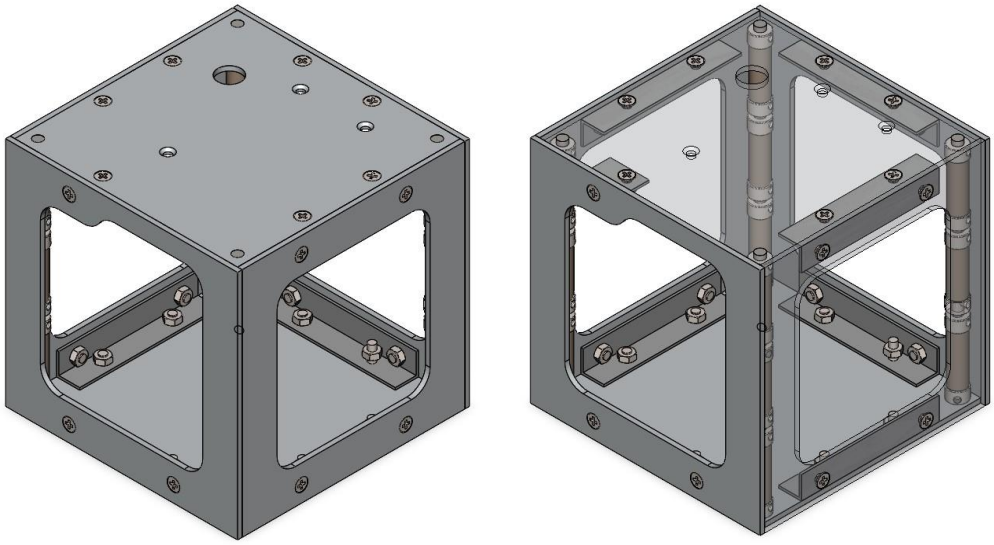

Figure 22: Frame of CubeSat

The frames are perfectly connected to achieve the precise dimensions of a 10x10x10 cm cube. The frame dimensions are calculated so that when they are attached together, they form a perfect cube. M3 bolts are countersunk into the frames to ensure that bolt heads don't protrude, maintaining a smooth exterior. The L brackets are attached from the inside, contributing to a beautiful cube frame without any protrusions.

6.1.b CubeSat Floors

The CubeSat is structured with a total of three floors, including the base and top frame. The tribometers are housed on the first floor, while the second floor accommodates the load mechanism for the pin-on-disk tribometer, an encoder seat, and enough space for the Arduino UNO with a custom PCB (shield design) attached to the top frame. The strategic arrangement of the floors is designed to increase functionality of each component. See figure below.

There are totally 3 floors in CubeSat (with base and top frame):

- Floor 0
  - 9V Battery and Battery seat
  - Motor support parts
  - L brackets mounting
- Floor 1
  - Pin-on-disk tribometer
  - Ball bearing tribometer
  - DC Motors mounting
  - Cage for ball bearing tribometer, load cell arm for pin-on-disk tribometer
- Floor 2
  - Pin-on-disk load mechanism
  - Encoder seat
- Floor 3
  - Arduino UNO with custom PCB (Shield design) and seat
  - L brackets mounting

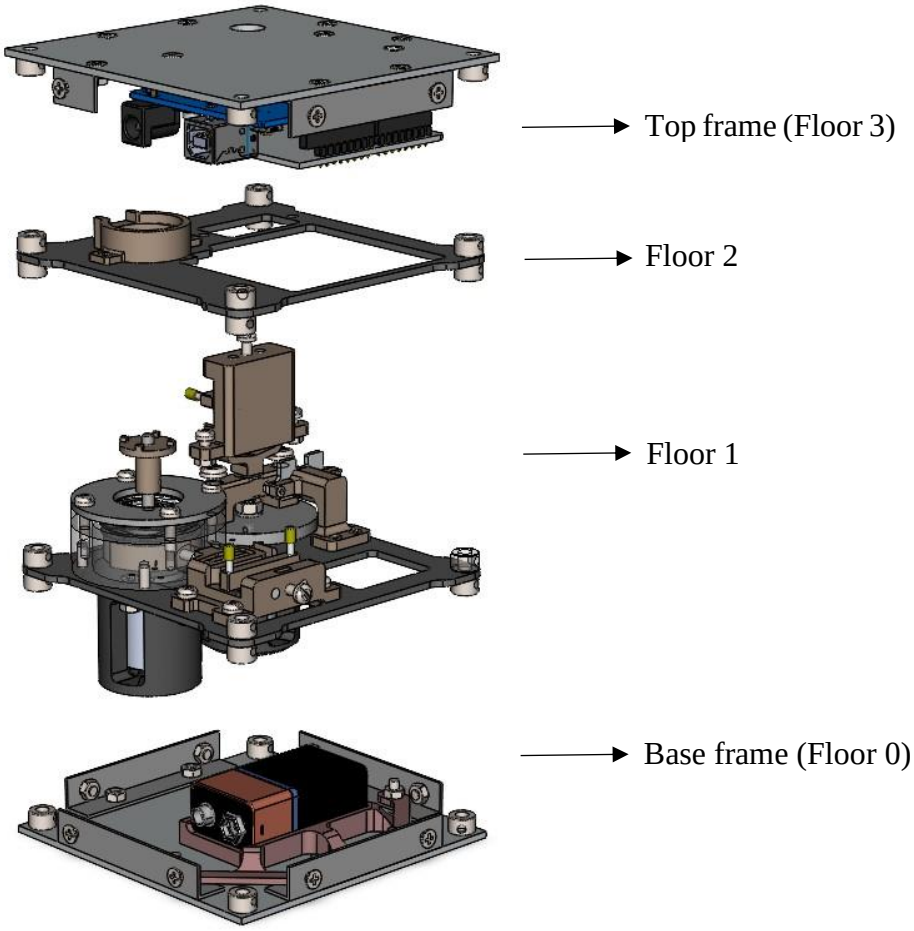

Figure 23: Exploded view of CubeSat

The CubeSat floors, constructed from 2mm aluminium sheet metal like the frames, are inserted into the CubeSat through the four rods at corners. These rods guide the floors into position, aided by cylindrical hollow 3D-printed parts that facilitate the alignment process. The floors are securely positioned with 4mm collars at the top and bottom of the frame in each corner, ensuring stability and proper placement. See figure below.

6.1.c Loading Systems

The loading mechanism serves the crucial purpose of adjusting the load applied to the pin-on-disc and ball bearing tribometers, facilitating experiments under variable loading conditions.

There are three distinct load applications on the tribometers: one axial and one radial load application on the ball bearing tribometer, and one axial load application for the pin-on-disk tribometer. The axial load on the ball bearing tribometer is fixed, adhering to SKF requirements. To control the radial load on the ball bearing tribometer and the axial load on the pin-on-disk tribometer, a 3D-printed spring load mechanism is employed. Both mechanisms are identical. The only difference is that the ball bearing load mechanism is horizontally mounted and the pin-on-disk mechanism I vertically mounted.

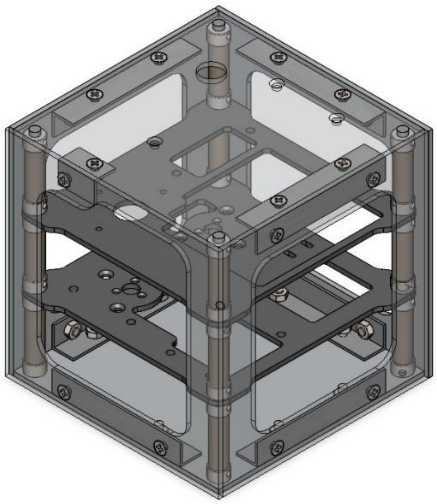

Figure 24: Floors with CubeSat frame

Pin-on-disc tribometer and ball bearing tribometer are mounted on the first floor shown in figure below.

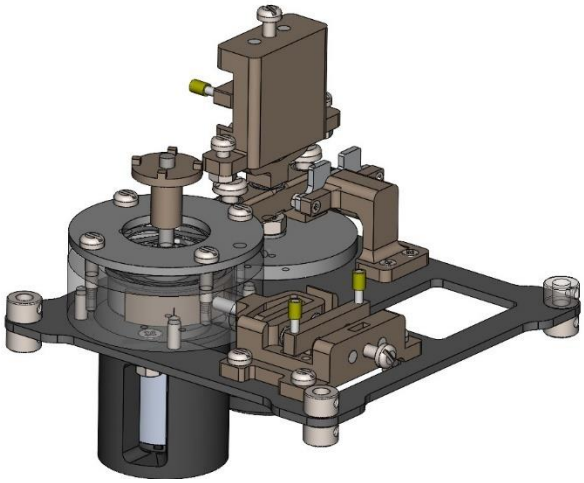

Figure 25: First floor configuration

The load is adjusted using M3 bolts that thread into M3 nuts fixed within 3D-printed part. These bolts provide sensitive adjustability. Connected to resin-printed parts, the bolts move along 2 parallel 3 mm metal rods, enabling them to change the length of the springs and thus adjust the load. Essentially, the 3D-printed load mechanism functions as a straightforward linear rail, give opportunity for precise control of the load applied to the tribometers.

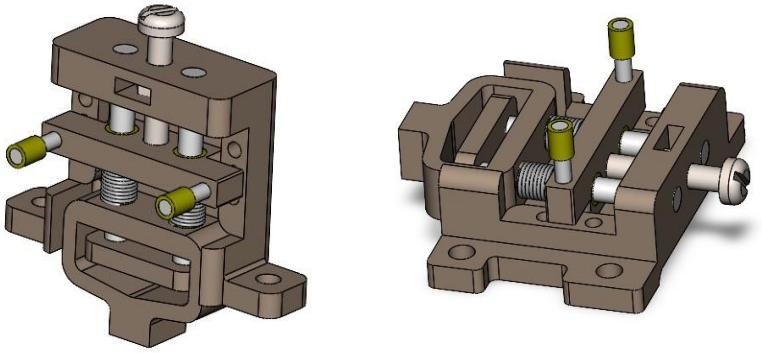

Figure 26: Loading mechanisms for tribometers

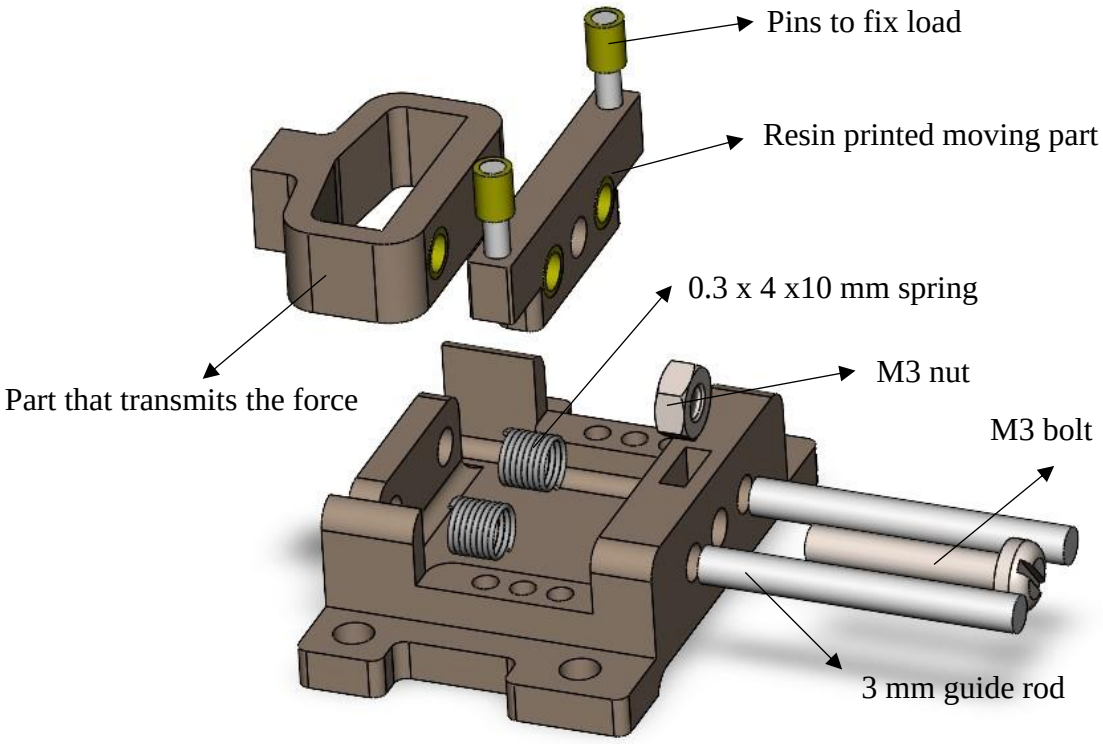

Figure 27: Exploded view of loading mechanism

The load mechanism incorporates three distinct presets, each corresponding to different compression levels on the springs. These load levels being calculated from test rig. To secure the moving part and prevent any unintended movement, 2mm pins are employed to fix the moving part securely within the designated load preset holes. This ensures stability and allows for precise control over the compression of the springs based on the selected preset.

6.1.d Pin-On-Disk Tribometer

The pin-on-disk tribometer features a disk connected to the motor via an external shaft. A resin printed two-leg part accommodates two cylindrical hollow metal components, each containing sample balls that contact the disk. Flanged bearings, positioned in the middle of the resin part,

are fitted onto a 3mm rod and connected to the loading mechanism on the other side. This two-leg pin setup design serves to distribute loading on the disk, preventing bending or wobbling issues.

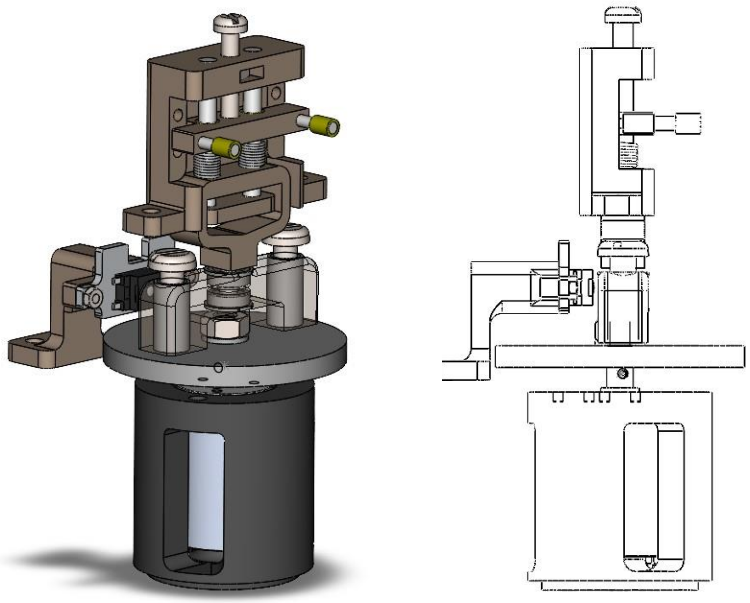

Figure 28: Pin-on-disk tribometer configuration

The normal load on the pin is predetermined from the test rig. A load arm leg is attached to the right end of the two-leg part, and at its extremity, a custom PCB is utilized for load cell attachment. When the balls contact the pin, frictional forces cause the two-leg arm to rotate until it reaches the load cell. This rotation provides data on the frictional forces, allowing for the calculation of the coefficient of friction.

The 3D-printed motor support part became essential due to the insufficient strength of the M1.6 threads on the motor, which were unable to securely hold the motor in place.

6.1.e Ball Bearing Tribometer

Bearings are commonly used in moving mechanisms and involve complex interactions like rolling and sliding. Designing a test rig to mimic these interactions is challenging and can lead to a complex and heavy setup, especially when fitting it into a CubeSat. However, a simpler approach is to directly use a bearing, avoiding the need for a specialized and complicated test rig.

The ball bearing setup is powered by a motor connected to the inner ring through an external shaft, allowing it to rotate freely with the motor. The outer ring is independent and can move, subject to both radial and axial loads. The radial load mechanism, connected to a U-shaped printed part, distributes the load evenly to the bearing's outer ring. Additionally, axial load is applied using a wave spring attached to the outer ring. A metal case secures the wave spring's position, and its compression is adjustable by changing the thickness of printed parts between top cover metal sheet and cage.

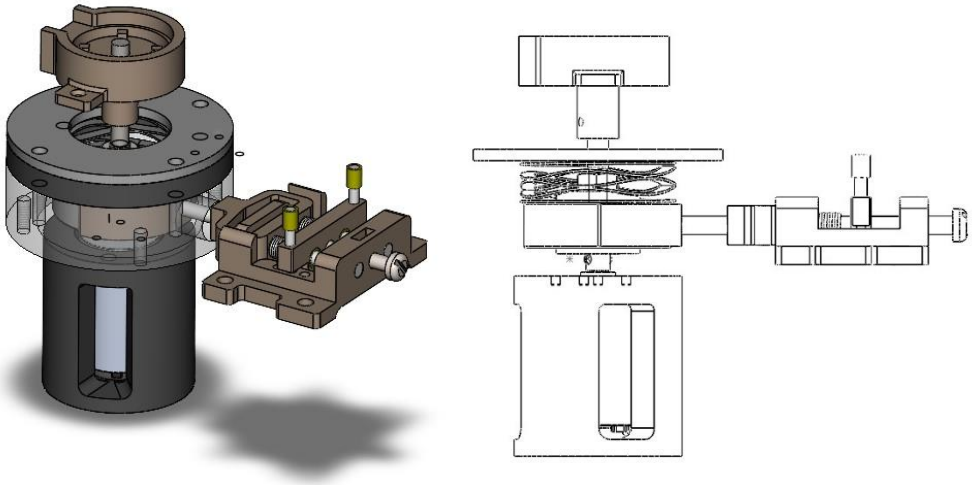

Figure 29: Ball bearing tribometer configuration

As the inner and outer rings engage with the rolling balls, reaction forces are generated on the outer ring, creating frictional torque. This torque is measured using an encoder attached to the shaft, which is in contact with the inner ring and motor. The rotation of the outer ring alters the RPM (revolutions per minute) at the shaft, and by monitoring these changes with the encoder, variations in the coefficient of friction can be calculated.

6.2 Space-compatible design CubeSat

The prototype design is good setup for the space-compatible design, but it needs to have some changes like material, some of components, electronics (space radiation) etc. The space-compatible design of the CubeSat involves several key considerations, primarily focusing on the CubeSat's weight limit, compatibility with industry-standard frames, and the ability to withstand extreme conditions during launch. Because of space environment are completely different from earth environment, it needed to have detailed investigations, considerations and requirements. Below is a summary of the possible changes, important considerations and components for the space-compatible design:

- Frame Lightweighting:
    - The CubeSat's maximum weight is 1.33 kg, and the frame should weigh a maximum of 200 g.
    - Consideration of different companies selling frames for various CubeSat sizes, the chosen structure can be a ISISPACE's 1U CubeSat frame, composed of modular parts with adjustable mounting points.

- Material Selection:
    - The frame material can be aluminium alloy 7075 which aligns with ESA/NASA standards for optimal strength and weight characteristics.

- Qualification Tests:
    - ISISPACE has conducted qualification tests for vibration, mechanical shock, thermal cycling, and thermal vacuum to ensure the structural integrity of the frame. So, some of the components must be chosen after this test.

- Component Stacking:

    - Mechanical and electronic components must be designed to be stacked in layers or panels known as floors like in prototype model.
    - Floors can be made of space-grade aluminium alloy, providing flexibility for component arrangement and attachment to frame rods.

- Vibration Considerations:
    - CubeSats experience extreme vibrations during launch, and the design must incorporate measures to withstand these vibrations.
    - A loading mechanism is implemented to vary the load on tribometers on prototype model and it must accommodate variable loading conditions and minimizing potential damage during vibrations.
    - The loading mechanism can be a piezoelectric actuator from Cedrat Technologies, previously used in NASA's space tribometer MISSE-7. The actuator has a loading force of 2.2 N, weighs 1.3 g, and operates within a voltage range of -20 to 120 V, requiring a dedicated piezo controller.

In summary, the space-compatible design ensures adherence to weight limits, utilizes industry-standard frames, undergoes rigorous qualification testing, and incorporates specialized components such as a piezoelectric actuator and load cell to address the challenges posed by launch vibrations and the space environment.

7. SIMULATIONS

Finite Element Analysis simulations were carried out in ANSYS Workbench to ensure the practicality of critical structural components. The structural strength and deformation of the loading mechanism, loading arm, sensor arm and the bearing shaft were simulated. Moreover, a modal analysis simulation was performed on the tribometer floors to evaluate the natural frequency of the structure. The materials used in the structure included Aluminium alloy, Structural steel, and PLA, and the material properties were preloaded in ANSYS. All the components were meshed with an element size of $1mm$ and all smaller parts were meshed to a finer element size of $0.5mm$.

The loading mechanism was designed for a maximum force of $1N$. Fig. 30(a) shows the loading mechanism used in the both the pin-on-disc and bearing tribometers in the CubeSat. The structure was manufactured using steel rods and 3D printed PLA material. A fixed support boundary condition is employed on the surface A and C, and a force of $1N$ was applied on the surface B. All sliding contact were assigned a frictionless contact condition, and all other contact were modelled as a bonded contact for simplifying of simulation. This simulates the condition where the spring-loaded mechanism applies the maximum rated force at the end C. Total deformation and the equivalent stress in the structure were simulated through static structural simulation in ANSYS. Fig. 30(b) shows the expected deformation of the loading mechanism for the maximum rated applied load. From the FEA simulations, a total deformation of $5.9\mu m$, and equivalent stress of $8.66\ MPa$ were observed. Since the total deformation was less than the allowable limit of $10\mu m$, the force applied by the spring would not be reduced and a constant force of $1N$ can be transmitted to the contact. Moreover, the equivalent stress was less than the yield stress of the material, thus making this part fully functional as expected.

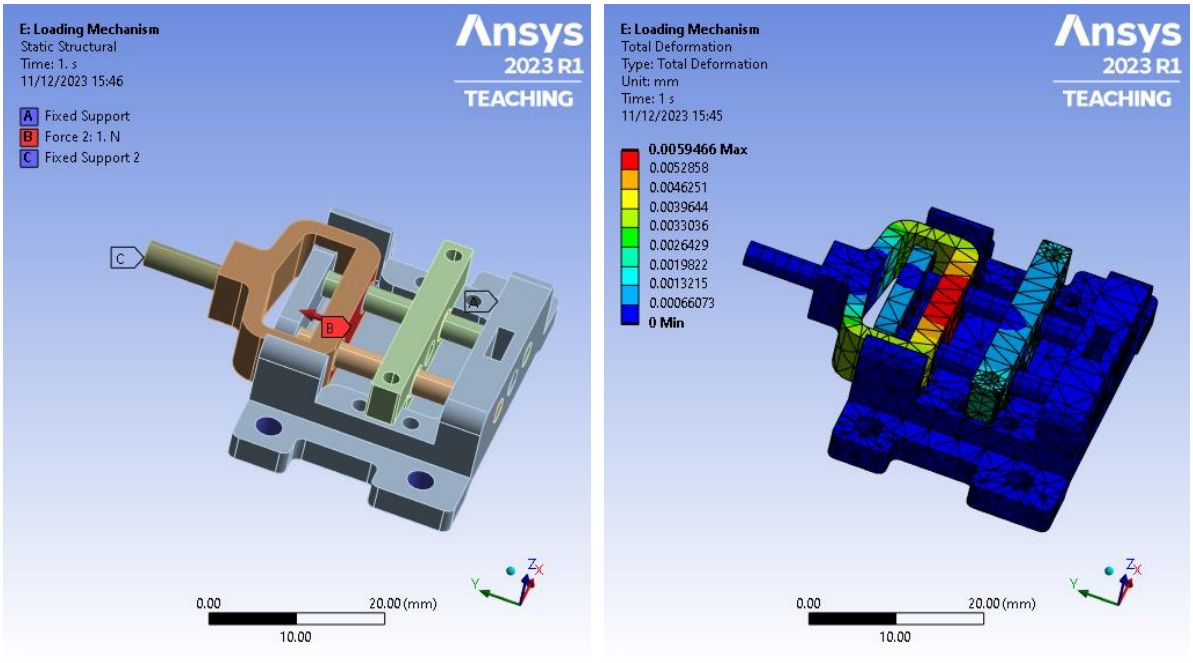

(a) (b)

Figure 30: The boundary conditions and the simulated deformation of the loading mechanism used in both tribometers.

Another critical component whose structural performance would determine the functionality of the pin-on-disc tribometer is the U-shaped loading arm. This part was manufactured using 3D printing with the PLA materials. Fig. 31(a) shows the boundary conditions imposed on the loading arm. A force of $1N$ was applied to the end connected to the loading mechanism, at surface B. A fixed boundary condition was imposed at the end that contacts the disc, on surface A. Since the load is acting only on one direction, a simple bonded contact condition was imposed on the part. Total deformation and the equivalent stress in the structure were evaluated using static structural simulations in ANSYS. Fig. 31(b) shows the total deformation of the U-shaped loading arm for the maximum rated load. It was observed that the total deformation of the arm was $0.2\mu m$, and equivalent stress was $0.25\ MPa$. With minimal deformation, and the equivalent stress being much lower than the yield stress of PLA, this part was expected to perform well even under the higher loads.

Fig.32(a) shows the sensor arm where the load cell that is used to measure the frictional force is loaded. The sensor arm was manufactured from PLA fused deposition modelling. The base of the sensor arm was given a fixed boundary condition, and the front end of the arm was given a force which corresponded to the expected frictional force. Generally, the friction coefficient of a sliding contact would go to about 0.25. Therefore, a force of $0.25\ N$ was applied on the surface B. This simulation aims to evaluate the deformation of the sensor arm. Any deformation of the sensor arm would result in the application of the frictional force at an angle to the sensor, which would provide wrong results for the friction coefficient. Fig.32(b) shows the total deformation of the sensor arm for the expected frictional force. From the ANSYS static structural simulations, the total deformation was observed to be $5\mu m$ at the top of the contact region. Since this is less than the allowable deformation of $10\mu m$, and the equivalent stress of $0.17MPa$ is less than the yield stress of PLA, the results from the load cell used for measurement of the friction force is expected to be accurate.

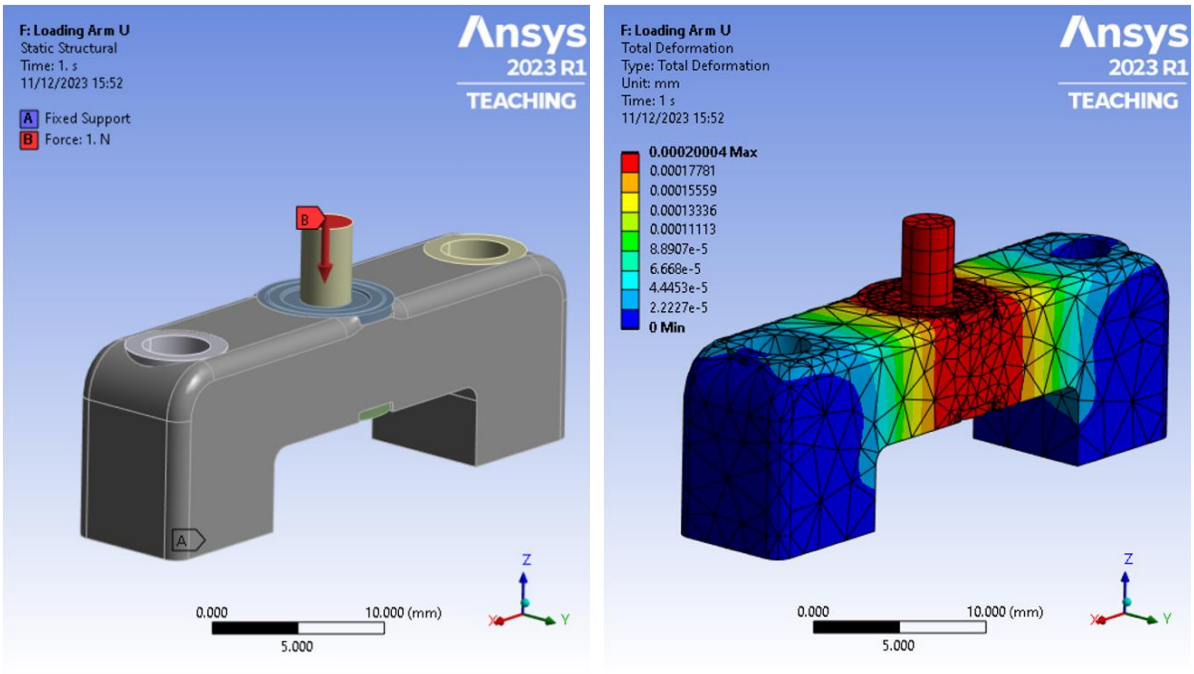

(a) (b)

Figure 31: The boundary conditions and the simulated deformation of the U-shaped loading arm in the pin-on-disc tribometer.

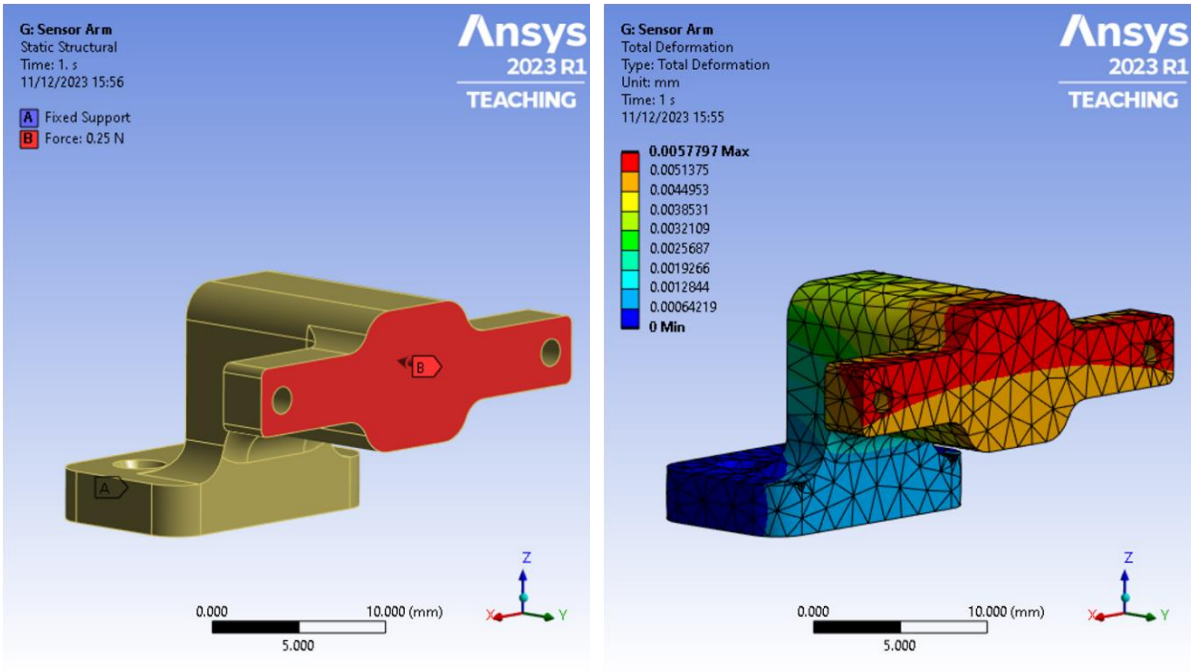

(a) (b)

Figure 32: The boundary conditions and the simulated deformation of the sensor arm in the pin-on-disc tribometer.

Since the bearing tribometer experiences a radial force of $1N$ and a maximum axial force of 80N, the bearing shaft is expected to deform. A rotary encoder is fixed at the top of the shaft to measure the RPM of the shaft. Any large deformation of the bearing shaft would interfere with the measurements of the encoder and could even destroy it. Therefore, understanding the

behaviour of the shaft for the loading and boundary conditions to which it is subjected is necessary. Fig.33(a) shows the boundary conditions imposed on the structure. A fixed boundary condition was applied on bottom end of the shaft on surface A to simplify the simulation. A radial force of $1N$ was applied on surface B and a maximum axial force of $80\ N$ was applied on the outer race of the bearing on surface C. Since rotation of the bearing is not involved in this condition, a bonded contact condition was established to evaluate the maximum deformation and stress. The total deformation at the top end of the bearing shaft, where the encoder is connected, is evaluated using ANSYS static structural simulations. Fig.33(b) shows the total deformation of the bearing tribometer assembly for the maximum rated loads. From the FEA simulations, the total deformation was observed to be $1.3\mu m$ at the top of the shaft. Since this is less than the allowable deformation of $5\mu m$, and the equivalent stress of $23.75MPa$ is less than the yield stress of steel used, the encoder can be loaded on to the bearing shaft with confidence.

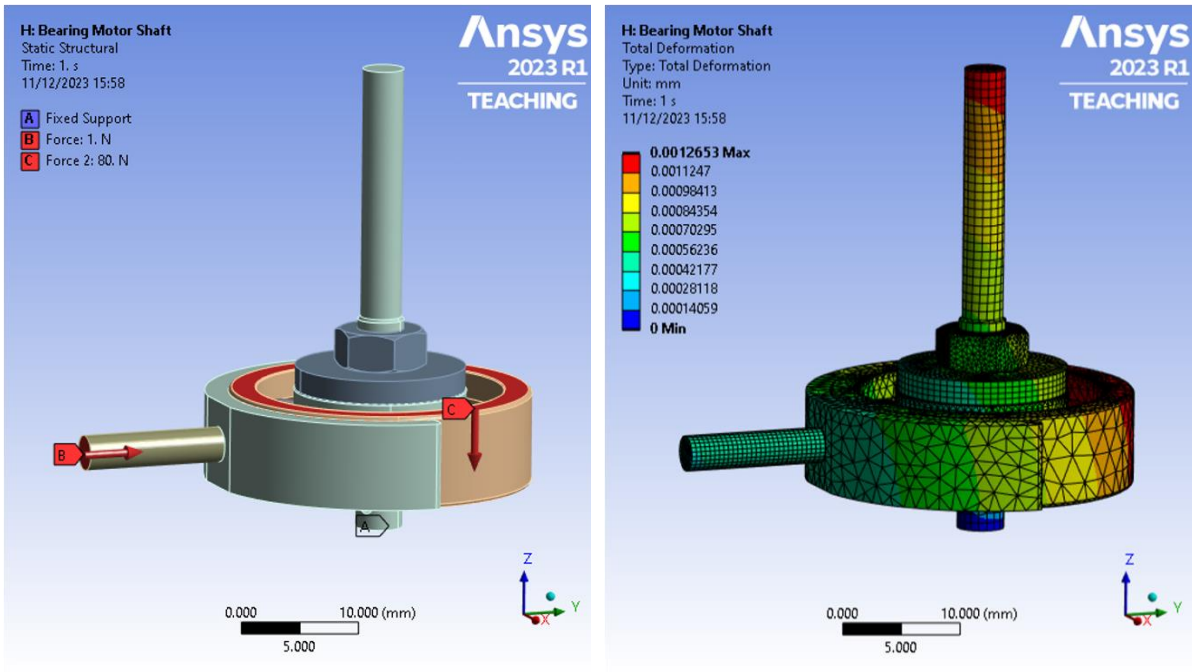

(a) (b)

Figure 33: The boundary conditions and the simulated deformation of the bearing shaft in the bearing tribometer.

A modal analysis simulation was carried out on the tribometer floors as shown in the Fig.34 to evaluate the natural frequencies of the system. This is performed to ensure that the tribometers are not run at the RPMs which correspond to the natural frequencies of the structure. In Fig.34(a), a fixed boundary condition was imposed on the bottom floor, and a radial load of $1N$ and axial load of $80N$ was applied on the bearing tribometer, whereas a normal load of $1N$ was applied on the pin-on-disc tribometer. A bonded contact condition was imposed on all contacts except for all sliding contacts where a frictionless contact was imposed for the simplicity of the simulations. Modal analysis simulations were performed on the prestressed structure in ANSYS. Table 6 shows the results from the FEA simulations where the natural frequency of the body modes of the structure is listed. Fig.34(b) shows a body mode of the structure with the natural frequency at 463.32 Hz. The tribometers are not expected to run at the frequencies listed in the Table 6.

Table 6: Natural frequencies of the tribometer floors.

Body mode	1	2	3	4	5	6	7	8
Natural Frequency [Hz]	81.097	103.67	113.43	417.5	463.32	464.12	499.47	584.25

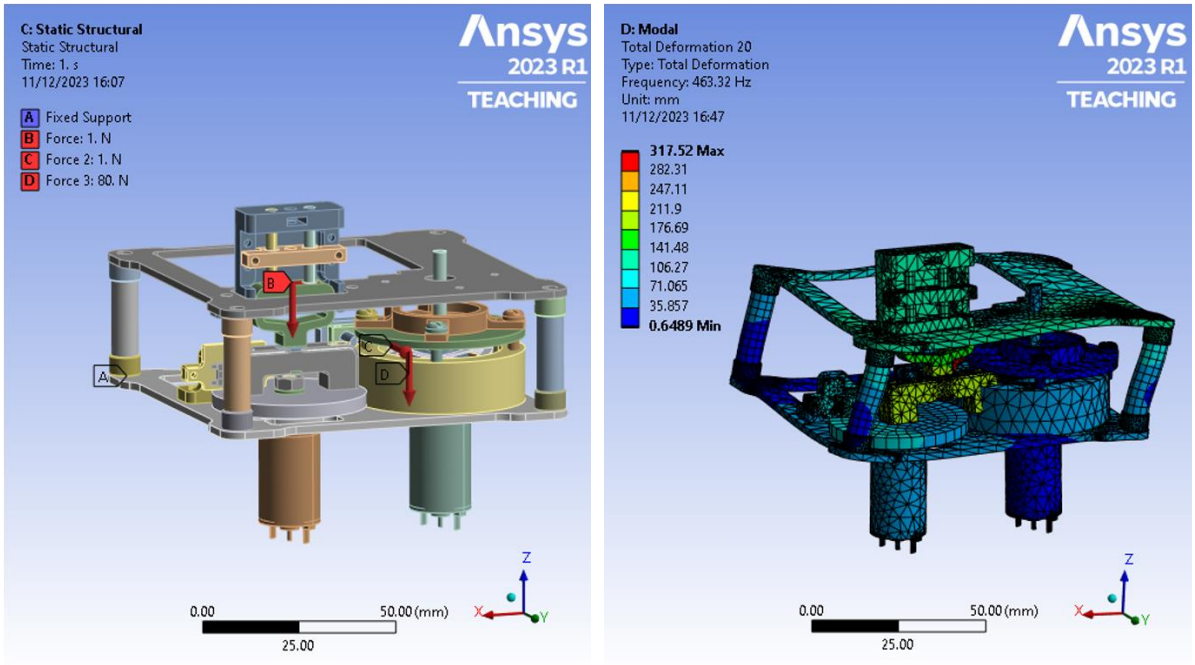

(a) (b)

Figure 34: The boundary conditions and a simulated mode shape of the tribometer floors.

The finite element analysis using ANSYS Workbench verified that the design and material combinations were apt for the loading and boundary conditions that the structure is exposed to. The results are used as reference for design iterations and experimentation.

8. ELECTRONICS

8.1. Electrical requirements for CubeSats and project constraints

Just like the frame and mechanical components of the CubeSat design the electrical system is subjected to strict construction and testing requirements. All CubeSats that are designed and built for space flight must comply with set rules from their mission integrators, and local space agencies [11]. All CubeSats must have a remove before flight (RBF) pin, separation switches that will separate the power system from the rest of the electrical system circuitry when the CubeSat is in the launch dispenser, and a power storage system before they can be integrated into a CubeSat dispenser. Before a CubeSat can be considered for launch and the integration process with dispenser can start, the electrical system must comply with the following regulations: wire runs are kept as short as possible, proper wire gauges are used between components, components are properly grounded, soldered, and insulated, components will not cause shorts or malfunctions of nearby components, safety and failure analysis is conducted on electrical parts, and an electrical report is created with wire diagrams/schematics, and all

components are listed along with their electrical properties such as voltage. All electrical components must also be tested using a bread board prior to fabrication of the electrical system and all parts must be tested separately and together before the assembly of the electrical system can begin. Finally, before the CubeSat is launched the electrical system must undergo intense testing such as FlatSat testing, radiation, vibration, thermal vacuum bakeout, shock, electromagnetic interference/electromagnetic compatibility, and Day in the Life testing, to ensure that the electrical system will function properly in a harsh space environment [11]. Once the CubeSat has passed all testing and is compliant with all electrical system requirements it will be considered for launch.

Since the testing requirements of a CubeSat are extensive and can be costly the prototype that was constructed in this project, which is a terrestrial model of a theoretical space-based CubeSat, was not tested to the same extent a CubeSat preparing for launch would be tested. This CubeSat is also designed to be a module of a larger 3U CubeSat so it does not have its own power system, and the battery used to power the two motors in the tribometers will be replaced when the module is integrated into the larger CubeSat setup. All components were tested on a breadboard to verify that the components were operational, and the components were tested separately and together once they were under code control and prior to assembly in the CubeSat module.

In figure 35, a wire diagram/schematic for the entire CubeSat module is seen. This CubeSat is supporting a pin-on-disc tribometer and a ball bearing tribometer, and besides the size constraints on the electrical set up, the motors that were used to power the tribometers were predetermined as they were salvaged from the previous iteration of the CubeSat module.

There was also a 10W power budget that could not be exceeded. Due to the size constraints for the tribometers it was decided that the pin-on-disc would use a Honeywell 1.53Kg load cell, and a SparkFun HX711 load cell amplifier breakout board. The bearing tribometer was originally planned to be measured using a variable resistance force sensor to measure radial loading and an encoder to measure the decrease in speed of the motor as friction in the bearing was increased. This sensor setup was later changed to relying solely on an encoder for the measurement of the friction in the bearing due to the readings from the force sensor being slow to react, and wildly variable and inaccurate over time as temperatures changed, making the variable force sensor no longer suitable for the needs of the project.

Two N-channel mosfets were used to control the two DCX 16 S Maxon motors. This allowed for individual control over each motor, efficient use of power allowances, easy integration into the electrical system due to their small size, and smooth integration into the software system as well. Finally, an LM35 ambient temperature sensor was integrated into the electrical system to measure the environmental temperature to predict the expected outcome of the tribology tests on different lubricants.

An Arduino Uno R3 microcontroller was chosen for this system because it had the most hard-wired pulse width modulation (PWM) enabled pins compared to that of the Raspberry Pi 3. The amount of the PWM pins was the deciding factor when choosing a microcontroller as many of the components in the electrical system relied on PWM usage. This would mean that for the Raspberry Pi, several PWM pins would have to be coded to produce PWM signals. This wouldn't have been ideal for the constraints of this setup as overloading the Raspberry Pi with PWM signals and data processing would ultimately affect the speed at which the microcontroller could produce PWM signals from non-hard-wired pins, and this could have affected the results of the data. To ensure all wire runs were as short as possible and that all components were properly grounded and fit inside the CubeSat a custom printed circuit board

(PCB), shown in figure 36, was designed to sit on top of the CubeSat's Arduino microcontroller.

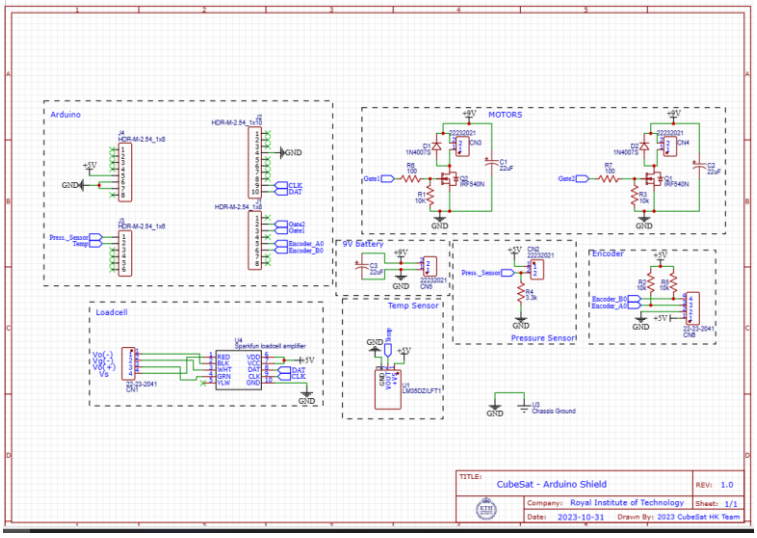

Figure 35: In this figure is the layout/wire diagram of the electrical system in the CubeSat.

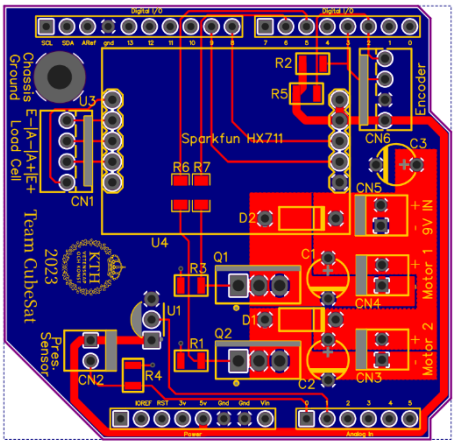

(a)

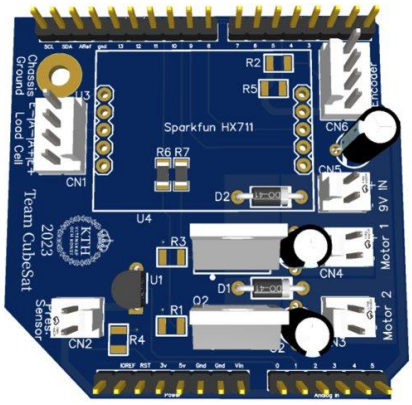

(b)

Figure 36: (a) Image a is a view of the wire running on the PBC. (b) Image b is a 3D view of the PCB board.

8.2. CubeSat electronics

8.2.a. Motors and controllers

This CubeSat used two DCX 16 S Maxon motors to power a pin-on-disc and a bearing tribometer [12]. These motors were controlled using N-channel mosfets. The mosfet on the pin-on-disc motor was set up to run the motor at a set speed, and the other mosfet ran the bearing tribometer at a set current, by using the PWM signals generated by the Arduino, based on the relationship between current and PWM, to run the motor. The maxon motors were chosen as they were used in the previous design of the CubeSat prototype and reusing them saved money and time in part acquisition. Previously these motors utilized an H-bridge to control them, and in the redesign the decision was made to switch to N-channel mosfets. N-channel mosfets instead of an H bridge were chosen in this iteration because it allowed for individual control of the motor. This allowed for one motor to be current controlled, meaning it received constant current, and the other motor to be speed controlled, meaning it can be run at constant speed.

8.2.b. Ball-bearing tribometer sensors

The sensors in the ball bearing tribometer were an encoder and a variable resistance force sensor (FSR). The FSR was going to be used to measure changes in radial loading of the bearing and the encoder was going to track the changes in RPM of the motor shaft as the friction in the bearing increased. These sensors were chosen for this tribometer because they allowed for efficient use of vertical space and removed the unknown and uncontrolled variable of load arm deflection found in the previous design, which used load cells and a strain gauge on a flexible loading arm to measure friction in the bearing. The idea behind the encoder and force sensor set up was that the radial loading would provide normal force to the bearing allowing for the calculation of the coefficient of friction in the system, and the encoder would track the motor RPMS, as the friction in a motor increases motors tend to slow down as they expend more torque to overcome the increased friction.

An optical rotary encoder with a resolution of 24 pulses per revolution was chosen to track the motor RPMs. Equation 8 was used to calculate the RPMs of the motor from the encoder pulses. The encoder that was used in this application was a cts series 292 20mm optical ring encoder, with an operating voltage between 3.3 and 5 Volts, and a max operational speed of 120 RPM. Each time the encoder moved, the disc inside the encoder would rotate and a light and photo sensor in the encoder would generate a pulse. The pulses were generated by the change in light each time the encoder passed over a hole in the encoder disc. An encoder with a resolution of 24 was chosen because for this system to be able to track small changes in motor speed an encoder resolution of at least 20 was required.

$$\textbf{(2)}\ RPM = \frac{Pulses\ in\ 1\ \text{sec} \times 60}{Pulses\ per\ revolution \times gear\ ratio}$$

The FSR had to be removed from the overall design at the last minute due to calibration and read out issues. FSRs work by changing the resistance as pressure is applied to them, and because of this they are slow to recover back to the non-load form and resistance, they also tend to have issues reading at the ends of the operating range. This is caused by the logarithmic curve of the sensor from changing resistance. These qualities made it difficult for the FSR to provide useful and reliable data about the applied radial load of the system, leading to the applied force of the loading mechanism to be calibrated and quantified using an external load cell and test rig. The encoder that was used also generated issues that ultimately lead to a last-minute pivot in design. The encoder generated too much rotational torque for the motor to rotate it and the bearing. This forced a switch to tracking motor RPMS using a phone camera

and a magnet. The phone camera tracked the fluctuations in the electrical field of the magnet as the speed of the motor shaft changed. In future design iterations the use of an encoder with a higher resolution for more precise measurements and with a lower rotational torque is suggested.

8.2.c. Pin-on-disc tribometer sensors

The pin-on-disc tribometer used a load cell to read the applied force from the pin rubbing on the disc. The load cell was calibrated off the CubeSat before it was integrated into the pin-on-disc tribometer. Calibration was done in a test rig where objects of known weight were placed on the load cell and a calibration factor using equation 9 was calculated. Implementation of the calibration factor in the loadcell code allowed for proper adjustments of the reading of the loadcell over the 1.53Kg working range. The load cell was placed in a load application test right, figure 37, where each loading preset of the load arm was measured. The load cell also uses a Sparkfun HX711 load cell amplifier breakout board that was mounted on the PCB to amplify the signals from the load cell when under loading to allow for the signals to be more easily read by the Arduino.

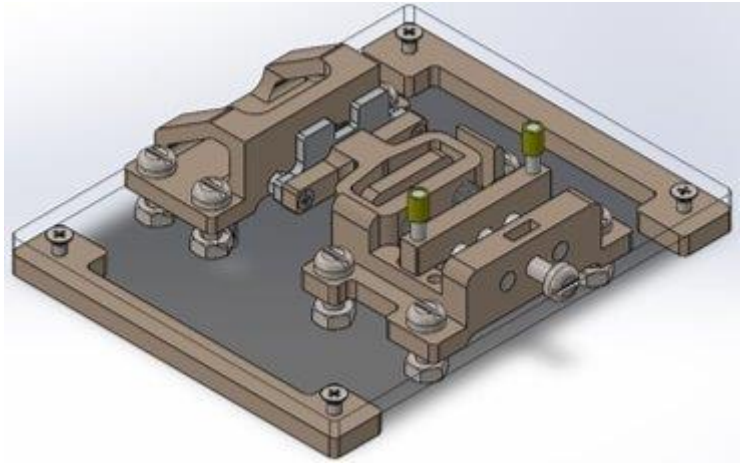

Figure 37: This is the CAD of the calibration rig that was used to measure the load applied at each preset of the load arm.

$$\textbf{(3)}\ calibration\ factor\ =\ \frac{load\ cell\ reading}{known\ weight}$$

8.2.d. Printed Circuit Board

The printed circuit board was designed to have a common ground plane on the bottom of the board and is a two-layer PCB. By making the bottom of the board grounded and connected to the ground pins on the Arduino the requirement of all electrical components having a common ground for CubeSats was met. The PCB also contained a chassis ground slot for a nut in bolt or cable to be soldered to it, and then connected to the metal frame of the CubeSat, ensuring that the CubeSat frame does not become electrically charged and that the potential effects of radiation on the CubeSat frame charge can be mitigated. This feature satisfied the requirement for CubeSats to not be electrically charged and to prevent electrical charges causing malfunctions or shorts in nearby components, as a charge frame can affect sensor readings especially on such a small scale. Molex KK 254 with friction lock pine headers were used on the PCB to keep all attached wire components securely in place to make the CubeSat able to withstand vibrations and rough handling, which is expected if it were to go to space. The PCB also allowed for all electrical components to be integrated into the CubeSat and maintain a small footprint to leave as much room as possible for the test components/instruments. This

allowed for the tribometers to have more robust designs and contributed to the overall compliance of the CubeSat with the electrical system requirements as the addition of a PCB allowed for short wire runs.

8.3. Adaptations for space environments

The majority of the electrical components used on the terrestrial twin CubeSat that was prototyped are not space compatible and were chosen because they were cost effective and did not require long lead times for part acquisitions. To bring the electrical system into compliance for space compatibility on the theoretical design twin, the motors running both tribometers should be replaced with brushless motors or a stepper motor as the system is designed to be run at low speeds that may encounter high torque loads on the motor, and these motors tend to best be able to dissipate built up heat and are less likely to fail under heavy load then brushed DC motors [13]. The loading arm mechanism will also be replaced with piezoelectric motors that apply a load when actuated. This is better suited for a space model because it does not rely on human interference to change the loading in the tribometer. Piezo electric motors also have several compact options that would fit well inside a CubeSat. A more robust encoder, likely of the mechanical type, should also be used in place of the optical rotary encoder on the bearing tribometer as it will be less prone to damage and radiation fluctuations in space compared to low-cost optical encoders.

9. SOFTWARE

All code to make the CubeSat run and calibrate sensors was done in C++ using the Arduino IDE and Arduino Libraries. Arduino IDE and C++ were used because the microcontroller on the CubeSat was an Arduino Uno R3, and this ensured that code written to run the CubeSat would be compatible with the designated microcontroller. Set up and run code was written for each sensor and then adjusted until sensors were calibrated and functioning correctly. Once sensors were calibrated, run code was created from them and used to verify that the sensors had been calibrated correctly. This process of running each component individually and checking that it was in working order complied with the electrical system regulation of running components separately before integrating them or using them with other sensors.

9.1. Load Cell calibration and operation code

The load cell reads out raw analogue values before they have been converted to usable numbers. To take the raw analogue values and make them usable a calibration factor using equation 9 above was created for the load cell. The calibration factor was subtracted from the raw readout value and the result was a load reading in grams. To set up the calibration code for the load cell the HX711 Arduino Library written by Bogdan Necula version 0.7.5 was used. This library provided a tare function to set the load cell to an initial reading of zero, a function called set_scale that allowed for the calibration factor to be set to correct load cell readout, a load cell reading function that averaged a specified number of load cell readings, and a power up and power down function that switched the loadcell between high power and low power modes to clear the previous readings and allow the load cell to take a new reading.

To calibrate the load cell, the first ten readings of the uncalibrated raw read out value of the loadcell when known weights were applied were taken. Then the averaged number was divided by the known weight that was used to gather weight readings. Finally, the load cell printed its calibration factor. The calibration factor was later used in the run script for the load cell using the set_scale function. This allowed for quick and easy calibration and readout adjustments.

When running the load cell, the load cell was switched between its high power (reading mode) and its low power (clear/sleep mode). This allowed for the load cell to be switched on and off every two seconds to get new reliable readings from the applied weights. Every reading from the load cell that was reported was an average of ten readings from the loadcell over the span of two seconds. The code that was used to calibrate and run the load cell can be seen in *Appendix 2*.

9.2. Encoder operation code

The encoder used in this setup has two signal channels, signal A and signal B. In this case, signal A of the encoder is the leading signal, and signal B is lagging by 90 degrees +/- 45 degrees. Using these properties, code was created to take advantage of the leading and lagging relationship. The encoder signals A and B were attached to Arduino digital pins 3 and 2, respectively. Digital pins 3 and 2 are interrupt enabled, meaning that the pins can be used when coded with an interrupt to pause the execution of the code script and run the function attached to the interrupt. In the code the rising edge, the transition point where voltage reading increases from ground state to powered state (in this case zero volts to five volts), of the encoder signal on signal line B triggered an interrupt. This interrupt used signal pin A to read off and then added a pulse increase of one for every pulse that passed in the one second read time before the interrupt ended and the remainder of the running code finished. The interrupts were attached in a loop function meaning that the interrupt code would continuously repeat to provide a constant readout for rotations per minute of the motor shaft to allow for efficient tracking of the expected speed decrease from increased friction.

9.3. Ball-bearing operation code

The ball bearing tribometer used a motor, a N-series mosfet, and an encoder to run and collect data. The motor for this tribometer was supposed to be run at constant current. When designing the printed circuit board, a current reading pin was not included due to design oversight. This forced the use of PWM duty cycle code to achieve the desired current to be fed to the motor. The Arduino generates a standard PWM cycle that most PWM enabled components use. A full PWM cycle is called a PWM duty cycle, and by changing the speed at which PWM signals are generated and sent to the motor controller the current of the motor can be controlled. To create the code for this application it was assumed that internal resistance of the motor would remain constant throughout the run time of the tribometer, and that voltage being fed into the system would also remain constant at five volts. Equation 10 was used to relate PWM duty cycling to motor current, allowing for the N-channel mosfet to run the motor at constant current.

$$\textbf{(4)}\ PWM\ cycle\ =\ \frac{motor\ current}{actual\ current}$$

The current that was being used was read off the gate pin of the N-channel mosfet as the gate pin on this type of mosfet is responsible for controlling the current between source and drain pins on the mosfet. Once the gate pin was tripped the motor was switched on and ran at constant current.

Data for this system was collected using an encoder. The coding and data acquisition process for the encoder was described in detail in the encoder operation code section. To summarize how the encoder works here in this system an interrupt is attached to the lagging signal pin and when the rising edge of the encoder, the point where voltage is increased from zero to one, is hit the interrupt triggers. This temporarily pauses the code and executes the interrupt code where the pulses being read off the leading signal on pin A is counted over the time frame of one second. Once the time frame of pulse counting has ended the code continues through the

remaining run code where RPMS of the motor shaft are calculated, and the process is repeated as the code reruns the function in the loop continuously.

Together the N-channel mosfet and the encoder work together to run the ball bearing tribometer and this sub system code was later integrated into the full system code.

9.4. Pin-on-disc operation code

The pin-on-disc tribometer uses a load cell to collect data, which has a code system explained in the load cell calibration and operation code section, and a N-channel mosfet. The N-channel mosfet in this system is used to run the motor at a set speed for testing. This is done by configuring the pin on the Arduino that the gate on the N-channel mosfet is connected to as an output. A new variable called speed was created and constrained to a range of 0 to 255. This means that if the desired speed value is less than zero it will be set to zero and if it is more than 255, which is the maximum PWM cycle the Arduino can generate, the speed variable is set to 255. This new variable is then mapped from a range of zero to 100 to the range of zero to 255 on for PWM signalling. Finally, the speed function is set up to run off the gate pin on the N-channel mosfet to the input speed parameter by using an analogue write function. The analogue write function sets the speed the motor will run at by setting the average voltage the motor will receive through a PWM signal.

9.5. Full system code

The full system code, found in *Appendix 2*, is composed of several small code portions written to control each separate component. The main running code in each function from the loop and setup sections of the code were placed into functions. These functions were used to call the setup and run codes for each component. This allowed for the components to all run at the same time, allowing for both tribometers to collect data in unison. The functions in the system code also allowed for quick adjustments to individual components to be made as the code for each part was easily findable. The set up of using multiple functions for each component also allowed for different components to be turned on and off in the run code using comments, making debugging easy and allowing for quick adjustments to be made in the case that only certain parts of the subsystem needed to be run to collect data. Finally, all data was printed to the serial monitor in the Arduino IDE and then placed into an excel spreadsheet. This data was then run through MATLAB for data calculations and manipulation, forming graphs and finding lines of best fit for the given data.

10. MANUFACTURING PROCESS

In the manufacturing process, we employed various methods and tools to create the components. Numerous parts were 3D-printed using PLA, and some were resin-printed. For the frames and floors, water jet cutting was utilized, and specific components were manufactured at the KTH Prototype Center, employing different machining tools. Additionally, certain parts were crafted at ELAB.

10.1. PLA 3D Printing

Many parts were crafted using PLA 3D printing (Prusa MK3 and Prusa MK3S printers). Numerous prototypes, in the form of initial prints, were generated to determine the optimal dimensions and features of these parts during the assembly process. After-processing was required to get smoother surfaces on printed parts (removing brims and supports and sanding). The test rig and load cell calibration parts also PLA printed. The PLA 3D printed parts include:

- Floor 0
  - 9V battery seat
  - Motors support part
- Floor 1
  - Ball bearing load mechanism assembly components
  - Half-circle radial load application part (to outer ring of the ball bearing)
  - Load cell arm for pin-on-disk tribometer
- Floor 3
  - Encoder seat
  - Encoder shaft coupling part
  - Pin-on-disk load mechanism assembly components
- Floor 4
  - Arduino UNO seat
- Test rig and load cell calibration parts

Some examples of initial prints and prototypes is in figures below.

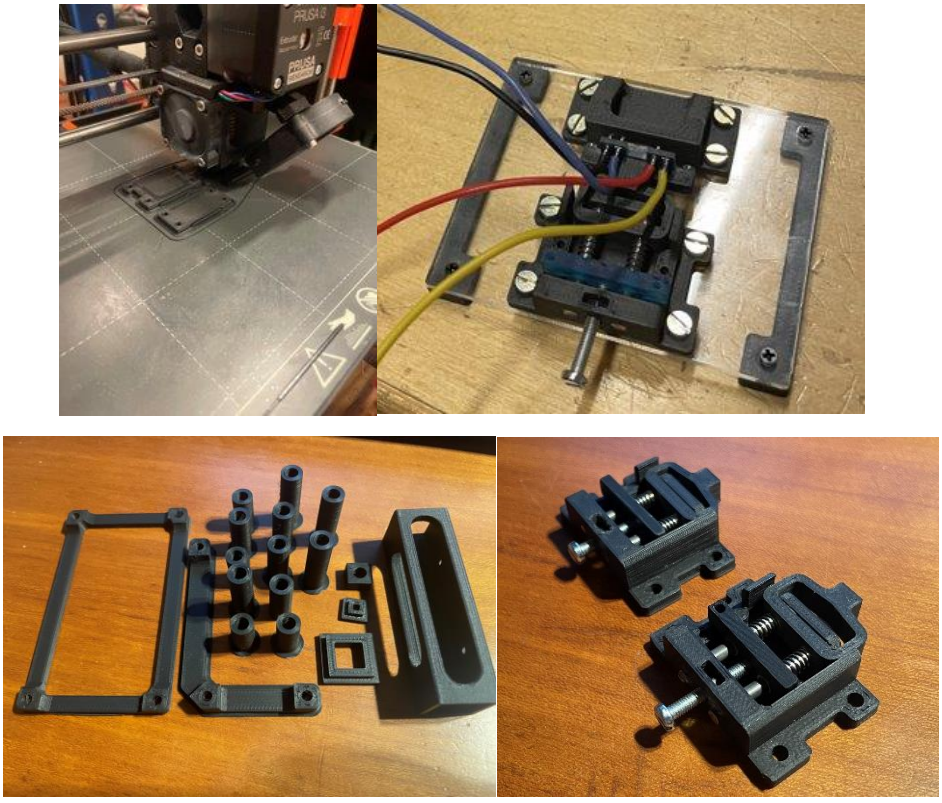

Figure 38: Printing process and prototypes

10.2. Resin 3D Printing

The moving part in the load mechanisms and the 2-leg part for the pin-on-disk tribometer are resin printed due to critical components that didn't perform as well as expected with PLA

printing. These parts became much better with resin printing. 2-leg part for pin-on-disk tribometer is in figure below.

Figure 39: Resin printed 2-leg part for pin-on-disk tribometer.

10.3. Water Jet Cutting

The external frames, floors and cage top cover part were produced through water jet cutting, utilizing 2 mm aluminium sheet metal. However, deviations from the original drawings necessitated post-processing, including the opening of countersinks for M3 bolt attachment. Sanding was also performed to achieve smoother edges and surfaces on frames and floors.

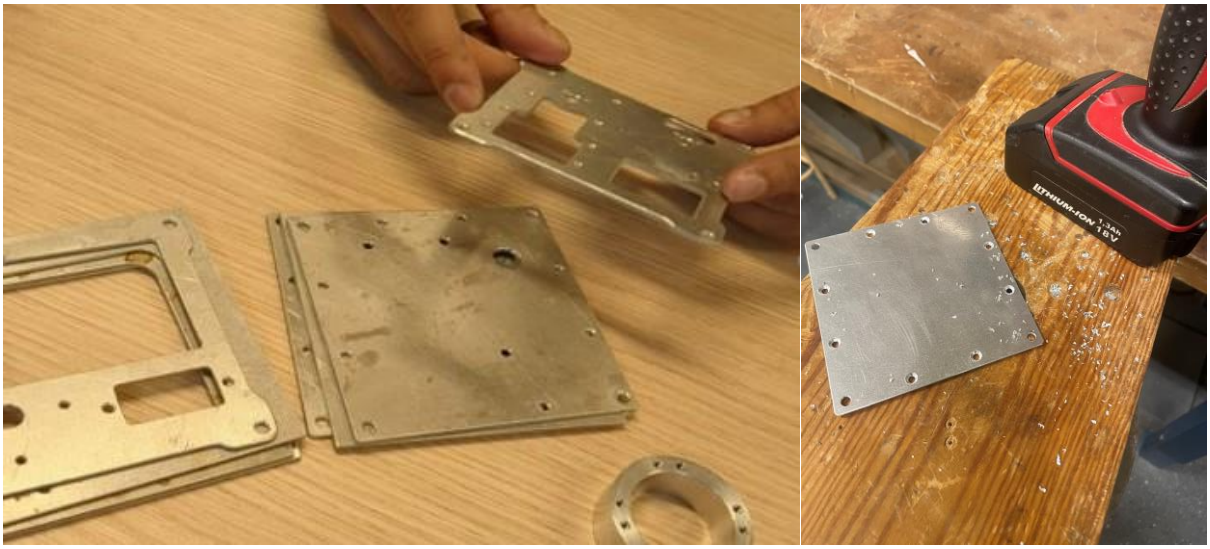

Figure 40: Water jet cut frames and floors.

10.4. Machining

Several machined parts, including motor shaft coupling parts, the cage part, the ball holder hollow cylindrical parts and the disk, were produced at KTH Prototype Center using machines such as lathe machines and press drills. Due to limited access compared to 3D printed parts, some of the machined parts did not achieve the desired accuracy, leading to post-processing requirements and necessitating design adjustments for support.

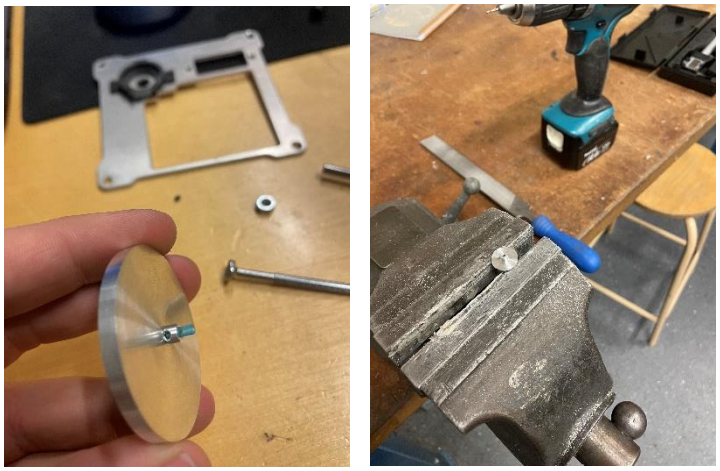

Figure 41: Machines part and after processing

10.5. Laser Cutting

The acrylic base plate was created using laser cutting on a 3mm acrylic plate.

Figure 42: Laser cutting test rig frame.

10.6. Processing of rods, L- bracket production

The 4mm rods on the edges were cut from longer rods to achieve the required length using a handsaw and then sanded with a metal file. Similarly, the 3mm rods used in the tribometers were cut to the required length with a handsaw and sanded with a metal file and bench grinder.

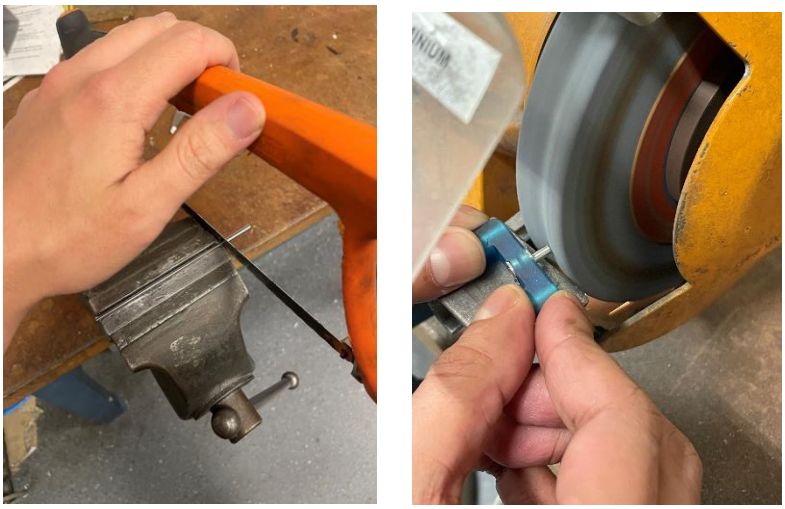

Figure 43: Rods cutting and sanding.

The L-brackets were cut from long aluminium angle profiles and refined with a metal file. Holes were drilled using a hand drill. To ensure precision in the length of the L-brackets and the position of the holes (critical for a proper fit with the water jet-cut frames), a 3D-printed mold-type part was printed and employed to facilitate sanding and cutting.

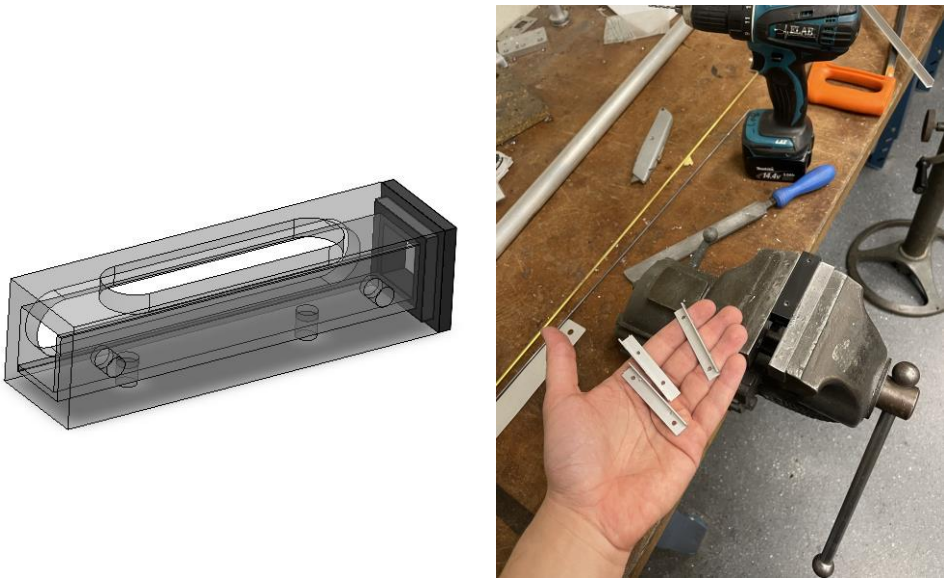

Figure 44: L-bracket production

10.7.Assembly

After soldering all electronic components to the custom PCB board, individual testing was conducted for each electrical element using the Arduino Uno and Arduino IDE software. Motor tests were performed to regulate the correct voltage for achieving a suitable rotational speed for the tribometer. Once the load cells were soldered to the custom PCB for load cell mounting, calibration (with known loads) and individual testing of each load cell were carried out before the assembly process. Extensive test runs using a breadboard were conducted to ensure the proper functionality of each component without any failures during testing of the PCB board. Test rig was performed to obtain load values for each preset of the load mechanism.

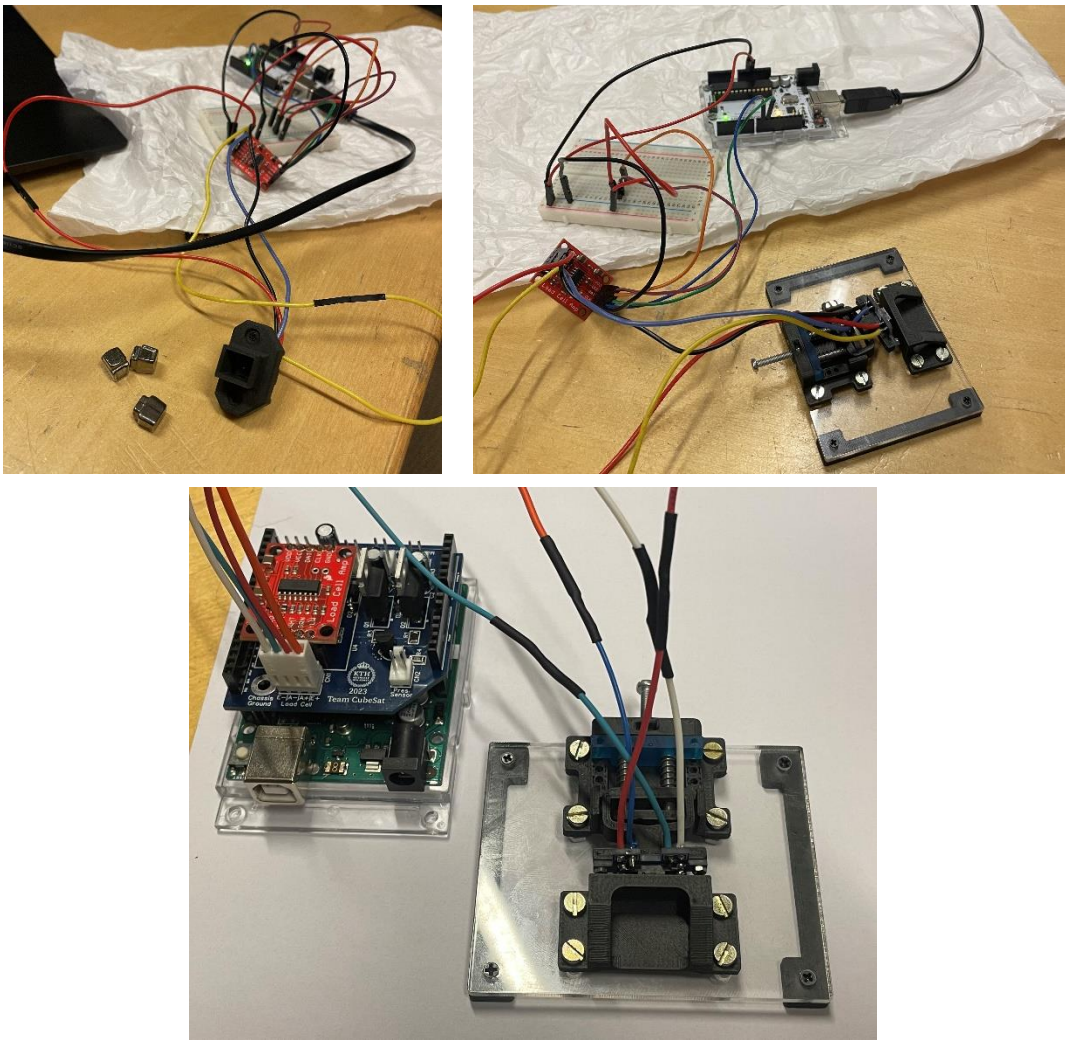

Figure 45: PCB test run for test rig to get load values of load mechanism.

After the dry slide test for the ball bearing, the bearing was lubricated with grease before assembling the entire assembly.

All electrical components were soldered with cables, and MOSFETs were used to insert pins into the right position on the PCB.

The CubeSat was assembled floor by floor, starting with the bottom frame and rods. The 4mm collars and 3D printed cylindrical hollow parts being used to secure the position of the floors. A 9V battery was placed inside the battery seat, and the seat was fixed to the bottom frame (Floor 0) using bolts from custom L brackets. Four L brackets were secured to the bottom frame.

Floor 1 was pre-assembled with two motors, each fastened with three set screws and coupled with respective shaft coupling parts to mount the test disc and bearing. The motor support parts were also attached to the same floor using three M3 bolts and nuts. The disc was secured with threads inside its hole and fixed with an M4 washer and nut. Simultaneously, the motor shaft coupling part for ball bearing tribometer was press-fitted to the inner ring, then fastened to the motor shaft, and the inner ring was secured with a water jet-cut disk and M4 nut. The loading

mechanism and load arm for the pin-on-disk tribometer were also attached to Floor 1 using various bolts and nuts.

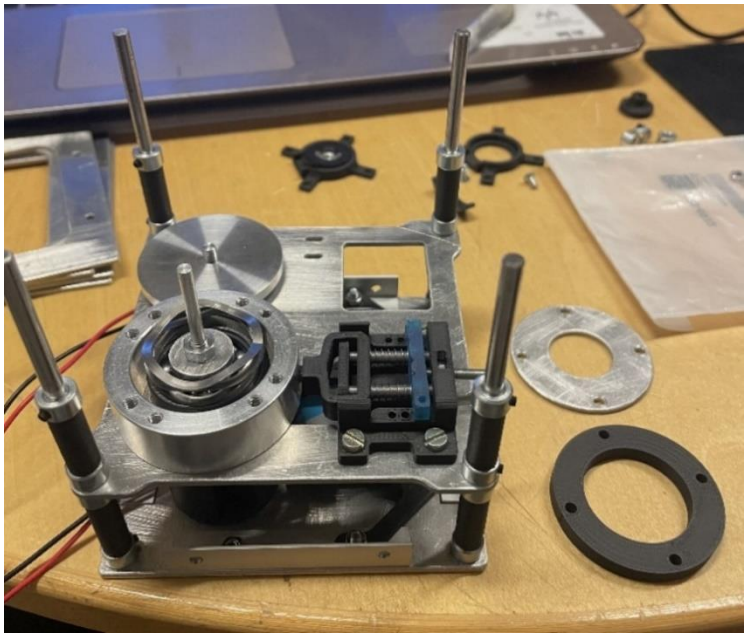

Figure 46: Assembling of the Floor 1

The encoder and load mechanism for the pin-on-disk tribometer were also attached to Floor 2 using various bolts and nuts. The encoder was fixed to the encoder seat, and the motor coupling shaft for the ball bearing tribometer was connected with a 3D printed coupling part designed to fix the encoder and shaft together. The Arduino UNO was secured to the top frame with a 3D printed seat using three M3 bolts and nuts and then the PCB board attached on the Arduino UNO.

The second floor was positioned accurately using 4mm collars and 3D printed hollow cylindrical parts through 4mm rods at the corners. Cable attachments were then completed. Finally, the top frame part was added after assembling all the floors. Two side frames were already attached before assembly to the base frame, and the other two side frames were also connected to the top frame before the final assembly, making the entire CubeSat assembly more efficient and easier. This approach helped avoid space constraints for tightening bolts and nuts through L brackets and frames during assembly.

The remaining connections between the frames and L-brackets were completed, and the final assembly was finished. This phase presented some challenges due to limited space for tightening the M3 bolts and nuts, but all mechanical and electronical connections were successfully secured. All cables were neatly arranged inside. While there could have been fewer cables to create more space inside the CubeSat. The design allowed for effective cable management, with cables transferred through floors and secured on the bottom frame, utilizing the available space efficiently. The final assembly of the CubeSat is in figure below:

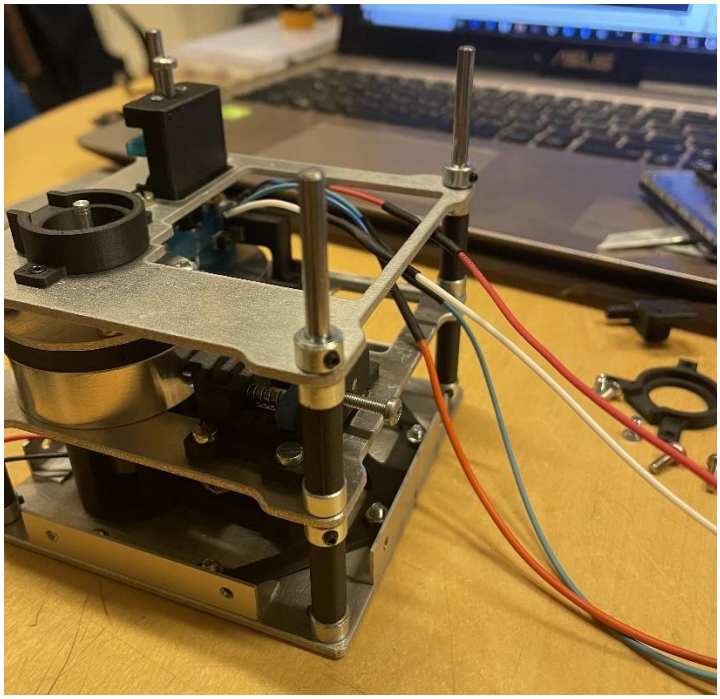

Figure 47: Assembling of the Floor 2

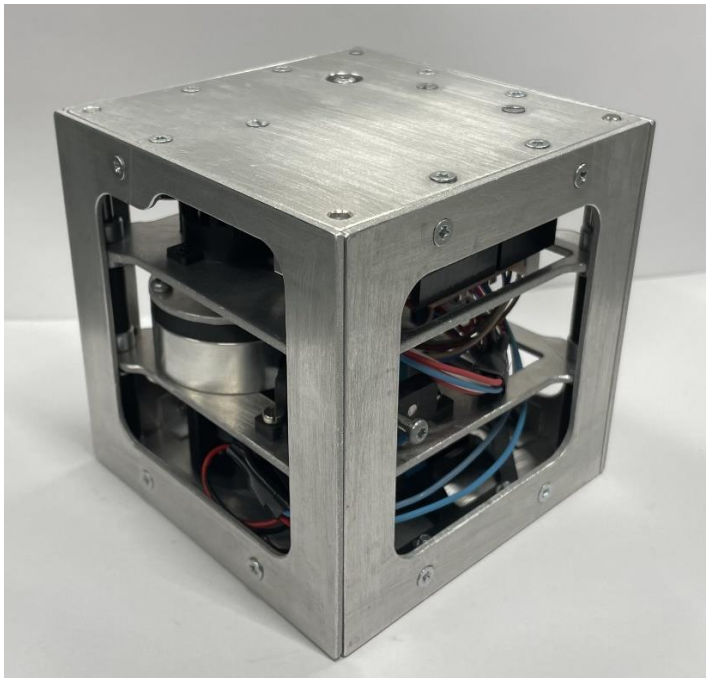

Figure 48: Assembled CubeSat

11. RESULTS

There were several key issues that were experienced throughout the data collection phase that negatively impacted the results and quality of data that was obtained in this process. The first issue in the pin-on-disc tribometer was that due to manufacturing imperfections and the motor shaft having a sharp and non-planer cut to its threads the disc did not sit level with the floor of the CubeSat. This caused significant problems in the system and oftentimes prevented the pin

from contacting the load cell, ultimately resulting in skewed data. When the loading applied from the load arm was high the issues with disc wobble were exacerbated and the motor would bind and stall. The maximum applied load that could be used in the pin-on-disc setup because of the issues with the disc was the weight of the load arm assembly. When load applied to the disc was equivalent to or greater than the load applied at preset one of the load arm, binding and motor stall issues were observed and no usable data could be collected.

In the ball bearing tribometer the key issue was compatibility between the motor and the encoder. The rotational torque of the encoder was too great for the motor. When the motor shaft was coupled to the encoder the frictional force was too great for the motor to overcome and this resulted in the motor stalling. Due to the inability to collect data from the bearing tribometer no usable data was able to be obtained. In an attempt to combat the issues of the encoder being too hard for the motor to spin it was replaced with a magnet. The magnet created changes in the magnetic field as the motor shaft rotated at different speeds and this was able to be tracked using a cell phone camera and app. The data collected from this set up was inconsistent and no real conclusions were able to be drawn from it, so it will not be included in this report.

10.1. Pin-on-disc

10.1.a. Pilot test

In figure 4, The graph of the pilot test for the pin-on-disc tribometer can be seen. From this graph it can be observed that once the motor has begun to reach its top speed, set in code, the coefficient of friction peaks at its highest point; this occurs between 30 and 35 seconds. Prior to the disc reaching its running speed the impact of the wobble on the data can be seen as the graph shows a line with many peaks and valleys. The peaks and valleys prior to roughly 30 seconds on the graph show a constant change in friction coefficients resulting from the pin temporarily losing contact with the disc and the application of uneven loading on the disc introduced by the wobble of the disc.

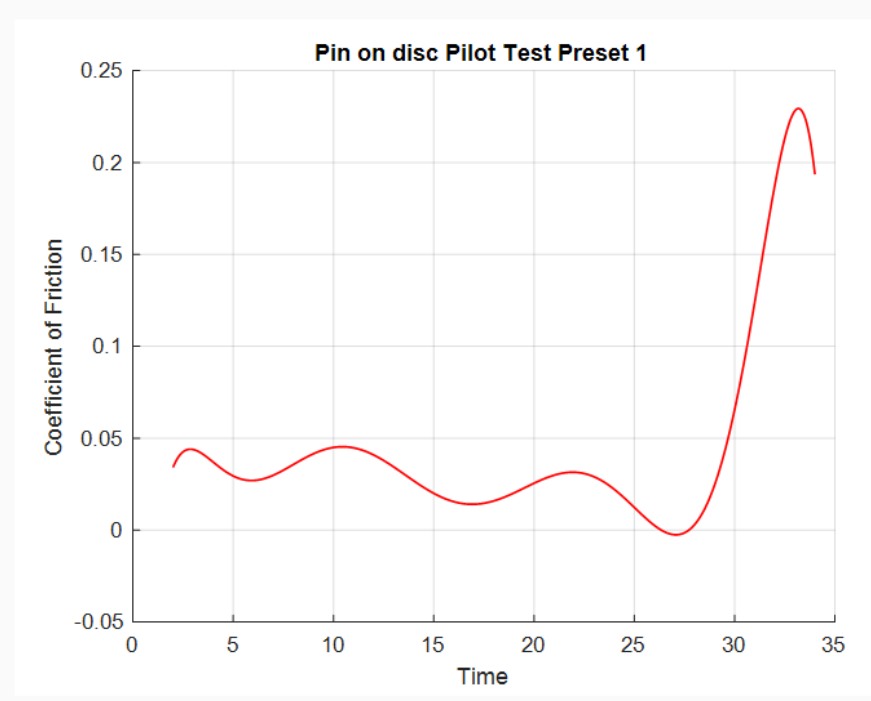

Figure 49: Trend line for pilot test data collected from the loaded position of preset one on the pin-on-disc.

10.1.b. Dry contact tests

Figures 5, 6, and 7 show the trendlines of the data obtained from running the pin-on-disc tribometer using the weight of the load arm mechanism and no additional loading. In figures 5 and 7 between zero and ten seconds the coefficient of friction reading rapidly increases; this is due to the motor going through the spin up process until it reaches its running speed. The rapid increase in speed causes the increase in friction. In figure 6 the friction coefficient starts at a high peak, due to the motor spin up process. Figure 6 does not show the rapid increase in friction that figures 5 and 7 show because by the point that data collection started, the motor had reached its running speed. The data in figure 5 remains stable and has little change to the coefficient of friction after the initial spin up period of the motor until motor power is cut and the disc slows down resulting in a lower coefficient of friction. Figures 6 and 7 both show a drop in the coefficient of friction over time after the motor has reached running speed until motor either stalls, resulting in a rapid increase in the coefficient of friction at the end of the run time in figure 6, or was turned off resulting in data collection ending in figure 7. The decrease in the coefficient of friction over the three test runs indicates that abrasive wear has occurred, meaning that the rough surface of the disc has become smoother.

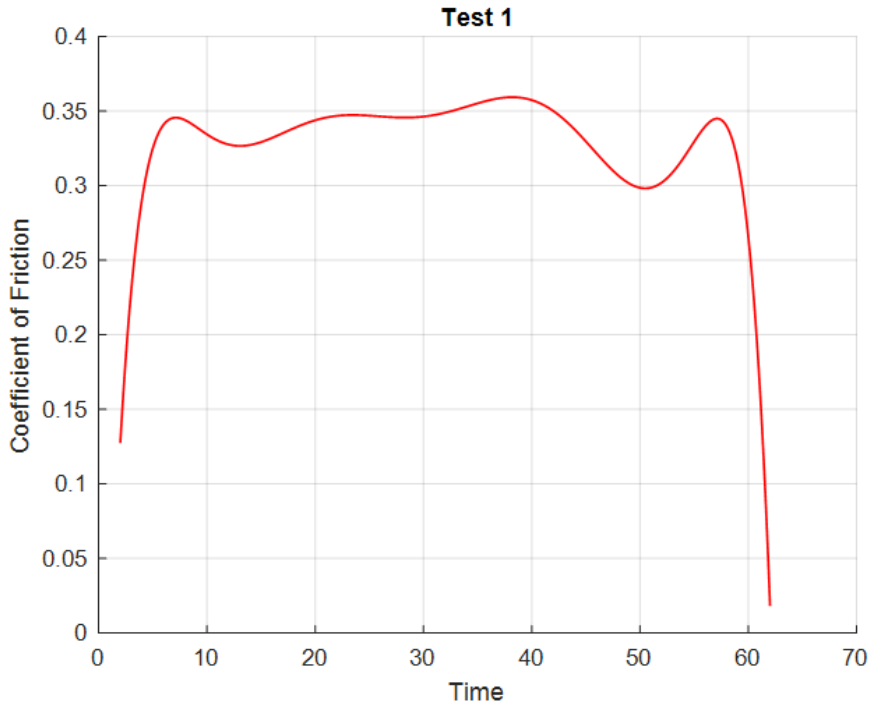

Figure 50: This is a graph of the data trends over time for the first test run on the pin-on-disc tribometer under the loading weight of the load arm assembly.

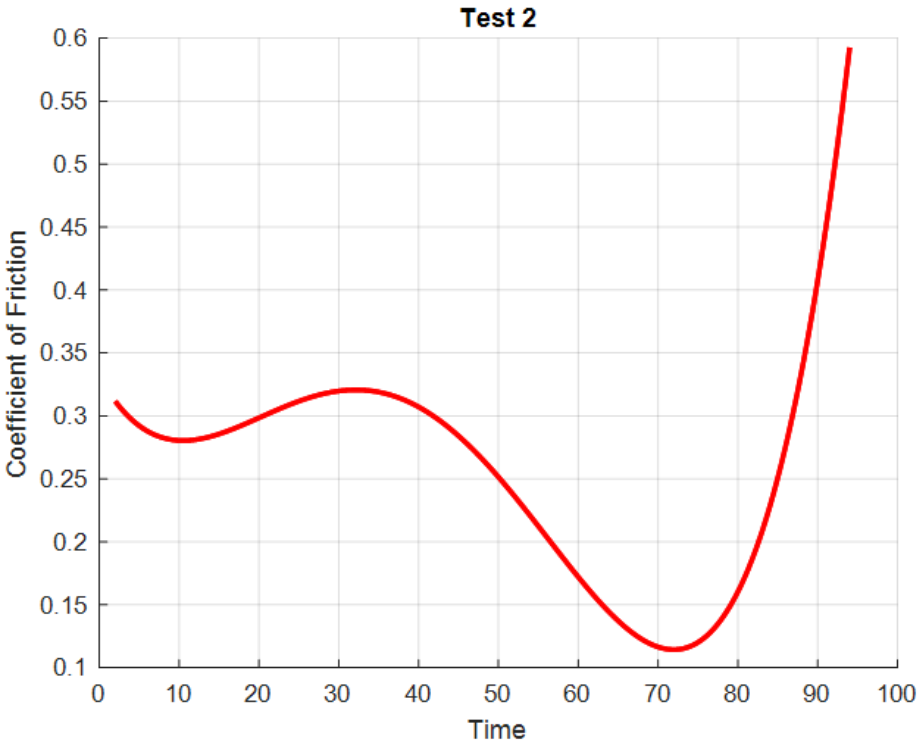

Figure 51: This is a graph of the data trends over time for the second test run on the pin-on-disc tribometer under the loading weight of the load arm assembly.

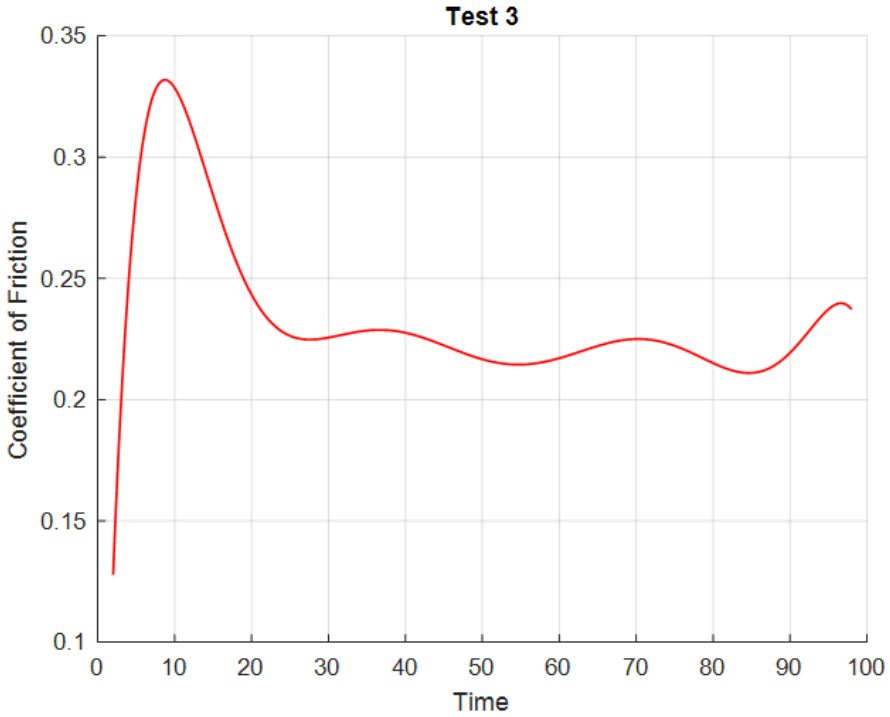

Figure 52: This is a graph of the data trends over time for the third test run on the pin-on-disc tribometer under the loading weight of the load arm assembly.

12. REFLECTIONS

This project helped the team understand the importance of critically evaluating past designs based on strict rubrics which allows us to gain a deeper understanding on the reasons of failures and scope of improvement.

The scale of working of the tribological elements and their components are extremely small, which requires precise modelling of both the components that make up the system and theoretical models used to understand the response of the same systems. This gave us an appreciation of analysing the finer details of any system.

The positive discourse between the team and the projects stakeholder allowed for the creation of concepts and ideas that considered and worked around many problems that the previous CubeSat design faced, hence improving our communication of queries and further bettering our understanding of technical problems.

Although the bearing system and encoder system worked smoothly independent of each other, when combined failure in the mechanism was brough about the unsurmountable increase in friction torque. This gave us the understanding that components must be studied and evaluated closely on both a unit level and a system level to ensure expected working to obtain usable results from the tests performed. A simulated test run of just the encoder detached from the ball bearing and its motor is presented below, which shows the expected coefficient of friction fitting well with the simulated trends of the SKF model, where an increase in RPM leads to an increase in the value of friction [14]. This graph indicated that these theoretical models can be implemented in the project.

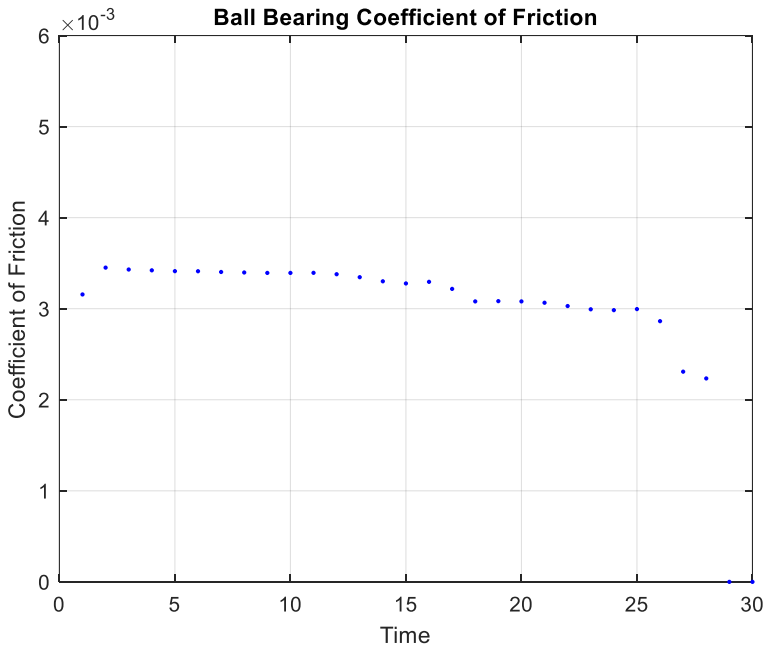

Figure 53: Expected graph of expected coefficient of friction vs time when just the encoder is manually rotated.

13. BROADER IMPACTS

This chapter serves to discuss the broader impacts of the CubeSat and its potential use for tribological data collection. In this chapter special attention is given to the topics of function, manufacturing, and distribution of the overall CubeSat product.

13.1. Engineering Ethics

The goal of this project was to redesign a space compatible CubeSat and prototype a terrestrial twin that can preform tribological tests on different types of lubricants to evaluate lubricants in space environments. This project adheres to the American Society of Mechanical Engineers (ASME) engineering code of ethics:

1. This project uses the knowledge and skills of all involved engineers to advance human welfare. The study and evaluation of different lubricants for spaced based applications provides the ability for engineers to make informed decisions in the design and construction process of space-based payloads. The information that this project seeks to lay the groundwork for can lead to more effective use of materials and designs ultimately limiting the amount of waste generated from rapid part wear and poor lubricant function in space environments. This can aid in further space exploration and research which can lead to new scientific discoveries.
2. This project was conducted and completed in an honest and impartial manner. The CubeSat was designed and prototyped to the best of our ability and all short comings were documented and discussed throughout this paper. Solutions to short comings and suggested future work was also documented in the future work section of this report.
3. This project strives to increase the competence and prestige of the engineering profession. This is accomplished in this project by the use of novel designs of tribometers in a CubeSat compatible size and format, as well as through the information that this project is designed to study and produce which is aimed at increasing the knowledge of space compatible lubricants and effective CubeSat based tribometers. This effectively increases the competence and prestige of the engineering profession by providing replicable designs and results that can be used to further space-based research objectives as well as serve to inform space-based payload designs.

13.2. Societal and Global Impacts

The potential impacts of this project are that the terrestrial prototype can increase interest and present the groundwork for the space-based counterpart to be funded and constructed. Funding of this type of research and the space compatible counterpart of this CubeSat will increase the understanding of long-term performance and effects of different lubricants in space, and potentially impact design criteria of space-based payloads and spacecrafts, which could lead to increases in space-based experimentation and exploration due to improved performance of materials like lubricants.

13.3. Environmental Impacts

The CubeSat prototype was designed with special consideration being given to reuse as many components from the previous prototype as possible. Parts such as the motors for the tribometers and the microcontroller were reused in the current prototype to limit the amount of waste generated in the redesign and prototype process. The space compatible version of the CubeSat was designed in accordance with the orbital debris mitigation requirements for CubeSats to ensure that the CubeSat module does not become space junk and completely burns

up on re-entry at the end of its lifecycle. This ensures that if the space compatible version is constructed it will not pollute the space environment or present harm to people or the Earths' environment. Furthermore, the information that can be obtained from this project about lubricants and their performance over time in space environments can further reduce material waste produced in space applications by identifying lubricants that will preform well in space and potently lengthen the life cycle of mechanical parts that experience frictional ware.

13.4. Codes and Standards

The CubeSat prototype and space compatible design were designed to conform to NASA and ESA standards for CubeSats. The prototype CubeSat was unable to undergo all testing outlined under theses standards due to the high cost the tests impose. The terrestrial prototype does not conform to the power supply standards set forth by NASA and ESA because it is designed to be a module of a larger 3U CubeSat and once it is integrated into the 3U CubeSat system it will be connected to that system's power system. The testing that was able to be conducted on the prototype was FlatSat testing and individual verification testing of all electrical components to ensure they were in working order prior to assembly. Both versions of the CubeSat conform to NASA and ESA standards regarding frame and floor setup/design, as well as electrical system regulations.

13.5. Economic Factors

In the CubeSats' current position, it does not impose any long-term economic costs or benefits. This is due to the space compatible design not being constructed and tested and due to the project being a stand-alone proof of concept. This means that it is not going into production past the level it is built and executed to at the current time. Should the Space compatible version of this CubeSat design be adjusted to remediate the short comings of the prototype CubeSat, the components be upgraded to space compatible parts, and the CubeSat undergoes the extensive testing required by NASA and ESA before it can be considered for launch a high cost will be incurred. On the other hand, the benefits to the global scientific community are sure to help offset the incurred costs of launching and operating this CubeSat module.

14. CONCLUSIONS

The aim of the project was to evaluate and redesign the previous iteration of the CubeSat and perform friction tests on its tribometers. This project took us over different phases such as evaluating previous designs, creating a Gantt chart, concept generation, concept selection, design, manufacturing, assembling, and testing.

The first phase of the project was mainly focused on conducting a Critical Design Review of the previous iteration of the CubeSat. This review resulted in identifying the key drawbacks in the CubeSat and focus on what aspects were to be improved. The issues were primarily in manufacturing and assembly due to small size of the CubeSat.

Upon determining we proceeded with generating conceptual solutions to improve the design of the tribometers. Five to four concepts were generated for each tribometer, and they were selected by using the Pugh Evaluation Matrices. The final concept for the bearing tribometer was based on rpm reduction at constant current to determine the frictional forces, and the pin on disc concept was based on diametrical loading and load cell sensor to detect frictional values.

The design process focused on iterating the loading mechanisms for both the bearing and pin on disc tribometers to achieve the necessary axial and radial loading for bearing tribometer and

axial loading for pin on disc tribometer. Majority of the parts were 3D printed to account for the difficulties in manufacturing at that size. 3D printing also allowed for rapid prototyping and adjustments in design of the mechanisms.

On the electrical side a custom PCB (Printed Circuit Board) was designed to reduce wire runs and make a more compact arrangement of the control module. The custom PCB was designed such that it was attached to the control module to keep it as a single unit. PCBs were also created for load cell sensor as they are very difficult to mount. This allowed for easier installation of load cell sensors and placement of battery within the CubeSat.

The manufacturing of most machined parts was done in house at KTH. Certain fits and tolerances could not be achieved which resulted in modifying the parts of the bearing motor shafts for alternative fixes. The assembly of the CubeSat was as expected however we faced an issue with the motor shaft attachment of the Pin on Disc tribometer. The disc when threaded onto this shaft would result in an inclined disc which would induce wobble into the disc.

The testing because of this was not as expected. Tests conducted on the pin on disc were affected by the wobble in the disc which can be seen in the collected data. Unfortunately, no data could be measured from the bearing tribometer as the motor did not provide enough torque to rotate the encoder.

The next iteration of the CubeSat should focus on getting new motors that can provide the necessary torque for the encoder or purchase encoders with lesser torque requirements.

15. FUTURE WORK

This year's CubeSat was based on the improvements as suggested in the Critical Design Review from the first half of the project.

In the design of the CubeSat, we successfully enclosed all the components within the frame of the CubeSat. The new compact designs and the inclusion of a custom PCB allowed for shorter wire runs and better spacing of the components in the CubeSat. However, there were some issues faced with design and manufacturing motor shaft attachments. For the bearing tribometer the motor shaft needed to be press fit with the inner ring of the bearing, since this was not possible, we made changes to the shaft to account for a nut and washer to couple the shaft to the inner ring of the bearing. On the Pin on disc tribometer we didn't account for the oblique thread to results on an inclined disc. Therefore, minor improvements in design and outsourcing the manufacturing would be the next step for this project.

As we were working with a custom PCB and with a range of sensors for the first time, our inexperience in selecting the sensors, resulted in the bearing tribometer not being able to measure the required data. The optical encoder we had selected required more torque than that provided by the motor. As we were improving on last year's CubeSat we proceeded to reuse as many components as possible. However, moving forward we would recommend getting stronger motors while keeping the same size constraint.

When it comes to the theoretical models of the CubeSat tribometers, the Pin on Disc and Bearing tribometer needs a model that also accounts for the temperature of the system. The encoder method of measuring friction doesn't isolate the friction experienced by the bearing it also accounts for the friction due to the encoder and motor bearings.

Calibration of encoder was also quite difficult to achieve as we did not have access to a laser tachometer, more work needs to be done on calibrating the encoder using alternative methods

such as Resor method. If the project continues to use the encoder bearing tribometer, it’s advisable to use a laser tachometer for calibration.

REFERENCES

[1] Globerson, Shlomo. "Impact of various work-breakdown structures on project conceptualization." International Journal of Project Management 12.3 (1994): 165-171.

[2] Knight, Paul, and James O. Jenkins. "Adopting and applying eco-design techniques: a practitioners perspective." Journal of cleaner production 17.5 (2009): 549-558.

[3] Roberts, E. W. "Space tribology: its role in spacecraft mechanisms." Journal of Physics D: Applied Physics 45.50 (2012): 503001.

[4] Fusaro, Robert L. Lubrication of Space Systems (c). No. NAS 1.15: 111740. 1995.

[5] Jones Jr, William R., and Mark J. Jansen. Space tribology. No. NAS 1.15: 209924. 2000.

[6] Thurston, Deborah L. "A formal method for subjective design evaluation with multiple attributes." Research in engineering Design 3.2 (1991): 105-122.

[7] Goncalves, David, et al. "Friction torque in thrust roller bearings lubricated with greases, their base oils and bleed-oils." Tribology International 107 (2017): 306-319.

[8] Ianuş, G., et al. "Power loss in grease lubricated ball bearings." IOP Conference Series: Materials Science and Engineering. Vol. 724. No. 1. IOP Publishing, 2020.

[9] B. Metz, “Optimising 3-component force sensor installation for satellite force limited vibration testing” 2014, 28th Space Simulation Conference - Extreme Environments: Pushing the Boundaries.

[10] Miyoshi, Kazuhisa. "Aerospace mechanisms and tribology technology: Case study." Tribology International 32.11 (1999): 673-685.

[11] “CubeSat101 - Basic Concepts and Processes for First-Time CubeSat Developers”, NASA CubeSat Launch Initiative For Public Release, Revision Dated October 2017.

[12] Maxon, DCX 16 S Ø16 mm, Precious Metal Brushes CLL, sintered sleeve bearings, last accessed 2023/12/11, <https://www.google.com/url?q=https://www.maxongroup.com/maxon/view/product/motor/dcmotor/DCX/DCX16/DCX16S01EBSL512?target%3DarticleDetail&sa=D&source=docs&ust=1671627916061902&usg=AOvVaw0YeN-pqvLy7nbSY607LY2F>.

[13] Wiwattananon, Peerawan, and Robert G. Bryant. Performance Comparisons and Down Selection of Small Motors for Two-Blade Heliogyro Solar Sail 6U CubeSat. No. NF1676L-21629. 2015.

[14] J. Wu, T. Liu, N. Yu. et al., “A Pin-on-Disk Tribometer for Friction and Lubricating Performance in mm-Scale”, Tribology Letters 69, Feb. 2021, Art. n. 36, doi:10.1007/s11249-021-01409-x.

APPENDIX 1: PROJECT PLAN

A1. Project Charter

Project Name	Redesigning and development of the CubeSat for friction testing in space	**Project Code**	3

Start Date	2023/02/09	**End Date**	2023/12/15

Sponsor	**Team Members**
Prof. Ian Sherrington	Abhay Menon
Project Manager	Dannel Jacob
Abhay Menon	Ananthakrishna Ayankalath Thekkepat
Support	Harun Gungør
Prof. Kjell Andersson	Samantha Rosenberg
Prof. Sergei Glavatskih	

Goals and Objectives	**Scope**
• To redesign and develop a modular tribometer instrument in a CubeSat format. • To enable friction testing in space and provide a framework for more accessible tribological validation of concept lubricant chemistries and materials. • To test a series of heritage space lubricants and novel ionic lubricants in a simulated space environment at KTH. • Design a modular instrument that can be easily assembled and disassembled for maintenance and testing purposes. • Develop a CubeSat format that allows the instrument to fit within the limited space and weight restrictions of a CubeSat. • Build a tribometer that can operate in a microgravity environment and	• Requirement specification and time plan • Concept development, evaluation, and subsequent selection of the best concept • Detailed design of the components, selection of the parts, driving system, and sensors • Manufacturing and assembling of the modular instrument. • Basic functional tests to commission the modular instrument.

withstand the harsh conditions of space. • Conduct friction testing on different types of lubricants, including concept lubricant chemistries, heritage space lubricants, and novel ionic lubricants, in a simulated space environment at KTH. • Collect and analyse data on friction and wear of the lubricants tested and compare the results to those obtained on Earth. • Publish the results in a scientific journal and share the findings with the wider research community.	

Approach
• Literature Survey • Product Design Specification • GANTT chart (Project Charge etc) • Concept generation • Concept evaluation • Detailed design and analysis (CAD) • Optimization of the design (after testing, CAE) • Manufacturing and assembling of prototype. • Testing • Weekly meetings and questionnaire

Milestones	**Dependencies/Related Projects**
• Completion of the tribometer instrument design (Month 1) • Development and integration of the CubeSat format into the tribometer instrument (Month 3) • Completion of the simulation testing setup at KTH (Month 4) • Testing of heritage space lubricants in simulated space environment (Month 6) • Testing of novel ionic lubricants in simulated space environment (Month 9) • Data analysis and report writing (Month 10-11) • Final report submission and project completion (Month 12)	

A2. Work Breakdown Structure

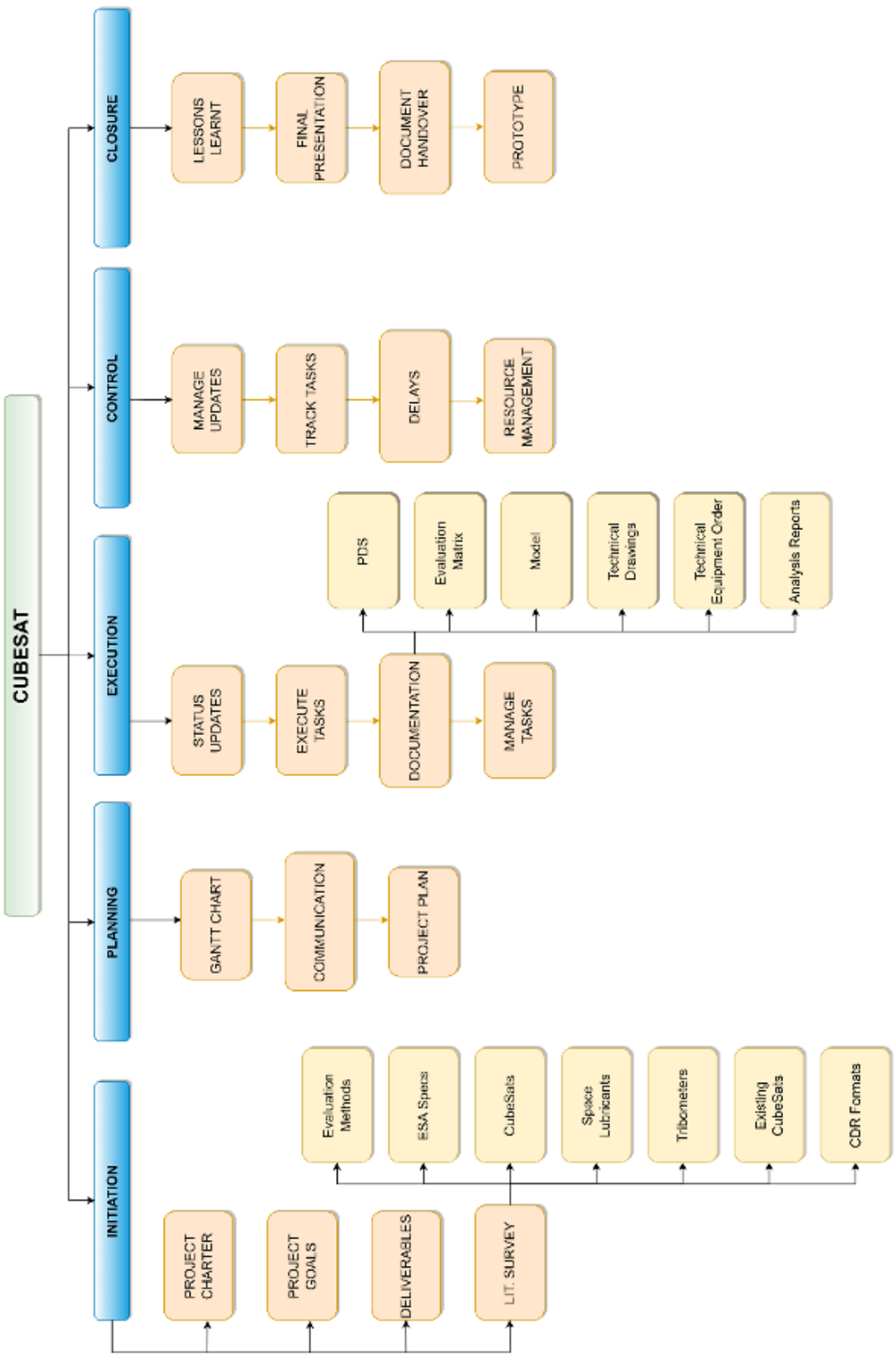

A3. Product Design Specification

Design Properties	Parameters	
	Description - Gathered Information	Current model – Implemented into our model
1. Performance	• Power: 10 W • Current: 4 • Voltage: 2.5 V	
2. Operating Environment	CubeSats works in the harsh environment of space that has high range of operating temperature and vacuum conditions of pressure. • Temperature: (-40, +80) ºC • Pressure: 10^{-6}	
3. Size	10×10×10 cm	
4. Weight	Maximum weight: 1.33 Kg	
5. Modules	• Control Module (Includes controllers for actuators and motors to control and monitor CubeSat to be placed inside the CubeSat. • Tribometer with Lubricant • Measurement Modules (Load cell and Temperature sensors) • Load applicators (new mechanism to apply variable load for both space and earth compatible cube designs)	
6. Tribometer	• Lubrication Region -Boundary Lubrication -Mixed Lubrication • The contact in Tribometer must represent real contact used in space Compactness of Tribometer is studied to allow for optimum space utilization Working Torque: 2-5 mNm	
7. Redundancy	Redundancy is required to ensure the entire mission does not seize in the condition of failure such as motor failure.	
8. Life in service	Maximum Life Expectancy: 1 year	
9. Maintenance	No maintenance system required; components must be robust enough to function throughout duration of mission	
10. Target product cost	To be decide based upon materials, prototyping and testing	

11. Installation	• CubeSat in installed into a Dispenser system which is usually of 3U size with the help of series of rails. • Bearing should be preloaded There must be no interference between components. • All bundles must be fixed on board to ensure modularity Once installed, all non-essential components are removed to meet expected weight and standard compatibility.	
12. Materials	• Material is chosen based on requirement of the project: -Aluminium 7075, 6061, 5005, Magnesium and Tin alloys. • To add materials suitable for earth compatible CubeSat • Lubricants properties must be of: -High viscosity index -Low pour point -Very low vapour pressure -Low volatility • Ex. Mineral oils, Perflouropolyalkylethers(PFPAE), Solid lubricants(MoS_2)	
13. Standards and Specifications	ESA specification: • ECSS-E-ST-33-01C Mechanisms • ECSS-Q-ST-70-01C Space Environment • ECSS-Q-ST-70-01 Cleanliness and Contamination Control	
14. Testing	Primary Tests • Flat Sat Test	
15. End of life	Burns up on re-entry	
16. Existing Products	• MISSE 7 - Seventh series of experiments products performed on the International Space Station • TRIBOLAB - Tribological tests on flight in European Technological Facility	

17. Quantity	One physical CubeSat for physical testing designed to allow for theoretic interfacing of other CubeSats	
18. Safety Issues	• Mechanisms containing electrical parts and circuitry shall be protected against overcurrent due to abnormal applied voltage. • Electromagnetic radiation shielding	
19. Timescales	Entire Project: Feb 2023 –Dec 2023 • Phase 1: Feb – Mar • Phase 2: Mar – May • Phase 3: Aug - Oct • Phase 4: Oct - Dec	

A4. Gantt Chart

CubeSat Evaluation & Design

Project Start	Thu, 09-Feb-23	Progress
Display Week	13	49%
Today	Tue, 23-May-2023	

Tasks	Outcome	Progress	Start	End
Phase 1		94%	09-Feb-23	02-Mar-23
Start-up meetings		100%	23-Feb-23	23-Feb-23
Literature Survery		60%	15-Feb-23	28-Feb-23
CubeSat		60%	15-Feb-23	28-Feb-23
Tribometer		60%	15-Feb-23	28-Feb-23
Lubricants		60%	15-Feb-23	28-Feb-23
ESA Guidelines		60%	15-Feb-23	28-Feb-23
Requirements Analysis		100%	28-Feb-23	02-Mar-23
Product Design Specification		100%	28-Feb-23	02-Mar-23
Work Breakdown Structure		100%	28-Feb-23	02-Mar-23
Evaluation		100%	02-Mar-23	02-Mar-23
	PDS	100%	28-Feb-23	02-Mar-23
	WBS	100%	28-Feb-23	02-Mar-23
Phase 2		100%	03-Mar-23	22-May-23
Concept Generation		100%	03-Mar-23	20-Apr-23
Concept Evaluation		100%	03-Mar-23	20-Apr-23
Concept Selection		100%	03-Apr-23	20-Apr-23
Concept Development		100%	18-Mar-23	20-Apr-23
Evaluation		100%	22-May-23	22-May-23
	Evaluation matrix	100%	22-May-23	22-May-23
	Morphological chart	100%	22-May-23	22-May-23
Phase 3		0%	21-Apr-23	20-Aug-23
System level design		0%	21-Apr-23	03-May-23
Detailed design		0%	21-Apr-23	03-May-23
Simulations		0%	21-Apr-23	03-May-23
Critical Design Review		0%	21-Apr-23	15-Jun-23
Design optimization		0%	04-May-23	19-May-23
Design Finalization		0%	04-May-23	19-May-23
Manufacturing Drawings		0%	20-May-23	23-May-23
Evaluation		0%	20-Aug-23	20-Aug-23
	CDR Report	0%	20-Aug-23	20-Aug-23
	CAD models	0%	20-Aug-23	20-Aug-23
	Simulation Reults	0%	20-Aug-23	20-Aug-23
	Manufacturing drawings	0%	20-Aug-23	20-Aug-23
Phase 4		0%	01-Jun-20	10-Jan-23
Ordering Parts		0%	19-May-23	05-Jun-23
Manufacturing		0%	24-May-23	15-Jul-23
Prototype development		0%	15-Jul-23	15-Aug-23
Testing		0%	15-Aug-23	15-Oct-23
Refinement		0%	15-Aug-23	15-Oct-23
Implementation		0%	15-Oct-23	10-Jan-23
	Testing protocol	0%	30-Sep-23	10-Jan-23
	Testing protocol	0%	30-Sep-23	10-Jan-23
	Test results	0%	30-Sep-23	10-Jan-23
		0%		10-Jan-23

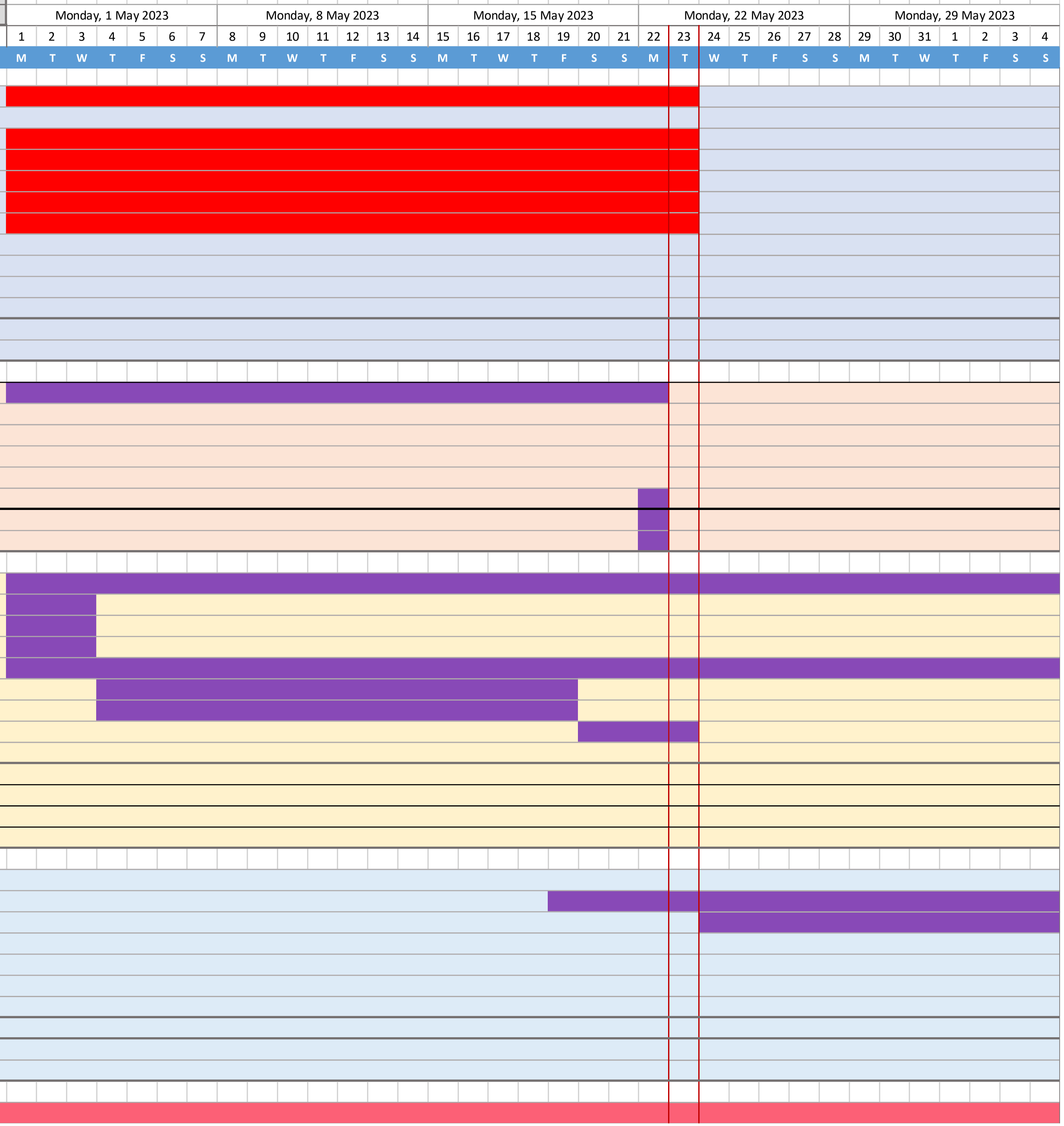

A5. Product Baseline Requirements

The Product Baseline Documents are the documentations of the components used in the CubeSat to measure the forces, amplify and transmit data.

The components used are:

- Motor: Maxon DCX 16 S

VALUES AT NOMINAL VOLTAGE	
Nominal voltage	6 V
No load speed	6580 rpm
No load current	29.6 mA
Nominal speed	3770 rpm
Nominal torque (max. continuous torque)	5.3 mNm
Nominal current (max. continuous current)	0.648 A
Stall torque	12.6 mNm
Stall current	1.48 A
Max. efficiency	74 %
CHARACTERISTICS	
Terminal resistance	4.06 Ω
Terminal inductance	0.131 mH
Torque constant	8.53 mNm/A
Speed constant	1120 rpm/V
Speed / torque gradient	533 rpm/mNm
Mechanical time constant	6.05 ms
Rotor inertia	1.08 gcm²
MECHANICAL DATA	
Bearing type	Waelzlager
Max. speed	8680 rpm
Axial play	0 mm, at radial load < 0.8 N
	0.1 mm, at radial load > 0.8 N
Radial play	0.015 mm
Max. axial load (dynamic)	0.8 N
Max. force for press fits (static)	18 N
(static, shaft supported)	300 N
Max. radial load	10 N, 5 mm from flange
OTHER SPECIFICATIONS	
Number of pole pairs	1
Number of commutator segments	7
Number of autoclave cycles	0
PRODUCT	
Weight	26 g

- Optical Encoder –

Electrical Specifications

Encoder Function

Parameter	Conditions & Remarks	Min	Nominal	Max	Unit
Input Voltage		4.95 2.97	5.0 3.3	5.50 3.63	VDC
Supply Current	5.0 VDC 3.3 VDC			30 20	mA mA
Dielectric Strength	For 1 minute			50	VDC
Insulation Resistance	At 50 VDC			10	MegΩ
Output Code	2-Bit Quadrature Channel A leads Channel B by 90°±45° during clockwise rotation				
Sink Current	5.0 VDC 3.3 VDC	2.0mA 1.0mA			
Power Consumption	5.0 VDC 3.3 VDC			150 80	mW mW
Logic Output	Logic High Logic Low	3.8		0.8	VDC
Resolution	24				Pulses per Revolution

Mechanical and Environmental

Wave Soldering	Maximum temperature of 260°C for 5 seconds
Operating Temperature:	-10°C to +85°C
Storage Temperature:	-10°C to +100°C
Rotational Life	3 million cycles (no detent @ 30 RPM) 1 million cycles (with detent @ 30 RPM) 500k cycles (with detent @30 RPM and 300 to 350 gf of side load)
Rotational Torque Non-detent Detent	 10 gf-cm max. 78 ± 30 gf-cm
Detent Position	Every 15° ± 3° of mechanical rotation
Travel	360° endless
Operational Speed	120 RPM max.
RoHS	Fully compliant to RoHS3 directive
IP Rating	IP 50
Marking	CTS logo, part number, date code
Packaging	Standard anti-static tray packaging
Weight	1.2g

All testing is performed at room ambient conditions except as noted. Users should verify device actual performance in their specific applications
RoHS3 Directive 2015/863 Amendments of Annex II on March 31,2015
Custom and value-added options available on request. Please contact your sales representative for additional information.

Mechanical Specifications

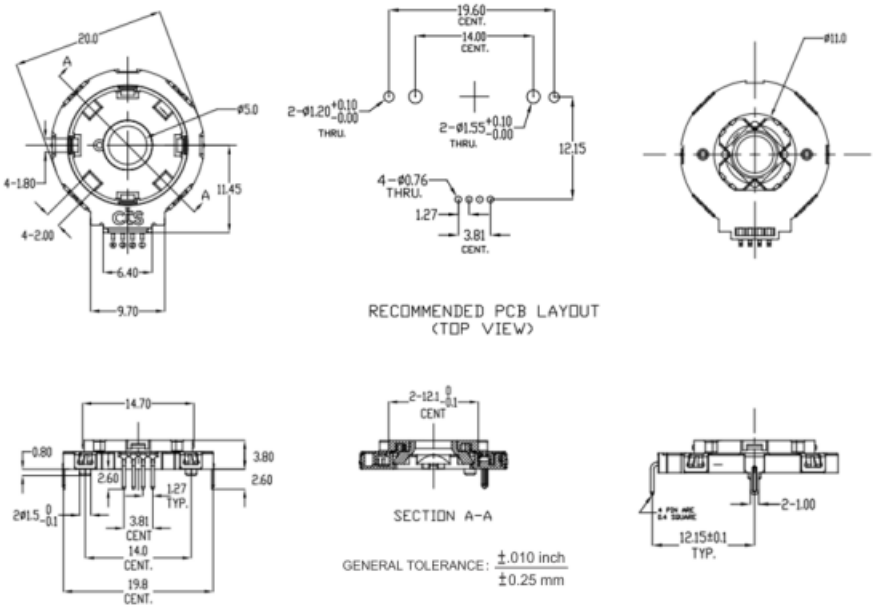

Electric Circuit And Waveform

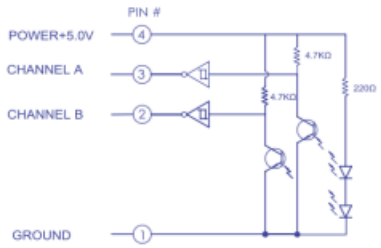

Schmitt trigger and pull-up resistor (4.7kΩ) are integrated into the optical encoder eliminating the necessity to use external pull-up resistors for the application circuit.

Standard Quadrature 2-Bit Code

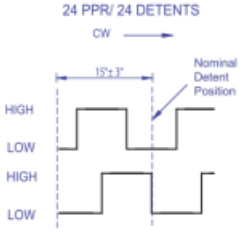

Channel A leads channel B in the CW direction, and lags in the CCW direction.

- Amplifier: HX711

Pin Description

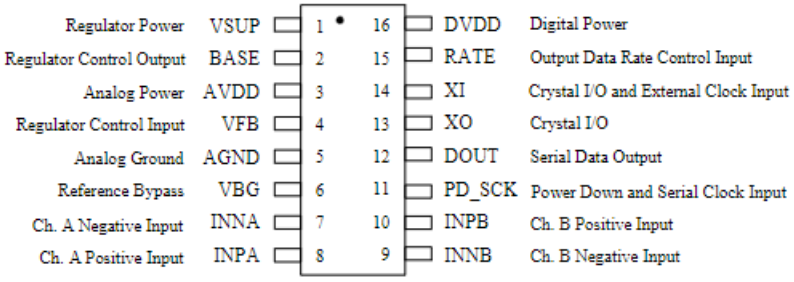

SOP-16L Package

Pin #	Name	Function	Description
1	VSUP	Power	Regulator supply: 2.7 ~ 5.5V
2	BASE	Analog Output	Regulator control output（NC when not used）
3	AVDD	Power	Analog supply: 2.6 ~ 5.5V
4	VFB	Analog Input	Regulator control input（connect to AGND when not used）
5	AGND	Ground	Analog Ground
6	VBG	Analog Output	Reference bypass output
7	INA-	Analog Input	Channel A negative input
8	INA+	Analog Input	Channel A positive input
9	INB-	Analog Input	Channel B negative input
10	INB+	Analog Input	Channel B positive input
11	PD_SCK	Digital Input	Power down control (high active) and serial clock input
12	DOUT	Digital Output	Serial data output
13	XO	Digital I/O	Crystal I/O (NC when not used）
14	XI	Digital Input	Crystal I/O or external clock input, 0: use on-chip oscillator
15	RATE	Digital Input	Output data rate control, 0: 10Hz; 1: 80Hz
16	DVDD	Power	Digital supply: 2.6 ~ 5.5V

Table 1 Pin Description

- Microcontroller: Arduino Uno Rev3

  - **ATMega328P** Processor
    - **Memory**
      - AVR CPU at up to 16 MHz
      - 32KB Flash
      - 2KB SRAM
      - 1KB EEPROM
    - **Security**
      - Power On Reset (POR)
      - Brown Out Detection (BOD)
    - **Peripherals**
      - 2x 8-bit Timer/Counter with a dedicated period register and compare channels
      - 1x 16-bit Timer/Counter with a dedicated period register, input capture and compare channels
      - 1x USART with fractional baud rate generator and start-of-frame detection
      - 1x controller/peripheral Serial Peripheral Interface (SPI)
      - 1x Dual mode controller/peripheral I2C
      - 1x Analog Comparator (AC) with a scalable reference input
      - Watchdog Timer with separate on-chip oscillator
      - Six PWM channels
      - Interrupt and wake-up on pin change
    - **ATMega16U2 Processor**
      - 8-bit AVR® RISC-based microcontroller
    - **Memory**
      - 16 KB ISP Flash
      - 512B EEPROM
      - 512B SRAM
      - debugWIRE interface for on-chip debugging and programming
    - **Power**
      - 2.7-5.5 volts

- Load Cell Sensor

Figure 1. Excitation Schematic (Excitation 5 Vdc Typ., 6 Vdc max.)

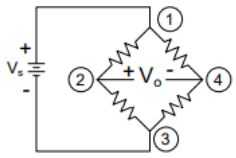

1. Circled numbers refer to sensor terminals (pins).
   Pin 1 = Supply Vs (+), Pin 2 = Output Vo (+), Pin 3 = Ground Vg (-), Pin 4 = Output Vo (-)
2. The force sensor may be powered by voltage or current. Maximum supply voltage is not to exceed 6 V. Maximum supply current is not to exceed 1.2 mA. Power is applied across Pin 1 and Pin 3.
3. The sensor output should be measured as a differential voltage across Pin 2 and Pin 4 (Vo = Vo(+)-Vo(-)). The output is ratiometric to the supply voltage. Shifts in supply voltage will cause shifts in output. Neither Pin 2 nor Pin 4 should be tied to ground or voltage supply.

Figure 2. Sensor Mounting Diagram (For reference only: mm/[in].)

FSS005WNGX, FSS010WNGX, FSS015WNGX, FSS020WNGX

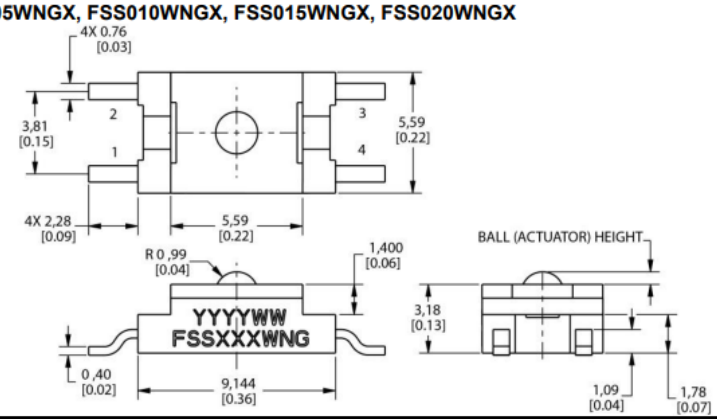

Force Sensing Range	Ball (Actuator) Height
0 N to 5 N	0.375 ±0.10 mm [0.0148 ±0.0039 in]
0 N to 10 N	0.452 ±0.10 mm [0. 0178 ±0.0039 in]
0 N to 15 N	0.504 ±0.10 mm [0.01984 ±0.0039 in]
0 N to 20 N	0.562 ±0.10 mm [0.0221 ±0.0039 in]

Suggested Land Pattern

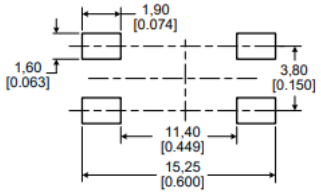

APPENDIX 2: FRICTION MODEL EQUATIONS

A.6 SKF Model Calculations

M = Total frictional moment

$\mathbf{M_{rr}}$ = Rolling frictional moment

$\mathbf{M_{sl}}$ = Sliding frictional moment

$\mathbf{M_{seal}}$ = Frictional moment of seals

$\mathbf{M_{drag}}$ = Frictional moment of drag losses, churning, splashing etc.

$\mathbf{M_{rr}}$ = Rolling frictional moment [Nmm]

$\boldsymbol{\phi_{ish}}$ = Inlet shear heating reduction factor

$\boldsymbol{\phi_{rs}}$ = Kinematic replenishment/starvation reduction factor

$\mathbf{G_{rr}}$ = Geometric variable

Depending on:

• The bearing type

• The bearing mean diameter d_m [mm] = 0.5 (d + D)

• The radial load F_r [N]

• The axial load F_a [N]

n = Rotational speed [r/min]

$\boldsymbol{\upsilon}$ = Actual operating viscosity of the oil or the base oil of the grease [mm^2/s]

e = Base of natural logarithm ≈ 2,718

Krs = replenishment/starvation constant:

= 3 x 10^{-8} for low level oil bath and oil jet lubrication

= 6 x 10^{-8} for grease and oil-air lubrication

$\mathbf{K_Z}$ = bearing type related geometric constant

$\mathbf{M_{sl}}$ = sliding frictional moment [Nmm]

$\mathbf{G_{sl}}$ = variable depending on:

• The bearing type

• The bearing mean diameter d_m [mm] = 0.5 (d + D)

• The radial load F_r [N] • the axial load F_a [N]

$$\mu_{sl} = \phi_{bl}\,\mu_{bl} + (1 - \phi_{bl})\,\mu_{EHL}$$

Where,

μ_{sl} = sliding friction coefficient

ϕ_{bl} = Weighting factor for the sliding friction coefficient

$$=\phi_{bl} = \frac{1}{e^{2.6*10^{-8}*(n*\vartheta)^{1.4}*d_m}}$$

A.7. Load Cell Calibration Code

```
#include "HX711.h"//include this library

HX711 loadcell; //name HX711 as loadcell (used throughout code)

const int loadcellDoutPin = 8;
const int loadcellSckPin = 9;
int knownWeight = 4; //This needs to be changed each time you change the weight you are putting on the loadcell
int long calFactor; //This will print in the serial monitor. Please save the value and use in the run code

void setup() {
  Serial.begin (57600); //start arduino
  loadcell.begin(loadcellDoutPin, loadcellSckPin); //set loadcell pins when loadcell is initialized
  Serial.println (loadcell.read());
}

void calibration(){
    if (loadcell.is_ready()){
    loadcell.set_scale(); //enter setup mode for loadcell
    Serial.println("Tare........"); //print message that loadcell is begining the tare process
    delay(5000); //10 second delay
    loadcell.tare(); //zero the loadcell
    Serial.println("tare done"); //lets the user know the loadcell has been zeroed (tare function)
    Serial.println ("Add known weight"); // prompt to know when to add weight to loadcell
    delay(10000); //10 second delay
    long reading = loadcell.get_units(10);
    Serial.print("results"); Serial.println(reading); // print loadcell results of reading
  }
  else{
    Serial.println ("could not find HX711"); //if above statement is not true print that HX711 is not found (error message)
  }
}
```

```
void calculateCalibrationFactor(){
  calFactor = loadcell.get_units(10) / (float)knownWeight; //calculate calibration factor. Take average of 10 reading of loadcell and divide them by known weight value entered in global vars.
  Serial.print ("calFactor"); Serial.println(calFactor); //print calibration factor. (Save this number it is important for the run code)
}

void loop() {
  calibration(); //fun calibration function above
  delay(5000); // 5 second delay
  calculateCalibrationFactor(); // run and calculate calibration factor
  delay(5000); //delay 5 seconds
  while(true); //break loop and stop readings
}
```

Load cell run code:

```
#include "HX711.h" //include this library

HX711 loadcell; //name HX711 as loadcell (used throughout code)

const int loadcellDoutPin = 8;
const int loadcellSckPin = 9;
int long calFactor= 6454;//This number will change based on what is calibrated in the calibration code



void setup(){
  Serial.begin(57600); //start arduino
  loadcell.begin(loadcellDoutPin, loadcellSckPin); //set loadcell pins when loadcell is initialized
  Serial.println("when stating loadcell:"); //print when loadcell starts this statement and the raw ADC val off loadcell
  Serial.print("Raw ADC value: \t\t"); Serial.println(loadcell.read()); //read raw ADC val
  loadcell.tare(); //after loadcell power on tare loadcell
  loadcell.set_scale(calFactor); //set calibration factor in loadcell
}
```

```
void loadcellRead(){
  Serial.print("loacell reading: \t"); //print loadcell reading statement
  Serial.println(loadcell.get_units(10));//print averaged loadcell readings
  loadcell.power_down(); //send loadcell into low power state to clear reading
  delay(2000); //delay for 1 second
  loadcell.power_up(); //send loadcell to high power mode to take a new reading
}

void loop() {
  // put your main code here, to run repeatedly:
  loadcellRead();//uncomment when running loadcell //run function in loop to read from loadcell
  }
```

A.8. System Run Code

```
//This script was written on 12/13/23
//This script controls the mosfets connected to the motors on the CubeSat, a loadcell, and an encoder, and a temp Sensor
//The motors are named Bearing Tribometer and Pin-On-Disc tribometer
//Pin-on-Disc uses a set speed function and is connected Motor 2 on the PCB
//Bearing tribometer uses a PWM cycling  and is connected to Motor 1 on the PCB

//This is where libraries are included
#include "HX711.h" //include loadcell library (by Bogdan Necula version 0.7.5 (if updated ensure all commands in this library work the same and adjust as needed) )

//setup naming convention as part
HX711 loadcell; //name HX711 as loadcell (used throughout code)

//This is where variables are declared
  //Motor variables
const int gatePin1 = 5; //initialize the pin connected to first mosfet gate for bearing tribometer
const int gatePin2 = 6; //initialize the pin connected to second mosfet gate for pin-on-disc tribometer
  //Loadcell variables
const int loadcellDoutPin = 8;
const int loadcellSckPin = 9;
int long calFactor= 46836;//This number will change based on what is calibrated in the calibration code
  //Encoder variables
const int encoderPinA = 3; //Pin connected to encoder A on Arduino
const int encoderPinB = 2; //Pin connected to encoder B on Arduino
volatile int pulse = 0 ;// encoder pulses
unsigned long lastTime = 0; // time when encoder was read last
unsigned long newTime = 0;
unsigned long deltaTime = 1000; //change in time variable
const int encoderPPR = 24; //Pulses Per Revolution in encoder is 24
unsigned long RPM = 0;//set up for rpm readings
  //Temp Sensor variables
const int tempSensor = A1; //LM35 connected to pin A1
```

```
float tempInCelcius; //variable to store temperature data in
//float tempInCelciusCorrected; //calibrated variable of tempInCelcius obtained from linearization (actual plotted against sensor reading)
//long int m = 100.8; //slope of line of best fit
//long int b = 40.34; //b intercept



//function to start up Pin-On-Disc Motor
void pinOnDiscMotor(){
  setMotorSpeed(255); //preset 1 run at 25 // no preset run at 8
}

//function turns off Pin-On-Disc tribometer
void pinOnDiscMotorOff (){
  //delay (300000);//5 min delay (gives run time of 5 mins)
  setMotorSpeed(0);
}

//function to start up bearing tribometer
void bearingTribometer(){
  setMotorCurrent(340);
//  delay(300000);

}

//function turns off bearing tribometer
void bearingTribometerOff(){
  //delay(300000);//5 min delay (gives run time of 5 mins)
  setMotorCurrent(0);
}

//function starts coms with loadcell
void loadcellStartUp(){
  Serial.println("when stating loadcell:"); //print when loadcell starts this statement and the raw ADC val off loadcell
  Serial.print("Raw ADC value: \t\t"); Serial.println(loadcell.read()); //read raw ADC val
```

```
  loadcell.tare(); //after loadcell power on tare loadcell
  Serial.println ("tare");
  loadcell.set_scale(calFactor); //set calibration factor in loadcell
}

void tempSensorStartUp(){
Serial.print ("RAW ADC VAL: "); Serial.println (analogRead(tempSensor)); //print first raw value from ADC for temp sensor
}

void setup() {
  // put your setup code here, to run once:
  Serial.begin (57600);
  pinMode (gatePin1, OUTPUT); //set gate pin as an output for bearing tribometer
  pinMode (gatePin2, OUTPUT); //set gate pin as an output for pin-on-disc tribometer
  pinMode (tempSensor, INPUT); //set tempSensor pin as an input
  pinMode(encoderPinA, INPUT);
  pinMode(encoderPinB, INPUT);
  loadcell.begin(loadcellDoutPin, loadcellSckPin); //set loadcell pins when loadcell is initialized
  loadcellStartUp();
  //set up interupt on encoder
  attachInterrupt(digitalPinToInterrupt (encoderPinB), pulseAdder, RISING);
  tempSensorStartUp();
}

//Function to control motor speed on Pin-On-Disc
void setMotorSpeed (int Speed){
  //Serial.println (Speed);
  analogWrite (gatePin1, map(constrain(Speed, 0, 255), 0, 100, 0, 255)); //run motor at set speed
}

//Function to handle PWM cycling (generates PWM signal based off calculation of desired current)
void setMotorCurrent (float current){
```

```
  int maxCurrent = analogRead(gatePin2);
  int PWM = (current/maxCurrent)*255 ;
  analogWrite (gatePin2, PWM); //run motor at set speed
}

void loadcellRead(){
  //Serial.print("loacell reading: \t"); //print loadcell reading statement
  //Serial.println(loadcell.get_units(10));//print averaged loadcell readings
  loadcell.power_down(); //send loadcell into low power state to clear reading
  delay(2000); //delay for 1 second
  loadcell.power_up(); //send loadcell to high power mode to take a new reading
}

//function adds pulses for encoder revolutions (triggered by interupt)
void pulseAdder(){
  if (digitalRead(encoderPinA) == HIGH){
    pulse++;
   }
}

//function reads encoder and calculates RPM
void encoderRead(){
   unsigned long newTime = millis();
if (newTime-lastTime >= 1000){
  unsigned long timeElapsed = newTime -lastTime;
  unsigned long rpm = ((float) pulse/(float)encoderPPR) *(60000.00 / timeElapsed);
  //Serial.print ("Pulses: "); Serial.println (pulse); //debug prints
  //Serial.print ("Delta Time: "); Serial.println (timeElapsed); //debug prints
  //Serial.print("RPM: "); Serial.println(rpm); //debug prints
  RPM = rpm;
  pulse = 0;
  lastTime = newTime;
  }
}
```

```
//function reads off temp sensor and can be changed to give calibrated value
void tempSensorRead(){
  tempInCelcius = (analogRead(tempSensor)*5000)/1023; //gets raw reading multiplies by 5000 mV and divides by 1023 bits
   //tempInCelciusCorrected = (m*tempInCelcius)+b; //calibrated temp sensor reading output
    delay (1000); //1 second delay
}

//this function makes it print in columns for all data
void printStatements(){
  //print averaged loadcell readings   //print comma       ///print RPM reading  //print comma //print temp reading (when calibrated switch for this print Serial.print (tempInCelciusCorrected))
  Serial.print(loadcell.get_units(10)); Serial.print(","); Serial.print(RPM); Serial.print(","); Serial.println (tempInCelcius);
}

void loop() {
  // put your main code here, to run repeatedly:
   loadcellRead(); //calls loadcell read function and gets data from loadcell
   encoderRead(); //calls function to read encoder
   tempSensorRead(); //calls function to read tempsensor
  pinOnDiscMotor(); //runs pin on disc motor
  bearingTribometer(); //runs bearing tribometer motor
  printStatements();  //prints data
}
```

APPENDIX 3: MANUFACTURING DRAWINGS

- Ball Holder

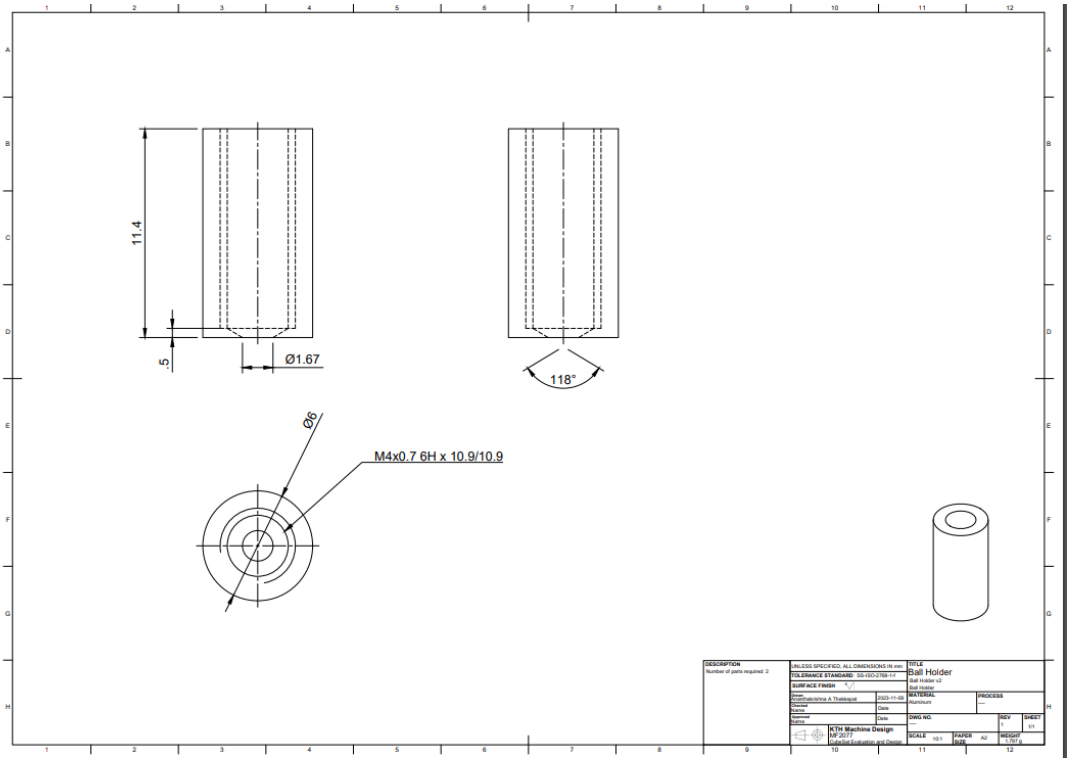

- Bearing Shaft

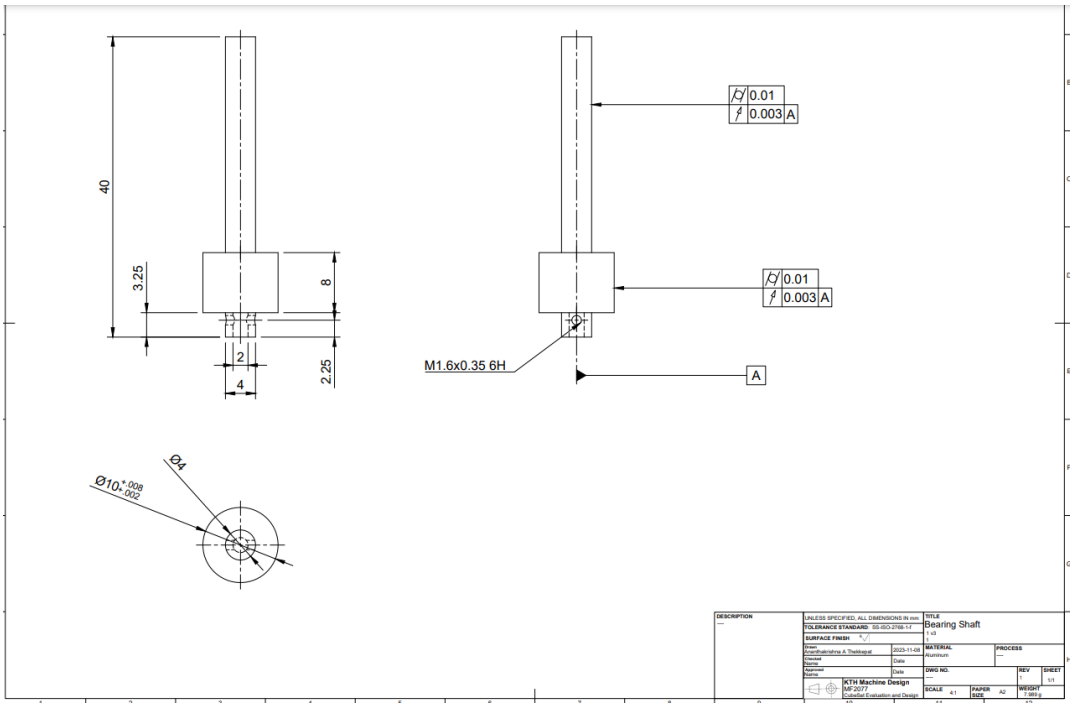

- Outer Ring Sleeve

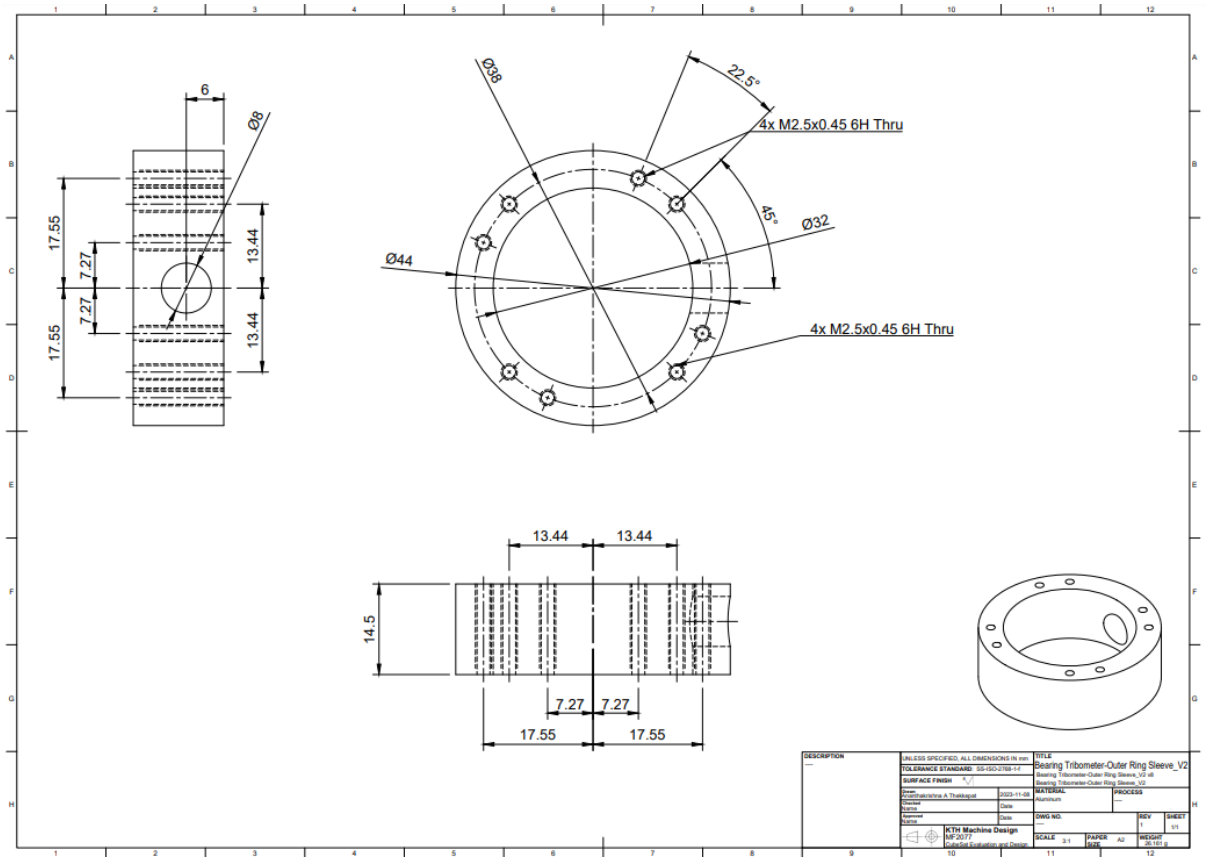

- Pin on Disc Motor Shaft